

Rainfall over the Netherlands & beyond: A remote sensing perspective

Manuel Felipe
Ríos Gaona

S P G

Rainfall over the Netherlands
& beyond:
A remote sensing perspective

Manuel Felipe Ríos Gaona

Thesis committee

Promotor

Prof. Dr Remko Uijlenhoet
Professor of Hydrology and Quantitative Water Management
Wageningen University & Research

Co-promotors

Dr Aart Overeem
Researcher, R&D Observations and Data Technology
Royal Netherlands Meteorological Institute, De Bilt, the Netherlands

Dr Hidde Leijnse
Senior researcher, R&D Observations and Data Technology
Royal Netherlands Meteorological Institute, De Bilt, the Netherlands

Other members

Prof. Dr Jordi Vilà-Guerau de Arellano, Wageningen University & Research
Prof. Dr Hagit Messer-Yaron, Tel Aviv University, Israel
Dr Marielle Gosset, Géosciences Environnement Toulouse, France
Prof. Dr Harald Kunstmann, Karlsruhe Institute of Technology, Germany

This research was conducted under the auspices of the Graduate School for Socio-Economic and Natural Sciences of the Environment (SENSE).

Rainfall over the Netherlands & beyond: A remote sensing perspective

Manuel Felipe Ríos Gaona

Thesis

submitted in fulfilment of the requirements for the degree of doctor
at Wageningen University
by the authority of the Rector Magnificus,
Prof. Dr A.P.J. Mol,
in the presence of the
Thesis Committee appointed by the Academic Board
to be defended in public
on Tuesday 20 June 2017
at 4 p.m. in the Aula.

Manuel Felipe Ríos Gaona

Rainfall over the Netherlands & beyond: A remote sensing perspective,
130 pages.

PhD thesis, Wageningen University, Wageningen, the Netherlands (2017)
With references, with summary in English

ISBN 978-94-6343-200-9

DOI <http://dx.doi.org/10.18174/414112>

Contents

1	Introduction	7
2	GPM-IMERG: Satellite Rainfall	19
3	Satellite- and Link-derived Rainfall	39
4	Errors in Dutch Rainfall Maps from CML	57
5	CML Rainfall in São Paulo, Brazil	75
6	Synthesis	91
	Appendices	97
	Bibliography	107
	Statement of authorship contribution	119
	Summary	121
	Acknowledgements	123

Chapter 1

Introduction

We live on planet Earth, and yes, the *cliché* that it should be called planet “Water” and not Earth is rather valid, for it is water the vital constituent that we live surrounded by and that we are made of. In fact, we should be called “aqualings” or “waterlings” instead of earthlings. By now, we are already familiar with the distribution of water on Earth (let’s keep calling “Earth” Earth in the meantime): 97.47% is salt water, with its vast majority found in the oceans. The remaining 2.53% is fresh water, out of which 69.6% is on glaciers, snow, and permafrost; and 30.1% is found as groundwater. 0.00759% of the total amount is the fresh water we usually survive with, i.e., rivers, lakes, soil moisture, atmospheric and biologic water (*Oki and Kanae, 2006; Shiklomanov and Sokolov, 1983*). The volume of salt water is huge ($\sim 1.36 \times 10^9 \text{ km}^3$) but this water is not appropriate for human consumption given its high salinity. The energy spent in seawater desalination is up to 10 times more than the energy spent in wastewater treatment (*Talbot, 2015a*), which is the main constraint for large-scale desalination. Nevertheless, Israel has achieved practical (cheap) levels of large-scale desalination, and 50% of its water supply now comes from seawater (*Talbot, 2015b*). “Global desalination output has tripled since 2000: 16,000 plants are up and running around the world,...” (*Talbot, 2015a*). Fresh water from glaciers and ice sheets and caps is trapped, and even though groundwater extraction has doubled in the last decades (*Wada et al., 2012*), it is within that tiny 0.00759% that earthlings flourished.

Where does water come from? Actually... we are not sure. One theory suggests that water was brought to Earth by the early impact of comets and asteroids. The whole $\sim 1.4 \times 10^{21}$ kg of terrestrial oceans could have been delivered by accretion of asteroidal material according to *Dauphas (2003)*, for instance. Another theory suggests the early lock/entrapment of water in Earth’s mantle when this latter formed billions of years ago (*Hirschmann, 2006; Smyth, 1987*), with more recent evidence of H₂O-bearing fluids in the lower/deep mantle, i.e., deeper than 660 km (*Palot et al., 2016; Hallis et al., 2015*). The potential volume of water within Earth’s mantle ranges from 1/4 to 4 times its ocean water (*Hirschmann, 2006*). This implies vast reserves of deep groundwater we just can’t reach (for now), and a much larger quantity of water than previously considered.

1.1 Rainfall and the Hydrological Cycle

Hydrology is the branch of Earth sciences that studies the fluxes and processes of fresh water on Earth. As with the distribution of water on Earth, we are also familiar with the hydrological cycle, i.e., the movement of water between the atmosphere and the continental crust. With the sun as the driving force, radiation heats all water surfaces, predominantly those of the oceans. Water rises to the atmosphere as water vapour and moves inland driven by wind currents. If enough condensation nuclei are present in the atmosphere, condensation takes place, and clouds are formed. If clouds grow enough, water precipitates as rain and/or snow. Water that is not intercepted by vegetation or urbanization reaches the ground, and infiltrates (and percolates) and/or runs to rivers, lakes and seas. Then, the hydrological cycle starts all over again. Over the oceans there is a surplus of evaporation, whereas over the continents there is a surplus of precipitation, partly due to the uneven distribution of water and land. This difference in net fluxes between precipitation and evaporation enhances the dynamics of the hydrological cycle back and forth.

The relevance of the study of the hydrological cycle cannot be stressed enough, given that it is within its dynamics that society exists. Take for instance groundwater, which has always been an alternative source of clean water, and has been extracted through *qanāts* (Biswas, 1970, p.26–29) for approximately three millennia (Solomon, 2011, p.487). There is also runoff and reservoir storage, from which we satisfy our increasing demand for fresh water for irrigation, and industrial and household consumption. Rivers are used not only for water supply, power generation and transport but also for dilution of pollutants. In fact, our interaction with the hydrological cycle is so intensive that it has led us to change the hydrological response of many catchments worldwide through the diversion of water flows, transformation of stream networks, alteration of drainage basins, and regional or global climate (Savenije *et al.*, 2014). This (deliberate?) huge impact on Earth and atmosphere driven by human activities since the late 18th century is now known as the *Anthropocene* (Crutzen and Stoermer, 2000). For more in-depth views on hydrology, the reader is referred to Melsen (2017); Brutsaert (2005); Biswas (1970) for comprehensive technical and historical reckonings on the science of hydrology.

Rainfall is arguably the most important process of the hydrological cycle. In the right quantity, it could sustain the food production of a nutritious low-meat diet year-round (Postel, 1997, p.57). If there is too little, life and nature struggle because the land becomes unproductive and uninhabitable. The state of California (USA) is seeing the end of a 6-year drought period (Carlton, 2017; Ehlers and Brown, 2016) that caused agricultural losses by 1.5 billion USD (Talbot, 2015a, p.46) in 2014 alone. If there is too much, life and human activities are threatened by natural hazards like storms, floods, and landslides. From 210 billion USD of economic losses due to these natural hazards in 2016, flooding was the costliest natural hazard with 62 USD billion, for the fourth time in a row (Impact Forecasting, 2017). About 1.28 trillion USD was the total insured values due to flooding from 2001 through 2012 in the USA (Kousky and Michel-Kerjan, 2015). In 2011 Thailand experienced economic losses of 45 billion USD due to widespread flooding between July and November, with 790 casualties (Gale and Saunders, 2013; Impact Forecasting, 2012). This

event ranked second in the costliest events for that year, the earthquake and subsequent tsunami in Japan was first (210 billion USD).

Rainfall is the product of hydrometeorological processes that extensively vary in time and space (Sene, 2013a; Hou *et al.*, 2008). It is not equally distributed over Earth's surface, and it is highly variable in time and space. Most of the rain falls along the equator (and within the tropics) substantially more over oceans than over land (Yong *et al.*, 2015). Continental northern latitudes experience more rainfall than southern latitudes, in terms of volume, as the proportion of land is larger in the northern hemisphere. The IPCC (2013) states that it is *likely* that the global water cycle has been affected by anthropogenic forcing (human influence) since the 60's, with an increased frequency of warm days and nights (climate change definitely is a fact!, folks). Therefore, under the current trends, it is expected by the end of the 21st century a *likely* increase in the annual mean precipitation at the equatorial Pacific Ocean, tropical monsoon areas, mid-latitude wet regions, and high latitudes (northern hemisphere mainly, e.g., most of Canada, northern Europe, and Russia (Henson, 2014, ch.5)). It is also expected a *likely* decrease in annual mean precipitation at mid-latitude and subtropical dry regions, e.g., most of Australia, southern Africa, the Mediterranean and Caribbean, and the south-west of USA and México (Henson, 2014, ch.5). The frequency and intensity of such heavy and/or extreme events is also *likely* to increase. With exceptional local exceptions, the apocalyptic global trend for the coming century is that wet places become wetter and dry places become drier (to paraphrase Henson, 2014, p.84).

To entertain ourselves a bit, it is worth to mention for instance, that the wettest place ever measured on Earth is Mawsynram (India) with 11, 871 mm of mean annual precipitation, officially (Burt and Stroud, 2007, ch.4). Unofficially, there are indications that the wettest spot is not Mawsynram but Lloro with 13, 300 mm·year⁻¹ (Burt and Stroud, 2007, p.112), and (Dolman, 2008, p.7). Lloro is located in Colombia (my *Matushka*), and it literally means "it cried". The maximum rainfall in 24 h was registered in La Réunion (French island east of Madagascar in the South Indian Ocean) with 1, 870 mm (in 1952 according to Burt and Stroud, 2007, p.121) or 1, 825 mm (in 1966 according to Cervený *et al.*, 2007, p.856). In 2007, the world records for the most rainy multi-day periods (3 up to 9 days) were shattered for this same spot (Quetelard *et al.*, 2009; Masters, 2007; NOAA-NWS, 2014). Also in India (Cherrapunji), we found the most consecutive and wettest 12- and 24-month rainfall period with 26, 461 mm and 40, 768 mm, respectively. Arica (Chile) is considered the driest spot on Earth, with a mean annual precipitation of 0.762 mm (Burt and Stroud, 2007; Cervený *et al.*, 2007); "although there are dry valleys in the interior of Antarctica that are believed to have not experienced precipitation in the last 2 million years" (Dolman, 2008, p.7).

1.2 Rainfall Measurements

As with any other natural phenomena, humans developed the need to measure rainfall to quantify its magnitude, and to account for its distribution in space and time. Measure-

ments help us to gain a better understanding of the natural environment that surrounds us. They are a necessary step towards the development of measures intended to somehow quantify the risks of natural hazards we are exposed to. Rainfall measurements are a valuable input in several applications, for instance: to infer the discharge that a catchment will produce at its outlet; to estimate the water balance (or water level) in a given reservoir (e.g., a dam) over which local authorities can elaborate water management programmes or mitigation plans, in case the dam is about to overflow (e.g., the case for the Oroville dam, CA, USA, *Henson (2017)*); to account for the water in the soil that may be available for root uptake and crop growth or that can cause landslides due to high pore pressures (*Posner and Georgakakos, 2016*); to estimate ground water tables and/or flood plains in hydrological models; in climate modelling, and the estimation of global water and energy budgets; to track waterborne (and vector-borne) diseases (*Kirschbaum and Patel, 2016*); to link rainfall as a weather hazard with the risk of motor vehicle crashes, injuries, and fatalities (*Black et al., 2017*).

Measuring rainfall is a whole science *per se* that has evolved in time. Rainfall measurement techniques are practically divided in two principles: direct measurements and indirect estimates.

I. Rain Gauges

Rain gauges (and maybe disdrometers) are examples of devices for (direct) measurements, whereas indirect estimates are provided for instance by radars, satellites and the like. A rain gauge is in essence a bucket in which the amount of rain that falls into is measured (or quantified). Up to date it is the only technology that directly measures rainfall, and thus the most reliable source when it comes to rainfall estimates. Because it is the most basic and ancient technology, it is the one with the longest records of rainfall measurements. Early rainfall measurements date back to the fourth century B.C. (*Strangeways, 2006; Biswas, 1970, p.75*). There are several types of rain gauges. The simplest one consists of a bucket with a graded funnel. Pluviographs include automatic graphing devices to generate the mass curve of the measured time series. Tipping buckets contain a system that counts the volume of raindrops falling into a scale system. There also exist vibrating-wire, weighing, and optical gauges. Disdrometers are a sort of rain gauges, but much cooler, because they not only do literally count the number of raindrops that fall on or through their sampling surface but also measure other physical properties like raindrop size and fall velocity. All of the above devices are mainly owned by meteorological institutes, water authorities or companies dedicated to hydrometeorological business. Nevertheless, the growing interest to measure and report precipitation by worldwide volunteers jointly with more accessible prices to (less regulated) weather stations have made “crowdsourcing” the uprising trend in rainfall measurements based on gauge technology (*de Vos et al., 2017; Reges et al., 2016*).

II. Radar

Radar has evolved a long way since it was devised for RAdio Detection And Ranging, and alongside with the cracking of Enigma, it is often regarded as the invention that helped the Allies to take the upper hand in World War II (*Buderi, 1997*). There was no meteorolo-

gical radar involved in the weather forecast for D-day, but the absence of rainfall did play a central role in the beginning of the end of World War II (*Fleming*, 2004). Radar detects objects that its pulse encounters in the atmosphere, and since its early origins, its potential application in meteorology was clear due to its capabilities to also detect storms and water droplets (*Buderi*, 1997, p.253). Radar estimates rainfall by quantifying all the back-scattered radiation from raindrops that the electromagnetic signal encounters when it propagates through the atmosphere. Bigger raindrops cause larger scatter than smaller ones. Thus, after a volume is scanned up in the atmosphere, we end up with the sum of backscattered powers from all raindrops found in that volume. The main components of a weather radar are the transmitter, receiver, pedestal, parabolic dish, feedhorn (device to convey the pulse to the dish), and the waveguide (hollow conduit where the pulse travels). The size of a radar is constrained by the size of the parabolic dish, which is a function of the transmitted pulse frequency and required beam width. For instance, C-band radars (4-8 GHz or 38-75 mm wavelength) have dish sizes ~ 5.0 m in diameter, whereas the typical dish diameter for X-band frequency radars (8-12 GHz or 25-38 mm of wavelength) is only ~ 2.5 m. It seems that the next step in radar technology for hydrometeorological applications is the phased-array antenna, which allows more frequent scanning, simultaneous targeting, and electronic steering of the pulse (*Hong and Courley*, 2014, p.102). The latter avoids the (mechanical) rotation of the parabolic dish, and thus reduces (regular) maintenance costs. Radar is an expensive technology, but if one would try to match up the capabilities of a radar with a network of gauges, the costs of such a task would be at least just as high.

III. Satellite

This year (2017), it is six decades since the first launch of satellites for scientific purposes, which have lead humans to gain a huge understanding about Earth processes on a truly global scale. The first rainfall estimates came from microwave and stratospheric sounders aboard Nimbus 5 back in the 70's (*NRC*, 2008, p.14). Nowadays, and since February 2014, for such a task we count on GPM (the Global Precipitation Measurement mission) which aims to advance global precipitation measurements from space (*Hou et al.*, 2014). GPM is a multinational platform of ~ 10 satellite programmes that offers worldwide precipitation estimates, which are freely available for everyone (with access to the Internet), as was the case with its predecessor TRMM (Tropical Rainfall Measurement Mission), which provided rainfall retrievals for 17 continuous years since 1997. Conversely to radars, satellites could long be considered as passive (remote) sensors. Their rainfall estimates come from measurements of radiation emitted or reflected by atmospheric hydrometeors. With missions like GPM (or TRMM), meteorological satellites can also be considered as active sensors due to the installation of radars aboard these platforms. Satellite platforms are divided in two categories: LEO (Low Earth Orbit), which orbit Earth at 800 km or lower, and GEO (Geostationary Earth Orbit), which orbit Earth at 36,000 km. The main advantage that satellite has over all other technologies is the continuous monitoring of rainfall over oceans and large proportions of land. Satellite measurements over the oceans help us, for instance, to identify and track Atmospheric Rivers which are known to produce extreme precipitation events (*Dacre et al.*, 2015; *Gimeno et al.*, 2014); and to study global ocean-atmosphere (interdecadal) cycles such as “El Niño” and/or “La

Niña”, which hugely influence the weather in the countries surrounding the Pacific Ocean (Henson, 2014, p.159).

IV. Microwave Links

Commercial microwave links (CML) as a technology for rainfall retrievals has gained momentum in the last decade. Microwave or radio links are pairs of transmitter and receiver antennas mainly used in telecommunication networks. Such networks are designed to transfer data/information from radio, tv, internet, and especially from cellular communication services. The measurement principle of CML is cemented on the near-linear relation that exists between rainfall and attenuation. The stronger the rainfall, the larger the attenuation an electromagnetic signal experiences when traveling along the link path, i.e. between transmitter and receiver antennas. The attenuation is the decrease of received power in the electromagnetic signal (or pulse). This phenomenon was promptly discovered after the invention of radar, and although experiments date back as far as five decades (Hogg, 1968), it was only after the uprise of cellular communications in the late 90's that the scientific community saw the potential of CML for rainfall estimation in the 21st century. The origins of CML and rainfall retrievals are rooted within the electronic communication networks, and thus avoid or forecast disruptions in the transmitted signal(s). The potential of such networks relies on its massive deployment worldwide despite the recent and continuous transition from CML to fiber optics for some areas. Fiber optics is more targeted for urban areas, whereas in rural areas there is still the necessity for CML as their deployment is cheaper compared to that of fiber optics (World Bank, 2012, p.32). GSMA (2016) and ITU (2016) report that the coverage of mobile cellular networks reaches 95% of Earth's population. Nevertheless, only 20% of Earth's land surface is covered by cellular networks (Overeem *et al.*, 2016a). Rainfall retrievals from CML can be seen as by-product of the network operation, which implies a potential scenario of costless estimates of rainfall.

This dissertation involves measurements of all the above technologies, i.e. CML, satellites, radars and gauges. Nonetheless, we are in the early stages of innovative approaches such as home TV-satellite links for rainfall retrievals (Mercier *et al.*, 2015), and umbrellas (Amos, 2014) and car windshields as moving rain gauges (Rabiei *et al.*, 2016).

1.3 Spatiotemporal Caveats

All the above technologies come with pros and cons linked to the spatiotemporal resolution at which they either retrieve or measure rainfall. Hence, it would be unfair to tag one technology above the others as “the best” or “most complete”.

Measurements from rain gauges are only representative of the rain that falls in their vicinity, due to the large variability of precipitation in space, and their small size. Kidd *et al.* (2017) estimate the representativeness of rain gauge measurements as $\sim 1\%$ of Earth's surface, and the actual coverage of gauge orifices as $5.93 \times 10^{-10} \%$, i.e., an area equivalent to less than half a football pitch! (yes, exclamation mark). Their temporal resolution

1.4. Why is it Important to Accurately Measure Rainfall?

depends on the type of gauge, and commonly goes from 10 min to 24 hours. 10-min gauges are also known as “automatic stations”, whereas 24-h gauges are mainly operated ad-hoc by a number of volunteers everywhere in the world.

A S- or C-band radar typically scans an area of $\sim 125,000 \text{ km}^2$ (for no-beam-blockage conditions) with a spatial resolution of $\sim 1 \text{ km}^2$. X-band radars typically scan a smaller areas at spatial resolutions of $\sim 1 \text{ ha}$. Radars also scan the vertical direction which offers a 3D-view of rainfall. The temporal resolution of radar estimates is $\sim 5 \text{ min}$ or less, the time in which information is retrieved from all directions. Currently, radar is the technology which offers the highest resolutions in rainfall retrievals.

The spatiotemporal resolution of satellite retrievals varies with the type of instruments carried aboard, and whether the satellite is LEO or GEO. For instance, infrared sensors aboard GEO satellites provide observations at resolutions of $\sim 10\text{-}30 \text{ min}$ (or hourly) and $1\text{-}4 \text{ km}$, whereas for LEO satellites, near-infrared imagers offer $\sim 1 \text{ km}$ or better, and GPM dual-frequency precipitation radar offers 5 km in the horizontal and $250\text{-}500 \text{ m}$ in the vertical, twice a day over a fixed spot on Earth. GPM gridded products span from 180°W - 180°E and 60°N - 60°S with spatiotemporal resolutions of $0.1^\circ \times 0.1^\circ$ every 30 min.

Power (attenuation) retrievals from CML can be logged at the sub-minute scale, with the most common sampling interval of 1 or 15 min. Their spatial resolution is given by the path length of the link that usually goes from hundreds of meters to tens of kilometers. Conversely to the other technologies, rainfall retrievals from CML are not volumetric or areal. Their estimates correspond to the accumulated rainfall over the path in which the link transmits its signal. Nevertheless, as CML networks are configured from multiple links, current interpolation techniques use tomographic (Zinevich *et al.*, 2008) or geostatistical (Overeem *et al.*, 2013) methods to generate rainfall fields at $\sim 1 \text{ km}^2$ or higher resolutions.

1.4 Why is it Important to Accurately Measure Rainfall?

Accurate rainfall measurements are of extreme importance not only for hydrological and climatological modelling but also because most of the times the purposes for which they are requested are directly linked to the economic welfare of a society. For instance, Uruguay now has to gauge the rainfall for the Rio Negro and Rio Uruguay basins (on which its hydro-power generation relies) to compile a weather index (Somanathan and Nageswaran, 2015). If the measured rainfall falls below a certain threshold, Uruguay will receive a payout from the World Bank that works as a “weather insurance”. This payout is intended to cover the purchase of alternative fuels for energy generation. In 2012, previous to the application of this payout system, the overtaxation of increased fares in electricity caused by an intensive drought had to be paid by the end-users. 80% of the power needs in Uruguay are supplied by hydro-electric generation. Another example is the design of hydraulic infrastructure which relies on the concept of “return period”, i.e., the time in which a given rainfall event would most likely surpass a certain threshold. The longer the return period

the stronger the event that is expected. For the hydraulic design of dams, channels, dikes, flood plains, box-culverts, sewers and the like, rainfall estimates are translated into water surface levels for which the structures should hold. If such structures fail, the socio-economic impact for a society can be devastating, as was the case in 2005 when hurricane Katrina hit the city of New Orleans, USA (Horowitz, 2016). As of 2017 it remains the third costliest natural disaster, 152 billion 2016 USD in economic losses (*Impact Forecasting*, 2017, p.56). Depending on the technology we use, we certainly have an idea about the intensity of the rain event, and how this develops. With regard to the temporal dimension, it is also very important to generate consistent rainfall measurements to avoid systematic biases that may lead to inaccurate rainfall aggregates in the long run.

1.5 On the Uncertainties

Rain gauges, radars, satellites, and CML offer distinct and diverse vantage points with regard to how and what they measure... but thou shalt not forget that these technologies are also plagued with a requiem of uncertainties. “Uncertainties” and “errors” are terms with interchangeable meanings. Sources of uncertainty in rainfall are mainly attributed to uncalibrated devices, poor sampling in the measurement process, intensity of the rain event, topography and location, and surroundings of the target and/or device, interpolation methodology, and the physical domain over which they perform. To give a detailed account of all possible (sources of) errors that affect rainfall estimation (from four technologies) is a behemoth task that serves a purpose beyond the scope of this thesis. Therefore, only a few examples are mentioned here for the sake of brevity.

If the rainfall event is too heavy, then a tipping bucket would stop measuring rainfall and thus the intensity would be underestimated. In the same way, a radar pulse would be lost due to strong attenuation. If the rainfall event is too light, then the tipping bucket won't record rainfall at all, whereas the radar echo would be lower than the detection threshold. CML (and radars) need to be shielded. Thus, in the case of CML a layer of water on the antennas may induce an attenuation not characteristic of rainfall that should be corrected for. This phenomenon is known as “wet antenna attenuation”.

We have to accept that nature (i.e., physical processes) and life (human and animal activities) are factors that impede perfect measurements. Local turbulence in the vicinity of gauges may withhold raindrops from falling into them. Solar radiation evaporates the upper layer of water inside a bucket. Trees may grow and buildings may be erected shadowing gauge measurements, which is especially the case for backyard-stations from volunteer or amateur networks. The volunteers' perception of the graded funnel in rain gauges may contribute to a slightly different measure of what actually fell. CML are commonly placed on building rooftops where maintenance cranes can interfere with the measurement path. Ground clutter and anomalous propagation, beam blockage, range degradation, and vertical variability of the precipitation system, are some of the most common error sources in rainfall retrievals from radar (Villarini and Krajewski, 2010).

1.6. The Truth About *Ground Truth*: An Ontological Disclaimer

The representativeness of each technique also contributes to the uncertainty, especially when comparisons between rainfall products from different technologies take place. Satellites often infer precipitation from top cloud measurements, whereas radar measurements represent an average rainfall field hundreds of meters above the ground. Because of their proximity to the ground CML are representative of rainfall depths tens of meters above the ground. Ironically, and despite their deficiencies, rain gauge measurements are the most representative of the actual amount of rain that reaches the ground surface, if they are well maintained.

To deal with sources of uncertainty is almost as important as to deal with the measurements themselves, because such errors propagate all the way through hydrological models. For instance, *Kirstetter et al. (2015)* developed a methodology for the generation of probabilistic quantitative precipitation estimates from radar. This certainly is of great value because now not only rainfall depths are provided but also their associated uncertainties.

1.6 The Truth About *Ground Truth*: An Ontological Disclaimer

Before we dwell on some of the uncertainties in rainfall products from satellites and CML over the continental Netherlands and beyond, a big disclaimer should be considered. The error analyses presented in this thesis come from the evaluation of rainfall products with regard to a framework of reference, something we like to call “ground truth”. It is always assumed that the ground truth is the most accurate representation of the actual rainfall field. This is never the case, technically speaking. First of all, our quest is to measure nothing less than rainfall, a quasi-continuous variable in discrete chunks, which by default implies an error in the source (uncertainties from sampling)... a “*contradictio in terminis*” if you will. Yet, still we have to measure something, right? (no purpose in going home empty-handed). By the way, hardcore scientists will tell you that rainfall is a discrete variable because you can actually count raindrops... don't let them trick you that easily. In Chapters 2, 3 and 4, a climatological radar data set from the Netherlands is fearlessly taken as the ground truth. There is no doubt that such a data set has been meticulously subjected to quality standards that make it suitable for evaluation purposes. The end result is a mosaic field from two C-band doppler radars, in which the rainfall estimates are adjusted with a manual and automatic gauge network (in the Netherlands, for the Netherlands). Despite its high quality, and truth be told, it is not the actual representation of the rain that falls, perhaps the most accurate representation, but not the actual one. This also holds for Chapter 5 in which gauge measurements represent the ground truth, although the quality of their estimates could not be verified. To make things worse, it was previously mentioned that uncertainties are introduced when techniques of different nature are compared against each other (representativeness). For instance, the evaluation of CML rainfall estimates against very local gauge measurements (Chapter 5) or 30-min satellite rainfall at 77 km² resolution against 30-min aggregations of 5-min rainfall fields at 1 km² (Chapter 2).

Hence, we should pensively remind ourselves that *ground truth* is just an abstraction for a reality we want to exist (but that doesn't), as all those rainfall measurements are abstractions of a phenomenon we want to quantify (but we technically can't). Here is where the ontology kicks in: In a philosophical sense we've just devoided/shattered the scientific foundation of the results presented in the following chapters, i.e., if the ground truth is a fallacy, why bother with rainfall measurements? An uncertainty within uncertainties, the mother of all uncertainties that actually and humorously cannot be quantified. For better or worse there is not a clear exit to avoid such a quintessential predicament. We saw how important rainfall is within the hydrological cycle and why we should measure it as ubiquitously as possible, or at least to believe that we accurately do so. The ground truth is not held in only one technology, what takes us one step closer to *that* ground truth is the study, understanding and combination of all possible rainfall measurement technologies and techniques.

1.7 What This Thesis Is About... and What to Expect

This dissertation is a quantitative assessment of state-of-the-art rainfall estimates from satellites and CML for the land surface of the Netherlands, mainly. The Netherlands is a relatively small country of $\sim 35,000 \text{ km}^2$ with a population of ~ 16.8 million inhabitants, located above the tropics ($5^\circ 33' \text{ E}$, $52^\circ 19' \text{ N}$) with a temperate climate (Cfb – Köppen-Geiger climate classification, *Peel et al.*, 2007), limiting to the west and north with the North Sea, to the east with Germany, and to the south with Belgium. Founder member of the European Union. The average winter and summer temperatures for the Netherlands are 2.6° C and 17.0° C , respectively, for the months of January and July. Its yearly average precipitation is 851 mm (climatology for 1981-2010). According to KNMI (2015), the average precipitation in the Netherlands is expected to increase 2.5-5.5% by 2050, and 5-7% by 2085, depending on the climate scenario.

The Netherlands has well-established automatic and manual gauge networks with 31 and 321 gauges, respectively (as of 2017). Two C-band doppler radars have been operating for ~ 20 years. It is within the reach of IMERG (Integrated Multisatellite Retrievals for GPM) rainfall products; and since one decade it has been one of the leading countries to continuously use CML in research for rainfall estimation. This data availability makes the Netherlands a suitable test bed for the evaluation of rainfall retrievals from innovative, alternative, and state-of-the-art technologies such as satellites and CML.

In this thesis, uncertainties in rainfall estimates from CML for a subtropical location are also explored and quantified. The test bed was the city of São Paulo, Brasil, with climatological conditions different than the Netherlands, e.g., a stronger precipitation regime characteristic of (sub)tropical latitudes. The topology of the CML network is also different from the Dutch one. Thus, this is an excellent opportunity to test and export the Dutch approach for CML rainfall estimation.

The first year of the research-version of IMERG is presented in Chapter 2. The evaluation is done for the land surface of the Netherlands, at half-hourly, daily, monthly, and yearly durations. IMERG calibrated and uncalibrated data sets are evaluated, and it is shown how calibration based on rain gauges is still necessary, despite the technological advances in satellite rainfall measurements. Nevertheless, once the correction is done, the performance of IMERG matches the rainfall distribution over the Netherlands. Hence, the value of such a product is demonstrated, which is especially relevant for places with no rainfall networks.

In Chapter 3 a similar exercise to that of Chapter 2 is carried out for 7 months (at half-hourly durations), not only for the IMERG product but also for two satellite products from a GEO platform, and one rainfall product derived from CML. The good performance of IMERG is once more confirmed, this time with regard to the GEO-satellite products. Nevertheless, the best performance is obtained for the CML product. These findings are used to further explore the potential use of CML in the eventual validation of satellite rainfall estimates at IMERG resolutions.

Chapter 4 is entirely devoted to explore the uncertainties due to the availability and interpolation methodology of rainfall estimates from CML. It is a continuation of the work conducted by *Overeem et al.* (2013) (exploring only 12 days at 15 min resolution) in which they demonstrated the suitability of CML to derive country-wide rainfall maps. Here, CML measurements are simulated from radar estimates to explore the uncertainties due to the interpolation methodology and the measurements themselves.

Chapter 5 is a straightforward application of the algorithm developed by *Overeem et al.* (2016b) for CML rainfall estimation, but for a different climatology and network topology than the one for which the algorithm was developed. The analysis is done for 3 months of 15-min CML data. It shows that even without locally optimal parameters of calibration the methodology offers accurate rainfall estimates for such subtropical conditions.

The discussion presented in Chapter 6 gives an overview of the evaluation of rainfall products for the Netherlands. It is also argued why there is no technology better than all the others, and how we can benefit from multiple types of rainfall measurements.

Chapter 2

GPM-IMERG: Satellite Rainfall

The Global Precipitation Measurement (GPM) mission is the successor to the Tropical Rainfall Measuring Mission (TRMM), which orbited Earth for ~ 17 years. With *Core Observatory* launched on 27 February 2014, GPM offers global precipitation estimates between 60°N and 60°S at $0.1^\circ \times 0.1^\circ$ resolution every 30 min. Unlike during the TRMM era, the Netherlands is now within the coverage provided by GPM. Here the first year of GPM rainfall retrievals from the 30-min gridded Integrated MultisatellitE Retrievals for GPM (IMERG) product Day 1 Final Run (V03D) is assessed. This product is compared against gauge-adjusted radar rainfall maps over the land surface of the Netherlands at 30-min, 24-h, monthly, and yearly scales. These radar rainfall maps are considered to be ground truth. The evaluation of the first year of IMERG operations is done through time series, scatterplots, empirical exceedance probabilities, and various statistical indicators. In general, there is a tendency for IMERG to slightly underestimate (2%) countrywide rainfall depths. Nevertheless, the relative underestimation is small enough to propose IMERG as a reliable source of precipitation data, especially for areas where rain gauge networks or ground-based radars do not offer these types of high-resolution data and availability. The potential of GPM for rainfall estimation in a midlatitude country is confirmed.

This chapter was originally published as:

Rios Gaona, M. F., A. Overeem, H. Leijnse, and R. Uijlenhoet, 2016: First-Year Evaluation of GPM Rainfall over the Netherlands: IMERG Day 1 Final Run (V03D). *J. Hydrometeorol.*, **17**, 2799–2814, doi: 10.1175/JHM-D-16-0087.1.

2.1 Introduction

On 28 February 2014, the National Aeronautics and Space Administration (NASA) and the Japan Aerospace Exploration Agency (JAXA) jointly launched the core satellite of the Global Precipitation Measurement (GPM) mission. GPM is the follow-on to the Tropical Rainfall Measuring Mission (TRMM), which orbited Earth for 17 years (scientific operations and data collection stopped on 8 April 2015). TRMM data were a valuable source of rainfall data for studies related to extreme convection and precipitation-related events such as tropical cyclones, floods, landslides, and drought; human impact on precipitation; high-quality climatology of rainfall; hydrological modeling to monitor streamflows, floods, and drought; tropical cyclone tracking and forecasting; climate and weather model validation and improvement; disease monitoring in flooded areas; and fire detection (Gran, 2014). In succeeding TRMM, GPM will provide a new generation of precipitation measurements from space to quantify the spatiotemporal variability of global precipitation with an improved accuracy and coverage at higher space-time resolutions. This will not only improve our knowledge of Earth's water and energy cycles and hydrological and climate modeling (Hou *et al.*, 2014), but also enhance relevant societal applications such as fresh water availability, flood forecasting, landslide warning, crop growth prediction, and storm tracking.

The key components of the core satellite of GPM are the Dual-Frequency Precipitation Radar (DPR) and the GPM Microwave Imager (GMI). The DPR consists of two phased-array precipitation radars (PR): 1) KaPR at 35.5 GHz, with a cross-track swath width of 120 km and vertical resolution of 250 or 500 m; and 2) KuPR at 13.6 GHz, with a cross-track swath width of 250 km and vertical resolution of 250 m. Both radars have a horizontal resolution of 5 km. The Ku band measures moderate-to-heavy rain, whereas the Ka band measures frozen precipitation and light rain. The GMI is a conical scanning passive microwave radiometer with 13 channels, from 10.65 to 183.31 ± 7 GHz. The mean spatial resolutions vary inversely with the frequencies from 26 to 6 km. At these frequencies GPM detects a wide range of precipitation intensities, from heavy to light precipitation. The detection of light and frozen precipitation is one improvement of GPM with regard to TRMM. GMI measures over a 140° sector, which represents a cross-track swath of 885 km. The GPM Core Observatory orbits Earth 407 km above its surface at $7 \text{ km} \cdot \text{s}^{-1}$ with an inclination of 65° to the equator. Its orbit is circular and non-sun-synchronous, with a period of 93 min (~ 16 orbits per day). A non-sun-synchronous orbit means that in about one month the satellite acquires measurements at all longitudes and times of day (NRC, 2008, p. 50). Gray and Hanson (2013), Hou *et al.* (2014), and Skofronick-Jackson *et al.* (2013) give detailed accounts of the technicalities of the GPM mission and Core Observatory. GPM was originally established as a cooperation between nine satellite programs, each with microwave radiometers on board and one with precipitation radar (GPM core satellite). Together, they can provide information on global precipitation with a revisit time of approximately 3 h.

GPM offers orbital and gridded products at three different levels of data processing. For instance, a level-1 orbital product is the calibrated GMI brightness temperature (1C-GMI),

whereas DPR Ka/Ku rainfall estimates (2A-DPR) or combined GMI-DPR rainfall estimates [2B-Combined Radar-Radiometer Algorithm (2B-CMB)] are level-2 orbital products. Level-3 products are gridded products, like combined GMI-DPR rainfall averages (3-CMB) or rainfall estimates combined from data of all active and passive microwave instruments in the GPM constellation, that is, Integrated Multisatellite Retrievals for GPM (IMERG; *Huffman et al.*, 2014). IMERG is a post-real-time research product that is of special relevance for hydrological purposes given its high spatiotemporal resolution of $0.1^\circ \times 0.1^\circ$ every 30 min. The main improvement of IMERG can be summarized as the combination of high space-time resolutions, the near-global coverage, and the high quality through the use of active instruments that support the use of passive instruments. GPM offers three different IMERG products: “Day 1 Early Run” is a near-real-time product with a latency of 6 h, “Day 1 Late Run” is a reprocessed near-real-time product with a latency of 18 h, and “Day 1 Final Run” is a post-real-time research product with a latency of 4 months.

Two high-quality precipitation-gauge products from the Deutscher Wetterdienst (DWD) Global Precipitation Climatology Centre (GPCC) are used in the calibration of IMERG products: 1) the full data analysis, which is a large database (from 1901 to 2010); and 2) the monitoring product, which is posted/produced two months after the month of observation and is based on synoptic observational data (SYNOP) and monthly aggregated data (CLIMAT) reports from $\sim 7,000$ to $8,000$ stations worldwide (*Huffman et al.*, 2015a). We studied IMERG Day 1 Final Run because it is not only the longest dataset among the IMERG products, but it also incorporates monthly precipitation-gauge analyses, which provides more accurate results (in regions with gauge information; *Huffman et al.*, 2015b). Its availability starts on 12 March 2014 with a latency of four months. IMERG Day 1 Early and Late Runs are available from 1 April and 7 March 2015, respectively, to present. *Huffman et al.* (2015a,c,b) offer extensive and technical information with regard to IMERG products. From here onward, unless stated otherwise, for simplicity we will refer to the IMERG Day 1 Final Run (precipitationCal) only as IMERG.

Extensive literature over the last decade has dealt with satellite rainfall products. Here we mention some relevant works to the hydrological sciences. *Kucera et al.* (2013), *Tapia-dor et al.* (2012), *Kidd and Huffman* (2011), *Kidd and Levizzani* (2011), and *Kidd et al.* (2009) offer detailed overviews of the state of the art in global precipitation measurements, especially TRMM, and how this technology has advanced in scientific and societal rainfall-related applications such as global high-resolution flux estimates of heat and moisture (energy and water cycle); monitoring of soil moisture, crops, drought, and health; water availability/scarcity; process and climate studies; and atmospheric aerosols, among others. Specific studies to characterize floods (*Wu et al.*, 2012; *Khan et al.*, 2011) and landslides (*Kirschbaum et al.*, 2012; *Hong et al.*, 2007a) have also been carried out. More details on satellite rainfall products such as merging techniques of satellite-based passive microwave (PMW) data, and precipitation radar algorithms are found in *Kummerow et al.* (2011), *Huffman et al.* (2007), *Rose and Chandrasekar* (2006), *Joyce et al.* (2004), and *Huffman et al.* (2001). Merging techniques between processed satellite rainfall products and rain gauges are presented, for instance, by *Nerini et al.* (2015) and *Tobin and Bennett* (2010). Thorough evaluations of several rainfall products developed so far have been done by *Wentz* (2015),

Yang and Nesbitt (2014), Kidd et al. (2012), Scheel et al. (2011), Dinku et al. (2010), Su et al. (2008), Ebert et al. (2007), and Villarini and Krajewski (2007). Kirstetter et al. (2014), Vergara et al. (2014), and Kirstetter et al. (2012) are validation studies against radar data over the continental United States. *Tang et al. (2015)* is one of the first studies on the evaluation of the IMERG product. Errors and uncertainties in satellite rainfall products are characterized and studied by *Gebregiorgis and Hossain (2015), Sarachi et al. (2015), Yong et al. (2015), Gebregiorgis and Hossain (2014), Tian and Peters-Lidard (2010), and Tian et al. (2009)*. *Xue et al. (2013), Bitew et al. (2012), Bitew and Gebremichael (2011), Hong et al. (2007b), and Nijssen and Lettenmaier (2004)* focus their efforts on runoff and streamflow modeling with satellite products as precipitation inputs.

Here, we analyze the first year of IMERG (from 12 March 2014 to 31 March 2015) over the land surface of the Netherlands (50.7° – 53.6° N, 3.3° – 7.3° E; $\sim 35,000$ km²). We assess the performance of satellite estimates at the scale of medium-size catchments by means of quantitative verification scores and cumulative time series of rainfall averaged over the land surface of the Netherlands. Pixel-by-pixel comparisons between radar and satellite rainfall maps are made to establish the accuracy of IMERG rainfall depths at 30-min and 24-h intervals. Radar rainfall maps are considered here to be the ground truth and are aggregated to match the spatiotemporal resolution of IMERG. To investigate the suitability of IMERG for extreme event analyses, empirical exceedance probabilities are also presented.

Our work is one of the first studies that extensively evaluates the performance of IMERG in its first full year of operations. The yearly evaluation of IMERG is novel given the recent long-term availability of this dataset. Although the validation is done for a relative small midlatitude country, we evaluate IMERG at 30-min scales, whereas the majority of the above-mentioned studies focus their analysis on 24-h scales. The use of high-quality gauge-adjusted radar data for evaluation purposes is another valuable asset of this study.

This chapter is organized as follows: Section 2.2 describes the rainfall datasets jointly with the metrics used to assess the accuracy of IMERG rainfall estimates. Section 2.3 presents the results and comparisons between satellite and radar rainfall maps and highlights our major findings. Summary, conclusions, and recommendations are provided in section 2.4.

2.2 Measurements and Methods

Data

The period under analysis extends from 0000 UTC 12 March 2014 to 0000 UTC 1 April 2015; 12 March 2014 is the first day IMERG became available for end users. Because Royal Netherlands Meteorological Institute (KNMI) gauge-adjusted radar data are not fully available either for 2014 or 2015, we chose 1 April 2015 as the end date to account for data losses.

Satellite data

From the available GPM rainfall measurements¹, we evaluated the IMERG dataset. This is the GPM postreal-time gridded research product, obtained from the intercalibration, merging, and interpolation of all microwave precipitation estimates from the GPM constellation (Huffman *et al.*, 2015a) combined with global gauge analyses of precipitation (Schneider *et al.*, 2015a,b). IMERG is 100% available for the studied period, with a temporal resolution of 30 min (also monthly) and spatial resolution [pixel size for the World Geodetic System 1984 (WGS 84) projection] of $0.1^\circ \times 0.1^\circ$ ($\sim 77 \text{ km}^2$ at the latitude of the Netherlands). At this resolution, the land surface of the Netherlands is covered by 593 pixels. There are two datasets embedded in the IMERG products: precipitationUncal and precipitationCal. Conversely to precipitationUncal, rainfall estimates in precipitationCal are calibrated by GPCC monthly precipitation-gauge analyses (Huffman *et al.*, 2015a). Here, the evaluation of IMERG is done for both datasets precipitationCal and precipitationUncal.

Radar data

Radar rainfall depths were obtained from the climatological rainfall dataset² of two C-band Doppler weather radars operated by KNMI. From these radars, a composite of radar reflectivity factors at a constant altitude [pseudo-constant-altitude plan position indicator (CAPPI) images] of 1, 500 m was derived every 5 min. The data were corrected for ground clutter. To avoid remaining strong residual clutter and hail, reflectivities above 55 dBZ were set to 55 dBZ ($\sim 100 \text{ mm} \cdot \text{h}^{-1}$). Next, reflectivity factors Z ($\text{mm}^6 \cdot \text{mm}^{-3}$) were converted to rainfall intensities R ($\text{mm} \cdot \text{h}^{-1}$) with a fixed $Z-R$ relationship (Marshall *et al.*, 1955), $Z = 200 \cdot R^{1.6}$. This results in 97 levels of rainfall intensities from 0.1 to $100 \text{ mm} \cdot \text{h}^{-1}$. A five-pixel median filter on nearest-neighbor pixels was applied to the rainfall depths to remove local outliers caused by accumulated residual ground clutter (Overeem *et al.*, 2011).

Radar data were adjusted with data from one manual and one automatic rain gauge network also operated by KNMI. The automatic network (32 gauges) gives 1-h rainfall depths every hour, whereas the manual network (325 gauges) gives 24-h rainfall depths. A 24-h spatial adjustment was combined with an hourly mean-field bias adjustment. The gauge-adjusted radar product has a temporal resolution of 5 min and a spatial resolution (pixel size) of 0.92 km^2 for the land surface of the Netherlands (38, 063 pixels). Note that gauge-adjusted radar estimates of rainfall are only available over the land surface of the Netherlands because no gauge data are available outside this area. This dataset is a reliable source given its accuracy, spatiotemporal resolution, and availability (99% for the studied period). For more elaborate descriptions on the construction and quality of this radar dataset, see Overeem *et al.* (2011, 2009a,b).

¹GPM rainfall datasets are freely available at the NASA portal: <http://pmm.nasa.gov/data-access/downloads/gpm>.

²KNMI climatological rainfall datasets are freely available at the Infrastructure for the European Network for Earth System Modelling (IS-ENES) climate4impact portal: <http://climate4impact.eu/impactportal/data/catalogbrowser.jsp?catalog=http://opendap.knmi.nl/knmi/thredds/.radarprecipclim.xml>.

Although both satellite and radar data are retrieved from two different and unrelated web portals, their complete independence cannot be guaranteed. This is because IMERG is combined with a monthly GPCC precipitation-gauge analysis (Huffman *et al.*, 2015a, section 3.8). Therefore, it is plausible to assume that some of the gauges used to adjust radar rainfall fields in the Netherlands (Overeem *et al.*, 2009b) are also involved in IMERG estimates. For the Netherlands, the average number of rain gauges used in the GPCC Full Data Product, version 7 (January-December 2013), and GPCC Monitoring Product, version 5 (January-December 2014), are ~ 120 and 35, respectively³. The latter agrees more or less with the number of gauges from the automatic network (32). At this moment, it is not possible to exactly determine which Dutch rain gauges are used in IMERG. Still, for evaluation purposes, we assume the radar dataset to be the ground truth and independent from the satellite dataset.

Spatiotemporal Aggregation

Two classes of rainfall maps were retrieved from the satellite and radar datasets: 30 min and 24 h. To match the spatiotemporal resolution of IMERG, radar rainfall maps were aggregated in time and space. The 5-min radar rainfall maps were simply aggregated, pixel by pixel, into 30-min rainfall fields. The spatial grids of both satellite and radar data were superimposed; thus, for every IMERG pixel, a set of radar pixels was identified. The mean rainfall value of every set of radar pixels was assumed to represent the spatial aggregation of radar rainfall maps (0.92 km^2) at IMERG resolution ($0.1^\circ \times 0.1^\circ$; $\sim 77 \text{ km}^2$ at the latitude of the Netherlands). This spatial average is less representative along the borders of the land surface of the Netherlands, where in most cases the spatial average was based on few radar pixels. Therefore, only those spatial averages of rainfall depths based on 62 radar pixels or more were taken into account for comparison purposes (against IMERG data); 62 is equivalent to 70% of the maximum number of radar pixels (88) that fit into one IMERG grid cell.

Error and Uncertainty Metrics

We quantified the accuracy and uncertainty in IMERG estimates over the Netherlands through 1) the relative bias, 2) the coefficient of variation, and 3) the coefficient of determination.

The relative bias is a relative measure of the average error between the satellite and radar rainfall fields (the latter considered as the ground truth):

$$\text{relative bias} = \frac{\bar{R}_{\text{res}}}{\bar{R}_{\text{radar}}} = \frac{\sum_{i=1}^n R_{\text{res},i}}{\sum_{i=1}^n R_{\text{radar},i}}, \quad (2.1)$$

³Visualization and access of GPCC Full Data and Monitoring Product is possible at <https://kunden.dwd.de/GPCC/Visualizer>.

where $R_{\text{res},i} = R_{\text{IMERG},i} - R_{\text{radar},i}$. \bar{R}_{res} represents the average rainfall residuals, \bar{R}_{radar} represents the average radar rainfall, $R_{\text{res},i}$ represents the rainfall residual (i.e., the difference between IMERG and radar rainfall depths) for a corresponding pixel and time step, $R_{\text{radar},i}$ represents the radar rainfall for any pixel at any time step, $R_{\text{IMERG},i}$ is the IMERG rainfall for any pixel at any time step, and n represents all possible pixels at all time steps for the period under consideration, that is, the first year of IMERG estimates. The relative bias ranges from -1 to $+\infty$, where 0 represents an unbiased rainfall field.

The coefficient of variation (CV) is a dimensionless measure of dispersion (Haan, 1977), defined in this case as the standard deviation of the residuals divided by the mean of the reference field, that is, the mean of the radar rainfall field:

$$\text{CV} = \frac{\sqrt{\widehat{\text{Var}}(R_{\text{res}})}}{\bar{R}_{\text{radar}}}. \quad (2.2)$$

The coefficient of variation is a measure of uncertainty. It ranges from 0 (a hypothetical case with no uncertainty) to $+\infty$.

The coefficient of determination is a measure of the strength of the linear dependence between two random variables, satellite and radar rainfall depths in this case. It is defined as the square of the correlation coefficient between the satellite and radar rainfall depths:

$$r^2 = \frac{\widehat{\text{Cov}}^2(R_{\text{radar}}, R_{\text{IMERG}})}{\widehat{\text{Var}}(R_{\text{radar}}) \cdot \widehat{\text{Var}}(R_{\text{IMERG}})}, \quad (2.3)$$

where r^2 ranges from 0 to 1, where 1 is the case of perfect linear correlation, that is, all data points would fall on a straight line without any scatter. Perfect linearity does not imply unbiased estimation because the regression line does not have to coincide with the 1:1 line, even if it captures all variability.

Quantitative Validation and Extremes

To assess the ability of IMERG to detect rainfall above a given threshold, we used two scores for deterministic detection of discrete events (Wilks, 2011): 1) the false alarm ratio (FAR) and 2) the probability of detection (POD). Deterministic detection means that there is no information about the uncertainty of the event. Although rainfall is considered to be a continuous variable, it becomes discrete when the scores are established for exceeding thresholds of rainfall. The quantitative verification is assessed by means of a 2×2 contingency table. As explained by Su *et al.* (2008), the contingency table is composed of a , where both satellite and radar rainfall depths are above a given threshold T ; b , for satellite rainfall above T and radar rainfall below T ; c , for satellite rainfall below T and radar rainfall above T ; and d , where both satellite and radar rainfall depths fall below T . The variables a , b , c , and d represent the total number of counts above the given threshold T .

The scores are defined as follows:

$$\text{POD} = \frac{a}{a + c} \quad \text{and} \quad (2.4a)$$

$$\text{FAR} = \frac{b}{a + b}. \quad (2.4b)$$

POD [Eq. (2.4a)] is a measure of discrimination, that is, the ability of IMERG estimates to reproduce radar observations above a given rainfall threshold. It is the ratio of IMERG detections to the number of times the event actually occurred. It ranges from 0 to 1, with 1 as the perfect case where all the events were correctly detected. FAR [Eq. (2.4b)] is a measure of reliability, that is, the proportion of IMERG detections that turn out to be wrong. It goes from 1 to 0, with 0 as the perfect case where no IMERG detection is wrong. Both POD and FAR were computed for spatial resolutions of $0.1^\circ \times 0.1^\circ$ and $0.5^\circ \times 0.5^\circ$. Rainfall estimates in the latter (non-overlapping) resolution were obtained from the simple average of 25 pixels at IMERG resolution. The $0.5^\circ \times 0.5^\circ$ resolution is equivalent to the average area of the 23 water authorities that the Netherlands is divided into, a relevant scale for local water management.

The empirical probability of exceedance assesses the ability of IMERG to detect high-intensity rainfall events. It is defined as the ratio of the number of rainfall measurements that exceed a given threshold of rainfall T and the total number of rainfall measurements. As with the other metrics, the empirical probability of exceedance is computed for IMERG and radar rainfall estimates.

2.3 Results and Discussion

Figure 2.1 compares two different cases of IMERG evaluation at 30 min. One is an example of how IMERG accurately detects one of the most intense rainfall events for the studied period. The other case is also an example in which IMERG fails to detect one typical rainfall event for the Dutch winter. In appendices A.1 and A.2, we present a few more visual comparisons of IMERG evaluation at 30 min and 24 h (Figs. A.1, A.2). The full monthly evaluation of IMERG is shown in Fig. A.3.

For the intense rainfall event shown in Fig. 2.1 (top), IMERG clearly detects the difference between areas where rainfall fell and where it did not. IMERG still gives some small differences along the transitions between rain and no-rain areas. Nevertheless, such differences fall below 1.0 mm when compared against radar (at IMERG resolution). One important feature is that IMERG is able to track high-intensity events, especially at higher temporal resolutions, that is, 30 min. This can also be seen in Fig. A.1, where the rainfall event on 28 July 2014 is shown practically in its entire duration. When it comes to rainfall estimates, IMERG performance is equally good. For the case in Fig. 2.1 (top), 47.9 mm is the rainfall depth retrieved by radar at its original resolution. When radar rainfall is scaled up to match IMERG resolution, this maximum rainfall depth becomes 20.5 mm. The maximum IMERG estimate for this event is 16.7 mm, which gives an indication of the good performance of IMERG at such higher spatiotemporal resolutions. Still, there

are some cases in which IMERG does not track the rainfall event nor is able to retrieve accurate rainfall estimates, as presented by the case in Fig. 2.1 (bottom).

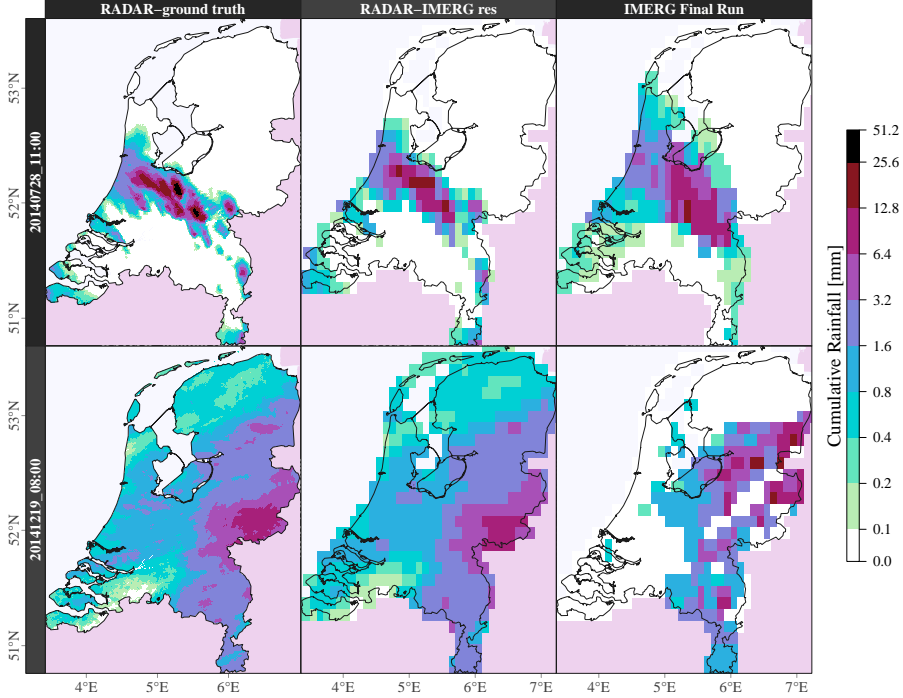


Figure 2.1: Comparison of 30-min rainfall maps. (left) Radar or ground truth, (center) radar at IMERG resolution, and (right) IMERG. The spatial resolution of the rainfall maps at the left is $\sim 1 \text{ km}^2$. These radar maps represent the actual rainfall fields for the time steps under consideration. The radar maps in the center are equivalent to the ground truth at IMERG resolution, that is, $0.1^\circ \times 0.1^\circ$ ($\sim 77 \text{ km}^2$ at the latitude of the Netherlands). Results are for one good evaluation case (top) and a bad one (bottom). Column labels indicate the end time (UTC) and dates at which the 30-min maps were obtained.

Pixel-by-Pixel Comparison

IMERG and radar rainfall maps were compared on a pixel-by-pixel basis at 30-min, 24-h, monthly, and yearly durations for the land surface of the Netherlands over the IMERG grid. The scatter density plots presented in Fig. 2.2 represent the pixel-by-pixel comparisons of IMERG estimates against radar rainfall depths. These plots only include data for which the radar rainfall depth is equal or larger than 0.1 mm (for 30 min) or 1.0 mm for all other cases. With such thresholds (significance condition), we concentrate upon more significant rainfall events. Thus, the statistics are not affected by frequent zeros.

Under the conditions of significance and representativeness (see section 2.2), the coefficient of determination at 30 min is very low ($r^2 = 0.11$), which indicates a poor linear correlation between IMERG and radar rainfall fields at high temporal resolutions. Large representativeness errors between radar and satellite retrievals, revisit time of GPM, and 30-min downscaling and interpolation procedures are some of the reasons for such a low 30-min correlation (~ 0.3). Nevertheless, the relatively low CV of 1.9 is a promising estimate for such a high spatiotemporal resolution, as seen in Fig. 2.2 (top left). Comparisons of 24-h rainfall estimates exhibit an r^2 of 0.40 (Table 2.1), which implies a correlation of ~ 0.6 , and a much lower CV of 1.15. This indicates a good performance in 24-h IMERG estimates. Such a good performance can certainly (but not exclusively) be attributed to the progressive smoothing of rainfall fields when aggregated at larger temporal and/or spatial scales (Huffman *et al.*, 2015c). The scatter density plots of 24-h rainfall depths reveal a relative bias of only -4.7% in IMERG (Fig. 2.2, top right; Table 2.1).

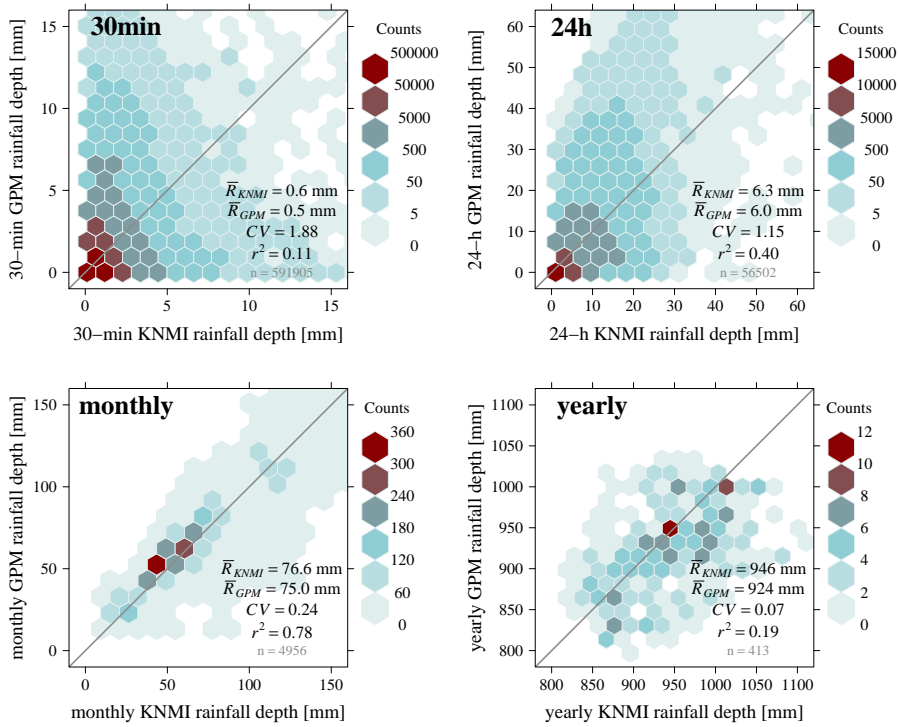


Figure 2.2: Scatter density plots of IMERG precipitationCal rainfall depths vs radar rainfall depths for 30-min, 24-h, monthly, and yearly accumulations, from 12 Mar 2014 to 1 Apr 2015. Paired data are only plotted when radar rainfall depths are equal to or larger than 0.1 mm (for 30 min) or 1.0 mm (for 24 h, monthly, and yearly).

All the above metrics are based on just 5.5% of the maximum possible number of data pairs for the 30-min evaluation, and 92.2% of all data pairs correspond to values below

0.1 mm. If no threshold is applied, the CV remains at ~ 7.0 either for the full coverage of the Netherlands or for 70% of its land surface (representativeness condition, see section 2.2 – Spatiotemporal aggregation). This means that the variability in rainfall estimates cannot be attributed to a poor representativeness of IMERG rainfall depths along the borders of the Netherlands. Instead, when only significant rainfall depths are accounted for ($R \geq 0.1$ mm), the CV decreases from ~ 7.0 to 1.9, which means that most of the discrepancies between rainfall estimates come from the inability of IMERG to properly retrieve the intermittency of rainfall.

Table 2.1 summarizes the values of the relative bias, the CV (of the residuals), and the coefficient of determination [Eqs. (2.1), (2.2), and (2.3), respectively] for the 30-min, 24-h, monthly, and yearly scales at two rainfall thresholds for the precipitationCal and precipitationUncal datasets.

Table 2.1: Relative bias, CV, and r^2 for 30-min, 24-h, monthly, and yearly cases, from 12 Mar 2014 to 1 Apr 2015. For the second column, the statistics are based on paired rainfall depths equal or larger than 0.0 mm for all cases. For the third and fourth columns, the statistics are based on paired data in which radar rainfall depths are equal to or larger than 0.1 mm (for 30-min cases) or 1.0 mm (for 24-h, monthly, and yearly cases). The second and third columns correspond to IMERG precipitationCal. The fourth column corresponds to IMERG precipitationUncal. For all cases the statistics represent at least 70% of the land surface of the Netherlands.

	precipitationCal		precipitationUncal
	$R \geq 0.0$ mm	$R \geq 0.1$ or 1 mm	$R \geq 0.1$ or 1 mm
Relative bias (%)			
30 min	-2.68	-21.88	-32.89
24 h	-0.96	-4.67	-17.15
Monthly	-2.06	-2.06	-18.03
Yearly	-2.30	-2.30	-15.97
CV			
30 min	6.98	1.88	1.97
24 h	1.83	1.15	1.44
Monthly	0.24	0.24	0.58
Yearly	0.07	0.07	0.15
r^2			
30 min	0.19	0.11	0.10
24 h	0.50	0.40	0.29
Monthly	0.78	0.78	0.27
Yearly	0.19	0.19	0.03
Number of pairs n			
30 min	7,541,380	591,905	591,905
24 h	147,441	56,502	56,502
Monthly	4,956	4,956	4,956
Yearly	413	413	413

Cumulative Distribution

Figure 2.3a presents the cumulative satellite and radar rainfall depths for the first year of IMERG. Figure 2.3b presents time series of IMERG 24-h rainfall depths, averaged over the land surface of the Netherlands. The date 21 October 2014 had the largest average rainfall depth (19.0 mm), although 28 July 2014 registered a local maximum of 135.4 mm.

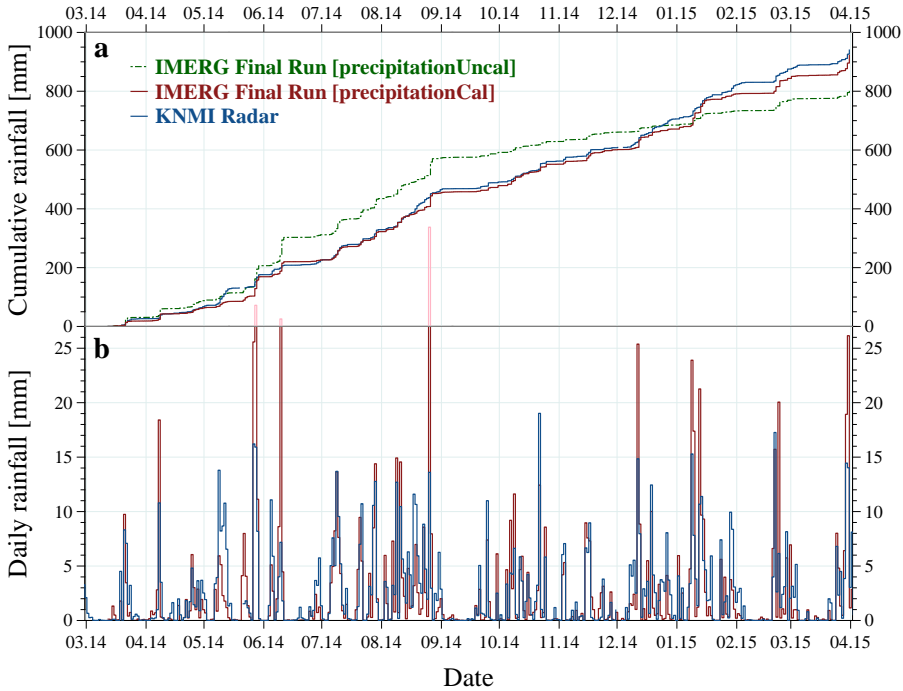


Figure 2.3: (a) Time series of cumulative rainfall depths averaged over the land surface of the Netherlands for KNMI radar data, IMERG precipitationCal, and IMERG precipitationUncal, from 12 Mar 2014 to 1 Apr 2015. (b) Time series of 24-h rainfall depths averaged over the land surface of the Netherlands for IMERG precipitationCal and KNMI radar dataset.

From Fig. 2.3 it can be seen that the yearly distribution of Dutch rainfall is well captured by IMERG. In general, rainfall events retrieved from IMERG, either significant or small, reasonably represent the yearly distribution of rainfall (~ 900 mm) across the land surface of the Netherlands ($\sim 35,000$ km²). On a yearly basis, there is a tendency for IMERG to underestimate 24-h rainfall, especially at low rainfall depths (Fig. 2.3b). Nevertheless, the tendency for IMERG to have a high bias for high precipitation rates has already been reported by Huffman *et al.* (2015c). This is clearly seen in Fig. 2.3b, where, for high-intensity rainfall events like those on 26 and 27 May and 25 August 2014, with averaged rainfall depths of 16.2, 15.9, and 13.6 mm, respectively, IMERG estimates were 25.6, 28.9, and 36.1 mm, respectively. Yong *et al.* (2015) found systematic negative biases in satellite rainfall products. Such negative biases are also seen here in the time series of cumulative rain-

fall depths (Fig. 2.3a).

The difference between the cumulative rainfall depths of IMERG and radar is just -1.9% at the end of the period under analysis (Fig. 2.3a). If the period under consideration is exactly one year, that is, from 12 March 2014 to 12 March 2015, the relative bias is -4.1% . A very similar relative bias (-4.0%) was found by *Tang et al.* (2015) for the IMERG Day 1 Early Run over a catchment twice as large as the Netherlands ($\sim 81,000 \text{ km}^2$, Ganjiang River basin, southeastern China). The low relative bias (-1.9%) is consistent with the relative bias between average yearly rainfall depths of IMERG and radar data (-2.3% ; Fig. 2.2, bottom right; Table 2.1). The difference is due to the way the metrics were computed. For the cumulative distribution, all rainfall is averaged over the land surface of the Netherlands, whereas for the scatterplots only rainfall with representative spatial average was taken into account (at least 70% of land surface coverage; see section 2.2 — Spatiotemporal aggregation). Figure 2.2 also shows the coefficient of determination for the yearly comparisons, that is, $r^2 = 0.19$. Given the low relative bias mentioned above, this lower coefficient of determination is related to the low variability of yearly accumulations. Conversely to r^2 , the good yearly performance of IMERG is also indicated by the very low coefficient of variation (~ 0.1).

Of all the scales studied here, the monthly duration is the one at which IMERG performs best. For average monthly rainfall depths, the relative bias is -2.1% , with a low CV of 0.24 and r^2 of 0.78, that is, a correlation of ~ 0.9 (Fig. 2.2, bottom left; Table 2.1). This good performance is mainly attributed not only to the monthly (and climatological) correction that IMERG is subjected to (*Huffman et al.*, 2015a,c,b), but also to the number of Dutch rain gauges included in the GPCC products used in the IMERG calibration (*Schneider et al.*, 2015a,b). The larger number of gauges from the Netherlands is included in GPCC (~ 120 ; see section 2.2 — Data). Figure A.3 shows all the monthly rainfall fields of IMERG against radar.

Quantitative Validation and Extremes

Quantitative validation was done for 30-min and 24-h IMERG rainfall fields. For each threshold of rainfall, metrics of discrimination (POD) and reliability (FAR) were computed on $0.1^\circ \times 0.1^\circ$ and $0.5^\circ \times 0.5^\circ$ resolutions. Figure 2.4 presents the curves of POD and FAR as a function of the rainfall threshold and their spatial resolution. As with the scatter density plots (Fig. 2.2), the POD and FAR curves are based on a spatial minimum representativeness of 70% (see section 2.2) for both resolutions. Analyses of extremes were carried out for several rainfall thresholds via empirical probability exceedance curves (Fig. 2.5). The empirical probability of exceedance is based on the total number of pixels for which a given threshold is exceeded within the studied period.

For very low rainfall depths, the POD for 30 min and 24 h are ~ 0.4 and ~ 0.6 , respectively (Fig. 2.4; $0.1^\circ \times 0.1^\circ$ resolution). Defined by Eq. (2.4a), the POD indicates the proportion of correct IMERG measurements with regard to rainfall events that actually occurred (radar measurements). At 30-min scales the POD decreases as higher rainfall thresholds

are evaluated, after which the POD becomes more or less constant at ~ 0.2 . At 24-h scales the POD remains more or less constant around 0.6. FAR gives better results at 24-h than at 30-min scales. At 24-h scales FAR starts at ~ 0.15 and steadily increases until ~ 0.9 beyond 30-mm rainfall depths. Similarly, at 30-min scales FAR starts ~ 0.45 and rises until ~ 0.95 beyond 8 mm. FAR indicates the proportion of missed (wrong) IMERG detections with regard to all possible detections [Eq. (2.4b)]. Thus, Fig. 2.4 indicates that most high intensities detected by IMERG are not justified. This is confirmed by Fig. 2.5, which shows how the overestimation pattern dominates IMERG estimates for higher rainfall intensities, especially above 9 mm (for 24 h) and 0.7 mm (for 30 min). Such overestimation implies that IMERG generates more high-intensity intervals, which leads to a relatively high FAR as seen from Fig. 2.4. High intense rainfall events rapidly evolve in time. Hence, the probability of direct detection of such events is reduced given the ~ 3 -h sampling of the whole GPM constellation and the twice-a-day overpassing of GPM core satellite over the Netherlands.

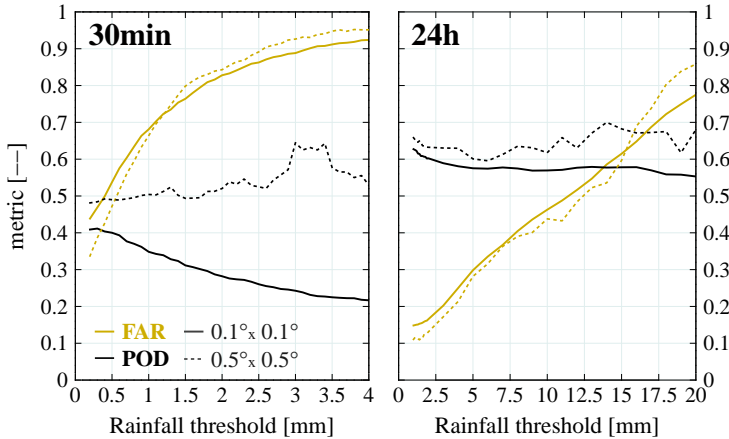


Figure 2.4: FAR and POD of IMERG precipitationCal for (left) 30 min and (right) 24 h as function of rainfall thresholds from 12 Mar 2014 to 1 Apr 2015.

On the other hand, it is not realistic to expect very high or perfect POD and FAR scores (1 and 0, respectively). As suggested by Ebert (2010), there are several sources of error inherent to the evaluation itself of satellite estimates against high-resolution reference data (radar), such as retrieval errors and representativeness of each type of measurement, sampling errors due to spatiotemporal mismatches between satellite and reference data, and the conversion of radiance and/or reflectivity to rainfall intensities. We applied a very simple neighborhood verification method in which both satellite and radar rainfall estimates were upscaled in space from $0.1^\circ \times 0.1^\circ$ to $0.5^\circ \times 0.5^\circ$ (which corresponds to the average scale of Dutch water authorities). Thus, Fig. 2.4 shows how there is a large improvement of POD at 30 min, that is, from ~ 0.4 (at $0.1^\circ \times 0.1^\circ$) to ~ 0.5 , without decreasing when larger rainfall depths are detected. The same holds for the POD at 24-h scale. For the $0.5^\circ \times 0.5^\circ$ resolution there is an improvement, particularly for POD at the 30-

min scale. A small improvement can be seen also for the FAR at both 30-min and 24-h scales for low rainfall depths. Nevertheless, after some rainfall threshold (~ 1.2 mm for 30 min, and ~ 15 mm for 24 h), the FAR gets worse with regard to that of $0.1^\circ \times 0.1^\circ$. This once more suggests the difficulty for IMERG to accurately detect higher rainfall intensities, even at larger spatial scales.

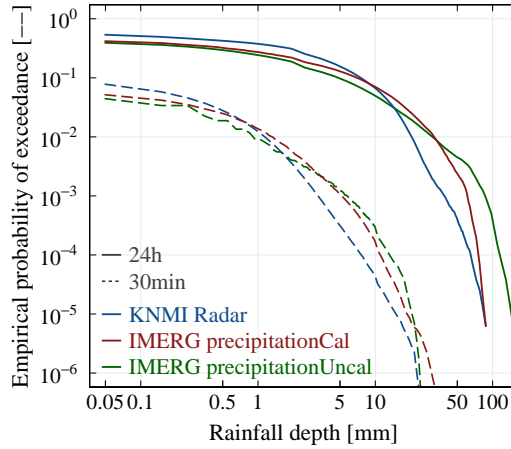


Figure 2.5: Empirical probability of exceedance curves for IMERG precipitationCal and IMERG precipitationUncal (red and green, respectively) and radar (blue) data for 30-min (dashed) and 24-h (continuous) rainfall depths, from 12 Mar 2014 to 1 Apr 2015.

IMERG precipitationUncal

Given the strong spatiotemporal variability of rainfall, it is an immense task for GPM to produce accurate rainfall estimates, especially when its core satellite samples more or less the same place only twice per day. Nevertheless, out of the $\sim 18,000$ 30-min time steps analyzed here, the proportion of cases in which IMERG performs well is larger than those cases in which its performance is bad. To some extent this reflects the recent advance of such a robust mission to estimate high-resolution rainfall rates across Earth.

One may assume that such a satisfactory performance in IMERG is due to the gauge-adjustment procedure. In fact, Fig. 2.3a clearly shows the key role of gauge adjustment in satellite rainfall estimates, where at the end of the studied period the cumulative distribution of IMERG precipitationUncal gives an underestimation of -14% (-16% when pixel-by-pixel comparisons are done; Table 2.1). Around the second full month of IMERG (May 2014), an overestimation in IMERG precipitationUncal took place. This overestimation abruptly increased because of the rainfall events on 26 and 27 May, 9 June, and 25 August 2014. Of particular interest is the apparent adjustment of IMERG at the end of 2014. We found that this adjustment was only carried out for the month of December. From

this point on, underestimation becomes the dominant pattern in IMERG precipitationUncal. Hence, the similarity in rainfall time series between IMERG and radar estimates confirms a large influence of the Dutch gauge network in the calibration of GPM rainfall retrievals (Fig. 2.3b). It is therefore expected that in places of lower gauge densities the performance of IMERG may not be as good as for the Netherlands. The monthly gauge adjustment of IMERG is a crucial step because it is where actual measurements of rainfall calibrate satellite retrievals and is used to back calibrate the 30-min rainfall fields (Huffman *et al.*, 2015b).

IMERG precipitationUncal was thoroughly evaluated as well. As with IMERG, uncalibrated satellite maps (IMERG precipitationUncal) were compared against radar data on a pixel-by-pixel basis. The comparisons (not presented here) were based on paired data for which the radar rainfall depth is equal to or larger than 0.1 mm (for 30 min) or 1.0 mm for all other cases. Therefore, the evaluation between IMERG and IMERG precipitationUncal is consistent for both datasets (Table 2.1). IMERG precipitationUncal is entirely based on satellite rainfall retrievals. Thus, and given the consistency among comparisons, the differences between IMERG and IMERG precipitationUncal performances are only attributed to the gauge calibration done for IMERG Final Run.

IMERG precipitationUncal performance is very similar to that of IMERG at 30-min scales. The relative bias is -32.9% , which represents 50% more underestimation of average rainfall over the Netherlands with regard to IMERG. The coefficients of determination and variation are slightly worse for IMERG precipitationUncal than for IMERG, just 10% and 5%, respectively. Thus, r^2 decreases from 0.11 to 0.10, whereas CV increases from 1.88 to 1.97 (Table 2.1). As with IMERG, the good performance of IMERG precipitationUncal improves as rainfall is accumulated at larger intervals. Nevertheless, such an improvement is not as significant as the one achieved by IMERG (Table 2.1). This highlights once more the importance of ground calibration satellite retrievals. It was previously discussed how promising IMERG is for rainfall estimation despite its low correlation (~ 0.3). We show here that practically the same correlation is found for IMERG precipitationUncal, which implies an actual step forward in satellite-only rainfall estimation. Note that our results are only transferable to a similar climate as experienced in the Netherlands. Still, such a relatively good performance of IMERG precipitationUncal is a trustworthy finding, as it is plausible that in some places or cases the latter outperforms IMERG itself (G. Huffman 2015, personal communication).

For quantitative validation of IMERG precipitationUncal, results remained practically the same for both spatial resolutions (also not shown here), especially at 30-min intervals where there is no significant distinction between POD and FAR metrics for IMERG and IMERG precipitationUncal. For the probability of exceedance, results are presented in Fig. 2.5, which reflect once more the similar performance between IMERG and IMERG precipitationUncal. Exceptions are the overestimates of extreme 24-h events by IMERG precipitationUncal: Fig. 2.5 clearly shows how 24-h IMERG precipitationUncal estimates surpass 100 mm of rainfall, something not even possible for IMERG. Therefore, it is expected that the POD for IMERG precipitationUncal decreases when compared to that of IMERG, more

drastically at 24-h than at 30-min scales. This is consistent with the sudden jumps in the cumulative distribution of IMERG precipitationUncal (Fig. 2.3a).

2.4 Summary, Conclusions and Recommendations

The aim of this work was to evaluate the first year of IMERG estimates (Day 1 Final Run) above the land surface of the Netherlands. Because of the TRMM orbit, TMPA products were not available for the Netherlands during the successful 17 years of TRMM operations. GPM has provided the impetus to generate precipitation estimates that extend to the latitudes of the Netherlands at $0.1^\circ \times 0.1^\circ$ resolution every 30 min.

To test the accuracy and performance of GPM rainfall estimates in its first year of operation, IMERG rainfall maps were compared against radar rainfall fields at 30-min, 24-h, monthly, and yearly durations. Gauge-adjusted radar rainfall maps are considered as ground truth. The quantitative evaluation of these comparisons was established through statistical performance scores, time series analyses, empirical exceedance probabilities, and scatter density plots (with their related error and uncertainty metrics).

We found an $\sim 8\%$ relative bias in IMERG rainfall estimates over the Netherlands. The relative bias is slightly negative (underestimation) for all temporal scales, that is, 30-min, 24-h, monthly, and yearly, and it is noticeable not only in the scatterplots (Fig. 2.2) but also in time series of cumulative 24-h rainfall depths (Fig. 2.3a). In the latter, it is clearer how, on average, IMERG tends to systematically underestimate rainfall in the Netherlands, although only by $\sim 2\%$. These low percentages of underestimation indicate the capability of IMERG to broadly reproduce the distribution of rainfall at medium-catchment scales, especially for longer durations, and hence the potential applicability of IMERG in hydrology and water management.

With regard to rainfall correlation, IMERG performs better at larger durations. Thus, at yearly and monthly aggregations the CV was 0.07 and 0.24, respectively, much better than for 24-h and 30-min aggregations (1.15 and 1.88, respectively). This better performance of IMERG for longer durations is corroborated by the coefficient of determination r^2 , which gradually improved from 0.11 for 30-min durations to 0.78 for monthly durations (with $r^2 = 0.40$ at 24-h scales). Much credit has to be conceded to the monthly gauge adjustment in the IMERG product (Huffman *et al.*, 2015a). IMERG precipitationUncal r^2 and CV were 0.10 and 1.97, respectively, for 30-min aggregations. These coefficients are very similar to those found for IMERG. This similarity implies an actual step forward in high-resolution satellite-only rainfall estimation, given that IMERG is a gauge-calibrated product whereas IMERG precipitationUncal is not. Given the expected similarity between the precipitationUncal datasets of IMERG Final and Early (or even Late) Runs, IMERG precipitationUncal results are promising for near-realtime applications, and particularly important for ungauged regions.

The monthly gauge adjustment in IMERG improves the 24-h, monthly, and yearly rainfall estimates with regard to IMERG precipitationUncal. For IMERG precipitationCal a low

correlation ($r^2 = 0.19$) is found for yearly rainfall estimates, which is mainly driven by the long period of the aggregation itself, the lack of spatial variability in the annual precipitation, and the few samples it was based on. A poor correlation for 30-min durations suggests room for improvement in IMERG estimates at such high resolution, at least over the land surface of the Netherlands. Nonetheless, we presented one good case (out of many) in which IMERG roughly retrieves a reliable spatiotemporal distribution of a 30-min rainfall extreme over the Netherlands. Figures 2.1 and A.1 show 30-min comparisons of rainfall fields from IMERG Final Run and radar (at IMERG resolution).

Better performances are expected at any spatiotemporal aggregation, where extremes and outliers tend to be filtered or canceled out. This was the case when POD and FAR were evaluated over a coarser grid ($0.5^\circ \times 0.5^\circ$), in which such scores perform better for 30 min and 24 h than their counterparts at $0.1^\circ \times 0.1^\circ$ resolution. Scores like POD or FAR are too severe in the pixel-by-pixel evaluation of satellite products against the reference data, especially at higher spatiotemporal resolutions. Therefore, it is advisable to evaluate IMERG through more sophisticated neighborhood verification approaches, such as those proposed by *Ebert* (2010) and *Ebert* (2008). Such an approach allows comparisons of estimates and observations within spatial and/or temporal neighborhoods to evaluate the accuracy of satellite estimates, given the spatiotemporal requirements of a particular application. Through a very simple neighborhood approach, we showed how these scores give better results for a spatial resolution 25 times coarser than IMERG. Figures A.2 and A.3 show 24-h and monthly comparisons of rainfall fields from IMERG against radar.

The evaluation carried out here heavily relied on the assumption of the Dutch radar data as the ground truth. Nevertheless, the gauge-adjusted radar dataset is not perfect either, particularly for 30-min duration. *Overeem et al.* (2009a) reported an underestimation for the most extreme rainfall amounts. There are also differences in representativeness between radar and satellite rainfall retrievals that may cause differences in both datasets.

With regard to GPCC data, it would be valuable if such a dataset gives detailed information about the gauge network used for IMERG calibration. Thus, the level of dependence between the ground truth and IMERG could be assessed. At present, GPCC gauge network details are not publicly available, conversely to all the other products involved in IMERG.

IMERG is now a valuable source of rainfall estimates at high spatiotemporal resolutions. The increased coverage and spatiotemporal resolution is certainly beneficial, especially in those areas (countries) in which other technologies (like ground-based weather radar for instance) or even standard gauge networks are scarce or too expensive to operate (or maintain). Applications such as hydrological modeling can now benefit from GPM products like IMERG. Flood monitoring and forecasting could be another area of application if IMERG near-real-time products are to be used.

2.4. Summary, Conclusions and Recommendations

Chapter 3

Satellite- and Link-derived Rainfall

High-resolution inputs of rainfall are important in hydrological sciences, especially for urban hydrology. This is mainly because heavy rainfall-induced events such as flash floods can have a tremendous impact on society given their destructive nature and the short time scales in which they develop. The spatiotemporal resolutions at which rainfall can be retrieved are becoming higher and higher, with the development of technologies like radars, satellites and (commercial) microwave links (CML). Such high resolutions provide not only more accurate rainfall estimates but also allow a better understanding of its spatiotemporal distribution

For the land surface of the Netherlands, we evaluate here four rainfall products, i.e., link-derived rainfall maps, IMERG Final Run (Integrated Multi-satellitE Retrievals for GPM - Global Precipitation Measurement mission), NIPE (Nighttime Infrared Precipitation Estimation), and MSG CPP (Meteosat Second Generation Cloud Physical Properties). All rainfall products are compared against gauge-adjusted radar data, considered as the ground truth given its high quality, resolution and availability. The evaluation is done for 7 months at 30 min and 24 h. Overall, we found that link-derived rainfall maps outperform the satellite products, and that GPM outperforms CPP and NIPE.

We also explore the potential of a CML network to validate satellite rainfall products. Usually, satellite derived products are validated against radar or rain gauge networks. If data from CML would be available, this would be highly relevant for ground validation in areas with scarce rainfall observations, since link-derived rainfall is truly independent from satellite-derived rainfall. The large worldwide coverage of CML potentially offers a more extensive platform for the ground validation of satellite estimates over the land surface of the Earth.

This chapter was submitted after revision to *IEEE Trans. Geosci. Remote Sens.* as:

M.F. Rios Gaona, A. Overeem, N. Brasjen, J.F. Meirink, H. Leijnse, and R. Uijlenhoet, "Evaluation of Rainfall Products Derived from Satellites and Microwave Links for the Netherlands," Mar. 2017.

3.1 Introduction

Rainfall is the key input in environmental applications such as hydrological modeling, flash-flood and crop forecasting, landslide triggering, waterborne disease propagation, and fresh water availability. Rainfall is the product of hydrometeorological processes that extensively vary in time and space *Hou et al.* (2008); *Sene* (2013a). It is extremely difficult to capture its inherent variability at high spatiotemporal resolutions, i.e., in the order of minutes and kilometers. The requirements of spatiotemporal resolutions are related to the applications for which rainfall inputs are deemed, for instance, urban vs. rural catchments *Schilling* (1991). In urban hydrology, rainfall-related events such as flash floods drastically impact society at short time scales. Thus, temporal resolutions of 30 min or less and spatial resolutions of 10 km or less are necessary *Berne et al.* (2004). Over history, devices and techniques have been developed not only to measure or estimate rainfall quantities but also to fill the spatiotemporal gaps in the data collected.

Rain gauges are the only devices that directly measure rainfall. They are a relatively low-cost technology due to their compact size and simplicity; consequently, large networks of rain gauges are found in many places over the land surface of the Earth *Becker et al.* (2013). If well maintained, measurements from rain gauges are accurate. However, they are point measurements, only representative of the area in their direct vicinity. The spatial variability of rainfall is not well captured by gauges given their sparsity, especially over the oceans, where practically no gauges are placed. Often, depending on the type of gauge, it is only possible to collect daily rainfall values, which is not desirable if hourly (or sub-hourly) analyses are needed. Yet still, rain gauges are the main and most reliable devices to validate more advanced platforms like weather radars and meteorological satellites.

Weather radar has greatly improved the spatiotemporal resolution of rainfall retrievals. After World War II radar (RADio Detection And Ranging) technology became popular for meteorological purposes *Rogers and Smith* (1996); *Atlas and Batan* (1990). Weather radar measures the power of the backscatter (reflection) produced by hydrometeors encountered by an electromagnetic pulse along its propagation path. The backscatter produced by raindrops can later be processed and transformed into precipitation intensity. Hence, rainfall is estimated for any given volume that radar scans up in the atmosphere. In general, weather radars scan azimuths (0° – 360°) with an angular resolution of $\sim 1^\circ$, and reach distances of ~ 100 – 300 km with horizontal resolutions of ~ 1 km. Such scans are also done for several elevations (0° – 90°) with regard to the horizon. Radar retrieves information from all directions with a typical time resolution of 5 min.

Satellite constellations provide global estimates of rainfall on a quasi real-time basis. Satellite rainfall estimates are obtained from remotely sensing the radiation emitted or reflected by atmospheric hydrometeors. This can be done by several techniques which depend on the type of sensor and the range of the spectrum they sense *Kidd et al.* (2010): 1) Visible (VIS) and infrared (IR) methods — in which measurements of reflectance and brightness temperature, or retrieved cloud properties such as water path, particle effective radius, and height are related to occurrence and intensity of precipitation; 2) Passive Mi-

crowave methods (PMW) — in which liquid or solid precipitation is identified through measurements of microwave radiation transmitted by both hydrometeors and the Earth, which is partly scattered and absorbed by hydrometeors; 3) Active Microwave methods (AMW) — in which rainfall information is retrieved from power measurements of the backscatter produced by the interaction of hydrometeors and electromagnetic pulses emitted by satellite-borne sensors, namely radars; 4) Multisensor techniques — in which the combination of data collected within a satellite constellation overcomes some of the deficiencies of the above techniques, for instance, temporal sampling, spatial resolution, and indirect measurements. An example of the latter is the Global Precipitation Measurement mission (GPM), which is the recent upgrade of the Tropical Rainfall Measurement Mission (TRMM). The GPM constellation consists of 9 satellites which offer global precipitation estimates between 60°N – 60°S at a spatial resolution of $0.1^{\circ} \times 0.1^{\circ}$ every 30 min, with a minimum latency of 6 h, i.e., in near-real time. *Hou et al.* (2014); *Skofronick-Jackson et al.* (2013) give a detailed account of all the technicalities of the GPM mission and its core observatory launched on 27 February 2014.

Meteorological satellites can be divided into two categories: Geostationary Earth Orbit (GEO), and Low Earth Orbit (LEO or polar). GEO satellites orbit the Earth at $\sim 36,000$ km, and maintain a fixed position to match Earth's rotation; thus, always the same area is scanned. Their instrumentation typically includes VIS and IR sensors, which provide observations at resolutions of ~ 10 – 30 min (or hourly), and 1 – 4 km *Sene* (2013b); *Wang* (2013). Examples of GEO satellites are those part of NOAA GOES (National Oceanic and Atmospheric Administration - Geostationary Operational Environmental Satellite system); and EUMETSAT (European Organisation for the Exploitation of Meteorological Satellites) with the MSG, which carries the Spinning Enhanced Visible and InfraRed Imager (SE-VIRI) aboard. LEO satellites orbit the Earth mostly in polar (sun-synchronous) orbits at ~ 800 km (407 km for GPM's core observatory). The resolution of their observations strongly depends on the type of sensor. For instance, LEO VIS-NIR (near IR) imagers typically have ~ 1 km or better; whereas PMW imagers are coarser, e.g., GMI (GPM Microwave Imager) is $\sim 6 \times 13 \text{ km}^2$ (depends on the channel). Since TRMM, AMW sensors such as precipitation radar (PR) or DPR (dual PR) are also placed on meteorological satellites. Examples of LEO satellites are those part of EUMETSAT MetOp and NOAA-N NASA (National Aeronautics and Space Administration) Aqua and Terra, which carries the MODerate resolution Imaging Spectroradiometer (MODIS) aboard. For more in-depth details on the state-of-the-art of rainfall estimation from satellites see *Kidd et al.* (2010) and references therein.

CML are a promising alternative for rainfall estimation, especially for places in which rain gauges are scarce or poorly maintained, or where ground-based weather radars are not yet deployed or cannot be afforded *Doumounia et al.* (2014). Rainfall rates can be retrieved from power measurements because rain drops attenuate the electromagnetic signal along the link path, i.e., between transmitter and receiver. Rainfall estimation via ML dates back nearly four decades *Atlas and Ulbrich* (1977); *Crane* (1977), but with the worldwide spread of wireless communication in the last two decades, this technique has become increasingly popular. *Giuli et al.* (1991) had previously reconstructed rainfall fields from si-

mulated microwave attenuation measurements. Nonetheless, *Messer et al.* (2006); *Leijnse et al.* (2007a) were the first to actually use CML to estimate rainfall rates. *Schleiss et al.* (2013); *Chwala et al.* (2014) developed methods to improve rainfall estimates from link measurements. *Overeem et al.* (2013); *Zinevich et al.* (2008) advanced in link rainfall maps for large datasets. When compared to satellite, weather radar or even rain gauges, links may outperform them in one or more of the following areas: they are just tens of meters above the ground, their spatial resolution is in the order of hundreds of meters to kilometers, and their temporal sampling is in the order of seconds to minutes. The massive availability of CML can potentially provide complementary rainfall information. Nevertheless, the success of this technology depends on the availability of received signal level (RSL) measurements from the providers of cellular communication.

We divide our study in two parts: 1) evaluation of satellite- and link-derived rainfall products, and 2) the potential of a CML network to validate satellite rainfall estimates. For the first part, we evaluate the accuracy of four gridded rainfall products: Cloud Physical Properties (CPP) and the experimental Nighttime Infrared Precipitation Estimation (NIPE), both from the GEO platform Meteosat Second Generation (MSG); Integrated Multi-satellite Retrievals for GPM (IMERG), of which the core satellite is a LEO platform; and rainfall maps from a Dutch CML network. The evaluation is done through pixel-by-pixel comparisons against radar rainfall maps at half-hourly (30 min) and daily (24 h) durations from 1 April 2014 to 1 November 2014, i.e., 7 months. Radar rainfall maps are considered here to be the ground truth. For the second part, we focus our analysis on the spatiotemporal availability of a Dutch CML network. Once we have established the accuracy of link rainfall estimates (first part), we are able to evaluate their performance against satellite estimates. We then assess the potential of a CML network as ground validation for satellite products for different link densities. This is of relevance due to the very high coverage of CML over the Earth's land surface, also in areas where no other infrastructure to measure rainfall is available *Overeem et al.* (2013).

This chapter is organized as follows: Section 3.2 describes the rainfall datasets, jointly with the evaluation metrics, and the methodology to assess the spatiotemporal performance of a Dutch CML network. Section 3.3 presents the evaluation of satellite and link-derived rainfall products. Results from the spatiotemporal analysis of a Dutch CML network are also presented in section 3.3. Section 3.4 highlights our major findings. Summary, conclusions and recommendations are provided in Section 3.5.

3.2 Measurements and Methods

The evaluation period is from 0000 UTC 1 April 2014 to 0000 UTC 1 November 2014. This period is limited by the availability of GPM data for the start date, and CML data for the end date.

Radar Data

Radar rainfall depths were obtained from the climatological rainfall dataset¹ of two C-band Doppler weather radars operated by the Royal Netherlands Meteorological Institute (KNMI). Radar data is adjusted with data from one manual and one automatic rain gauge network (325 and 32 gauges, respectively) also operated by KNMI. The gauge-adjusted radar product has a temporal resolution of 5 min, and a spatial resolution (pixel size) of 0.92 km² for the land surface of The Netherlands (38, 063 pixels). This dataset is considered here as the ground truth, and it is a reliable source given its accuracy, spatiotemporal resolution and availability (99.05% for the studied period). For its complete description see *Overeem et al.* (2011).

Microwave Link Data

Rainfall maps were derived from one Dutch CML network. These rainfall maps, LINK hereafter, are derived from the methodology established by *Overeem et al.* (2016b), which can be briefly explained in six steps: 1) a link is considered for non-zero rainfall retrievals if the received power jointly decreases with that of nearby links, i.e. a wet-dry classification is applied; 2) the RSL is subtracted from a reference signal level representative of dry weather, i.e. the median signal level of all dry periods in the previous 24 h; the result is the attenuation estimate; 3) links for which specific attenuation (accumulated over 1 day) deviates too much (from that of nearby links) are excluded from the analysis; 4) a dew filter is applied to correct for dew formation on antennas *Overeem et al.* (2016a); 5) 15 min average rainfall intensities are computed from a weighted average of minimum and maximum rainfall intensities obtained by a power-law relation with specific attenuation, assigned to the middle of the link paths *Atlas and Ulbrich* (1977); and 6) for each grid cell over the land surface of the Netherlands, the 50 nearest rainfall intensities are interpolated via Ordinary Kriging. The spatiotemporal resolution of these rainfall maps is 0.92 km², which corresponds to the radar grid, every 15 min. Examples on rainfall maps from CML are provided in *Overeem et al.* (2016a, 2013) (the latter with supplemental information exclusively on rainfall maps).

RSL storage is not fully continuous for most of the links within the network (Fig. 3.1a). This is mainly due to storage issues at the communication provider's server or replacement of links by fiber optics in urban areas. Consequently, rainfall retrievals for individual links are unevenly distributed in time for the land surface of the Netherlands. Still, it is possible to derive rainfall maps even with missing links because the methodology does not rely on the full availability of the network. Only when none of the links within the network retrieves RSL, rainfall fields cannot be derived. For the studied period, the availability of the CML dataset is 85.2% (59.1% the average availability of individual link paths). Most CML operate at a microwave frequency between 37 and 40 GHz. The average link-path length 4.43 km, with maximum and minimum path lengths of 19.68 km and 0.16 km, respectively.

¹KNMI climatological rainfall datasets are freely available at the IS-ENES climate4impact portal: <https://climate4impact.eu/impactportal/data/catalogbrowser.jsp?catalog=http://opendap.knmi.nl/knmi/thredds/catalog/radarprecipclim/catalog.xml?>

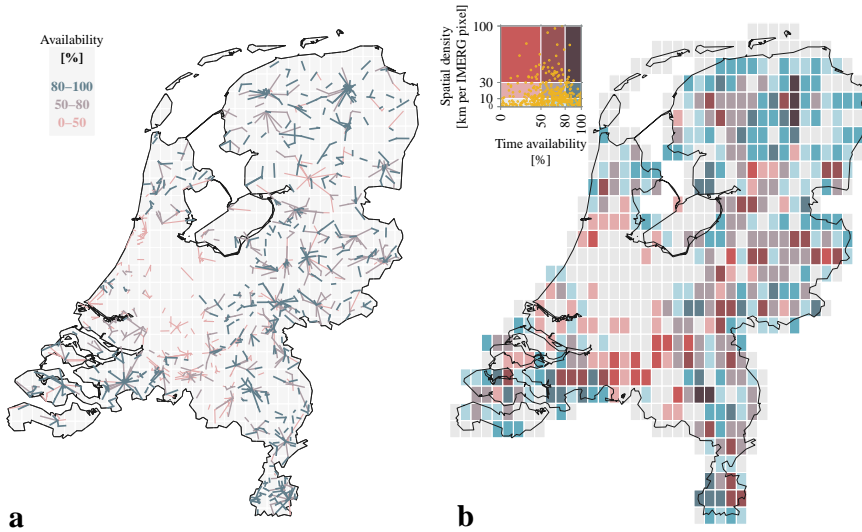


Figure 3.1: a) Topology and temporal availability of one Dutch CML network, for the period between 0000 UTC 1 April 2014 and 0000 UTC 1 November 2014. b) Bivariate choropleth map for the spatial density at IMERG resolution ($0.1^\circ \times 0.1^\circ$), and the temporal availability of the CML network shown in a).

Satellite Data

IMERG

GPM offers orbital and gridded products processed at three levels². IMERG Day 1 (V03D) is a level-3 product with a spatiotemporal resolution of $0.1^\circ \times 0.1^\circ$ every 30 min, for a global coverage of $180^\circ\text{W} - 180^\circ\text{E}$ and $60^\circ\text{N} - 60^\circ\text{S}$ Huffman *et al.* (2014). IMERG is the result of intercalibration, merging and spatiotemporal interpolation of all microwave precipitation estimates from the GPM constellation Huffman *et al.* (2015a) combined with IR data from geostationary satellites and calibrated with global gauge analyses of precipitation Schneider *et al.* (2015a,b). These gauge analyses come from two high-quality precipitation-gauge products from the DWD (Deutscher Wetterdienst) Global Precipitation Climatology Centre (GPCC), i.e., the Full Data Analysis which is a large data base (from 1901 to 2010), and the Monitoring Product which is based on synoptic observational data (SYNOP) and monthly aggregated climatological data (CLIMAT) from $\sim 7,000$ to $8,000$ stations worldwide Huffman *et al.* (2015a). There are three IMERG products, which target different user requirements for latency and accuracy: Early Run (flash flooding), Late Run (crop forecasting), and Final Run (research product; Huffman *et al.* (2015a,c)). Their latencies, i.e., the time after they become available are 6 h, 18 h, and 4 months, respectively. The main variable embedded in each IMERG product is “precipitationCal”, in which the rain-

²GPM rainfall datasets are freely available at the NASA (National Aeronautics and Space Administration) portal: <http://pmm.nasa.gov/data-access/downloads/gpm>.

fall estimates are calibrated by GPCC monthly analyses of gauge precipitation. *Huffman et al.* (2015a,c,b) offer extensive and more conceptual information with regard to IMERG products. *Rios Gaona et al.* (2016) provides examples on rainfall maps from IMERG.

We chose IMERG Final Run because it is considered the post-real-time research product, it is the only IMERG product available for the studied period, and provides more accurate results *Huffman et al.* (2015b). For simplicity, we refer (from here onwards) to the IMERG Final Run (precipitationCal dataset) only as IMERG. For the analyzed period, IMERG availability is 100%, and overlaps that of the CML dataset (Sec. 3.2). At the latitude of the Netherlands, the IMERG spatial resolution [pixel size for the World Geodetic System 1984 (WGS 84) projection] is equivalent to $\sim 77 \text{ km}^2$. Hence, the land surface of the Netherlands is covered by 593 IMERG pixels.

Although both IMERG and radar data are retrieved from two different and unrelated web-portals, their complete independence cannot be guaranteed. This is because IMERG is combined with a monthly GPCC precipitation gauge analysis (*Huffman et al.*, 2015a, sec. 3.8). Therefore, it is plausible to assume that some of the gauge (stations) used to adjust radar rainfall fields are also involved in IMERG (~ 30 , according to *Rios Gaona et al.* (2016)). Still, for evaluation purposes, we assume the radar dataset to be independent from the satellite datasets.

MSG

MSG is a series of GEO-satellites which carry the Spinning Enhanced Visible and InfraRed Imager (SEVIRI) aboard. The latter is an imager with 12 narrow-band channels in the VIS to IR spectral range. We use data from Meteosat-10 (MSG3). Two SEVIRI products developed by KNMI were evaluated: CPP and NIPE. Both products are available every 15 min at the MSG-SEVIRI native spatial resolution, i.e., $4 \times 7 \text{ km}^2$ over the Netherlands³. Correction for parallax effects is not included.

The CPP product relies on the retrieval of cloud optical and microphysical properties from a combination of VIS and shortwave-IR channels. More specifically, precipitating clouds and rain rates are retrieved from cloud condensed water path, particle effective radius, cloud thermodynamic phase, and cloud height measurements. Due to the shortwave channels, CPP is only available during daytime (i.e., solar zenith angle smaller than 78° , $\sim 12 \text{ h}$). This leads to an overall availability of 42.96% for the 30-min resolution for the period under analysis. The algorithm is calibrated with radar data from another period. More details on the algorithm and its validation can be found in *Roebeling and Holleman* (2009); *Roebeling et al.* (2012).

NIPE is an algorithm designed to estimate precipitation rates solely from MSG-SEVIRI IR imagery. It is based on a cloud type dependent precipitation index in which brightness temperatures and brightness temperature differences are combined with corrections for

³MSG CPP rainfall datasets are freely available at the KNMI portal: <http://msgcpp.knmi.nl/portal/>.

atmospheric moisture and cloud top structure. This precipitation index is then converted to precipitation rate by statistical mapping which aims at unbiased statistics on the precipitation estimates. The algorithm used here has been trained with rainfall data from the Dutch radar network from another period. More details on NIPE can be found in *Brasjen and Meirink* (2015). The availability of the NIPE product for the period under analysis is 92.4% for the 30-min resolution.

Spatiotemporal Aggregation

Half-hourly rainfall maps are retrieved from radar, satellite and CML data. All rainfall maps are upscaled to match the spatiotemporal resolution of IMERG, which is considered here as the resolution of reference. The spatial upscaling is done through the simple average of all the values within the resolution of reference. For instance, the spatial grids of IMERG and radar data are superimposed, and for every IMERG pixel a set of radar pixels is identified. The mean rainfall value of every set of radar pixels is assumed to represent the spatial aggregation of radar rainfall maps (0.92 km^2) at IMERG resolution ($0.1^\circ \times 0.1^\circ$). This procedure is done for all datasets given their higher resolutions when compared to IMERG. For the temporal upscaling, rainfall maps are simply aggregated (pixel-by-pixel) into 30-min rainfall fields, which are also aggregated into daily rainfall maps. Daily aggregations in the NIPE dataset are based on a minimum availability of 95% of the half-hourly rainfall maps.

Spatiotemporal Availability

The topology and time availability of link paths within a network are highly variable (Fig. 3.1a, and Sec 3.2). Translating such spatiotemporal features into a 2D-domain, one obtains a visualization of the spatial density of the network (defined as the total CML path length per IMERG pixel) and its availability for a given resolution, e.g., at IMERG resolution (Fig. 3.1b). The temporal availability of any link within the network is represented as 1 or 0 whether the link was active or not (respectively) for a given time step. Thus, the spatial density of the network at any given time step is equivalent to the sum of all active path lengths within one pixel of the IMERG grid (resolution of reference). For the topology presented in Fig. 3.1a, the spatial density extends from 0 to 97.39 km per IMERG pixel for the entire evaluation period. If such a range of spatial densities is binned into few categories, one can explore the influence of the spatial density of a CML network in link-derived rainfall maps against any other rainfall product. In this case, we compute statistics for four spatial density bins between LINK and radar rainfall maps to quantitatively assess the role of CML as potential alternatives for ground validation in satellite rainfall estimation.

Figure 3.1b shows the distribution of the spatial density against the time availability for every (Dutch) IMERG pixel (see also its legend for the link distribution in such a 2D-space). In this figure, the time availability of the network is given by the average relative availability of all the link-paths within each pixel. The relative availability of one link is the number of 30-min time steps in which RSLs were retrieved with regard to the total number

of 30-min time steps in which at least one link was active (theoretical maximum). The maximum time availability for the evaluation period is 99.8%.

Error and Uncertainty Metrics

We evaluate the performance of rainfall estimates from satellites and CML through the relative bias, the coefficient of variation (CV), and the coefficient of determination (r^2).

The relative bias is a measure of the average systematic error between a given rainfall product R_{product} and radar rainfall fields R_{radar} (the latter considered as the ground truth):

$$\text{relative bias} = \frac{\bar{R}_{\text{res}}}{\bar{R}_{\text{radar}}} = \frac{\sum_{i=1}^n R_{\text{res},i}}{\sum_{i=1}^n R_{\text{radar},i}}, \quad (3.1)$$

where $R_{\text{res},i} = R_{\text{product},i} - R_{\text{radar},i}$ and n represents all possible pixels at all time steps for the period under consideration. $R_{\text{res},i}$ are the residuals, i.e., the difference between $R_{\text{product},i}$ and $R_{\text{radar},i}$. \bar{R}_{res} and \bar{R}_{radar} are the average of the residuals and radar rainfall measurements (in mm), respectively. The relative bias ranges from -1 to $+\infty$, where 0 represents an unbiased rainfall field.

The coefficient of variation is a dimensionless measure of dispersion *Haan (1977)*, defined in this case as the standard deviation of the residuals $\sqrt{\widehat{\text{Var}}(R_{\text{res}})}$ divided by the mean of the reference field, i.e., the mean of the radar rainfall field:

$$\text{CV} = \frac{\sqrt{\widehat{\text{Var}}(R_{\text{res}})}}{\bar{R}_{\text{radar}}}. \quad (3.2)$$

The coefficient of variation is a measure of uncertainty. It ranges from 0 (a hypothetical case with no uncertainty) to $+\infty$.

The coefficient of determination is a measure of the strength of the linear dependence between two random variables, satellite (or link) and radar rainfall depths in this case. It is defined as the square of the correlation coefficient between the rainfall depths of a given rainfall product $R_{\text{product},i}$ and its equivalent radar rainfall depths $R_{\text{radar},i}$:

$$r^2 = \frac{\widehat{\text{Cov}}^2(R_{\text{radar}}, R_{\text{product}})}{\widehat{\text{Var}}(R_{\text{radar}}) \cdot \widehat{\text{Var}}(R_{\text{product}})}, \quad (3.3)$$

where $\widehat{\text{Var}}(R_{\text{radar}})$ and $\widehat{\text{Var}}(R_{\text{product}})$ are the variance of radar rainfall measurements and a given rainfall product, respectively; and $\widehat{\text{Cov}}^2(R_{\text{radar}}, R_{\text{product}})$ the squared covariance between these two variables. r^2 ranges from 0 to 1, the latter in case of perfect linear correlation, i.e., where all data points would fall on a straight line without any scatter. Perfect

linearity does not imply unbiased estimation because the regression line does not have to coincide with the 1:1 line, even if it captures all the variability.

3.3 Results

IMERG, LINK, CPP and NIPE products are compared against radar rainfall maps on a pixel-by-pixel basis for the land surface of the Netherlands for seven months, at half-hourly and daily scales over the IMERG grid. The pixel-by-pixel comparisons are done through scatter density plots of satellite and link-derived estimates against radar rainfall depths. Scatter density plots based on half-hourly paired rainfall depths are presented in Figure 3.2. These half-hourly plots only include data for which radar rainfall depths are equal to or larger than 0.1 mm.

Table 3.1 summarizes the values of the relative bias, the coefficient of variation of the residuals, and the coefficient of determination [Eqs. (3.1), (3.2), and (3.3)], respectively] at half-hourly and daily scales. Except for the relative bias, the metrics at daily durations are based on rainfall pairs for which the radar depths are equal to or larger than 1.0 mm. For half-hourly durations the analysis is split into daytime (0600 to 1800 UTC), and nighttime (1800 to 0600 UTC) (Table 3.1, 3rd and 4th columns).

Figure 3.3 shows the coefficients of determination and variation between LINK and IMERG, and between LINK and radar rainfall depths for bins of spatial density of the CML network (Fig. 3.1). Similar to the scatter density plots, these metrics are computed for radar rainfall depths equal to or larger than 0.1 mm (30 min), and 1.0 mm (24 h).

3.4 Discussion

The main focus of this study is the evaluation of rainfall products at half-hourly scales.

Rainfall Intercomparison

Out of the four products, LINK is the one which best reproduces the spatiotemporal distribution of rainfall over the land surface of the Netherlands. It is the product with the lowest CV of 1.16 and the highest r^2 of 0.37 (Fig. 3.2, and Table 3.1, 30 min, day+night). The latter indicates a linear correlation of ~ 0.6 which can be described as good for such fine resolutions. These results are consistent with those obtained by (Overeem *et al.*, 2013, Fig. 4, right panel) (CV = 1.13 and $r^2 = 0.49$). Overeem *et al.* (2013) performed a similar analysis for 15-min rainfall accumulations for 12 days from 2011, with a higher average link density. The similar results between their work and ours imply that the algorithm developed by Overeem *et al.* (2016b) (Sec. 3.2) is able to accurately retrieve rainfall fields under different network topologies (availability issues included), which would be beneficial and convenient for GPM ground validation (see Sec. 3.4). Our results are based on the comparison of $\sim 10,000$ time steps, compared to the $\sim 1,000$ they considered. Our results for 30 min are also consistent with those in (Overeem *et al.*, 2016a, Table 1 - 'outlier + dew filter' row, 'entire period' dataset), i.e., CV = 1.08 and $r^2 = 0.35$. Their analyses

were done for a much more complete network for 15-min durations at 74 km², and for 2.5 years of CML data. In winter, solid precipitation is a known factor that worsens link rainfall retrievals. Rainfall estimates from LINK on average underestimate rainfall by 8.88%. IMERG and NIPE also yield low relative biases, i.e., < 10%. *Mei et al. (2016)*; *Nikolopoulos et al. (2010)* found that errors in similar and coarser satellite rainfall products result in predicted runoff with a relative error of the same order.

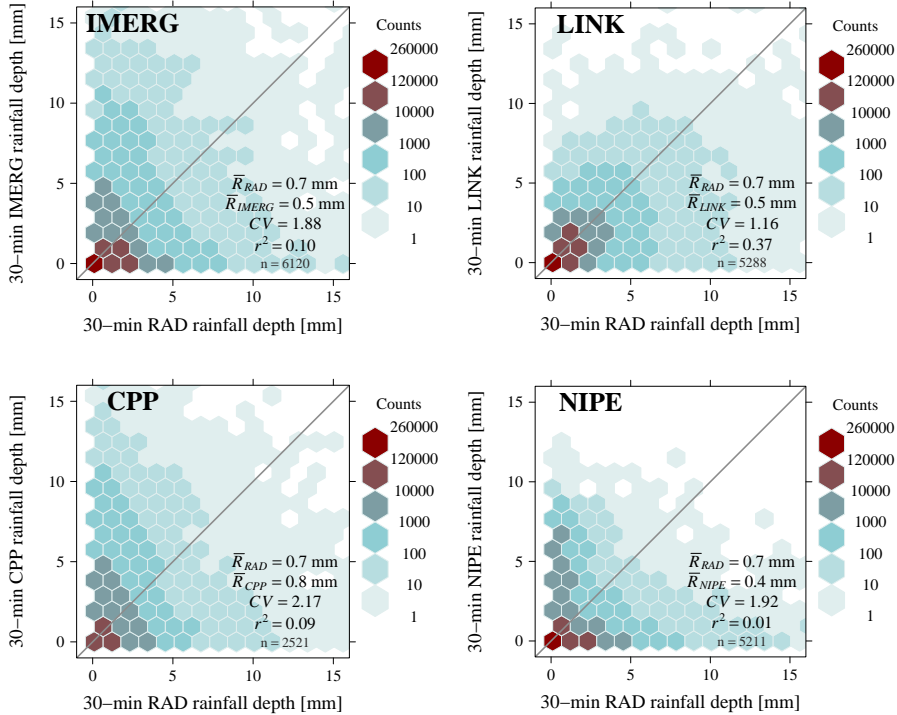


Figure 3.2: Scatter density plots of IMERG, LINK, CPP and NIPE vs. radar rainfall depths for half-hourly accumulations, from 1 April 2014 to 1 November 2014. 'n' represents the number of half-hourly intervals the comparisons are based on.

For IMERG, results are less appealing with a CV of 1.88 and r^2 of 0.10. Nevertheless, *Rios Gaona et al. (2016)* showed that such results are typical for the Netherlands in the first year of IMERG operations, i.e., CV = 2.30 and r^2 = 0.08. The low linear correlation ~ 0.3 is partly attributed to the few direct measurements the GPM constellation is able to retrieve over the Dutch surface. The GPM core satellite carries a state-of-the-art DPR (dual precipitation radar) and GMI (GPM Microwave Imager), but only overpasses the land surface of the Netherlands twice a day on average. The revisit time of GPM constellation is approximately 3 h. Therefore the probabilities to detect and track heavy storm events are low, given the relative small size of the Netherlands ($\sim 35,000$ km²). Still, IMERG also relies on GEO-satellite IR data and continental rain gauges to merge and downscale all

data to obtain an almost instantaneous global snapshot of precipitation. For the analyzed period the relative bias is low, i.e., -1.51% (Fig. 3.2 and Table 3.1). This is due to the gauge adjustment IMERG is subjected to, especially at monthly scales *Huffman et al.* (2015a); *Rios Gaona et al.* (2016). Note that IMERG offers a $\sim 15\%$ higher availability with regard to LINK. This is an advantage of IMERG given that in many places around the world radars and/or CML are not yet operational, and most gauge networks are too sparse to offer high-resolution and continuous rainfall estimates.

Table 3.1: Relative bias and coefficients of variation and determination for half-hourly and daily rainfall depths from IMERG, LINK, CPP and NIPE. For the second column all possible 30-min steps are considered. The third column only considers 30-min steps where CPP retrievals were available, i.e., daytime (0600 to 1800 UTC). The fourth column considers 30-min steps where CPP retrievals were not available, i.e., nighttime. The results for the daily aggregation of 30-min steps are shown in the fifth column. The CV and r^2 are computed on paired rainfall depths equal to or larger than 0.1 mm for 30 min; and equal to or larger than 1.0 mm for 24 h. These thresholds are used in all the analyses, i.e., Day, Night, and Day+Night. For the relative bias no threshold was applied.

	30 min			24 h
	Day+Night	Day	Night	Day+Night
Relative bias (%)				
IMERG	-1.51	-14.88	+9.89	-1.49
LINK	-8.88	-10.88	-2.92	-8.88
CPP	—	+60.41	—	—
NIPE	+5.33	+31.63	-32.50	+0.37
CV				
IMERG	1.88	1.80	2.06	1.17
LINK	1.16	1.21	1.14	0.58
CPP	—	2.17	—	—
NIPE	1.93	2.17	1.50	2.01
r^2				
IMERG	0.10	0.10	0.11	0.36
LINK	0.37	0.34	0.40	0.66
CPP	—	0.09	—	—
NIPE	0.01	0.01	0.02	0.06

CPP is the rainfall product with the highest relative bias, i.e., $+60.41\%$. In general, CPP tends to overestimate rainfall at high solar zenith angles. Conversely to IMERG, CPP is entirely based on MSG which monitors the Netherlands once every 15 min. Thus, the probability to detect rainfall and track storms is very high with this platform. However, CPP measures cloud properties such as optical thickness only in daylight conditions. Thus, for the studied period, the comparison is based on just $\sim 50\%$ of the availability with regard to LINK. Table 3.1 (third column) also presents the analyses of all the other products for daytime to facilitate consistent comparisons between products. Despite its high CV of 2.17, the highest among all products, it is still remarkable how CPP broadly matches the

performance of IMERG in terms of CV and r^2 . This is more clear when the coefficients of determination (r^2) are compared, i.e., 0.09 for CPP and 0.10 for IMERG. The relative bias of the latter increases to -14.88% when only daytime steps are considered. Still, neither CPP nor IMERG are able to approach the performance of LINK. This can be attributed to the fact that CML provide more direct estimates of surface rainfall than satellites, which have larger measurement and sampling uncertainties.

NIPE is the rainfall product with the worst statistics either for daytime or nighttime. Although its CV of 1.93 is very similar to that of IMERG, its very poor r^2 of 0.01 basically suggests no linear correlation (~ 0.1). In principle, NIPE is expected to perform better during nighttime (in all aspects, i.e. bias and correlation) because during daytime the radiance observed in the SEVIRI IR channel at $3.9\ \mu\text{m}$ has a solar component which has to be corrected for. This is confirmed by the evaluation of NIPE during nighttime where its CV decreases from 1.93 to 1.50. Such an improvement suggests the separate use of MSG CPP for daytime and NIPE for nighttime. For daily durations CV and r^2 improve due to the smoother rainfall fields result of the temporal aggregation. The last column of Table 3.1 shows how for nearly all cases, and all metrics, daily rainfall maps are more accurate than half-hourly maps. Unlike IMERG and LINK, the relative bias between 30-min and 24-h NIPE differs because not all half-hourly steps are included in the daily aggregations (we only aggregate to daily accumulations if at least 95% of 30-min data is available for any given day; Section 3.2).

CML for Satellite Ground Validation

As shown in section 3.3 (Table 3.1, Fig. 3.2), LINK rainfall estimates at the IMERG pixel scale are more accurate than IMERG rainfall retrievals, in the sense of being closer to gauge-adjusted radar rainfall estimates, considered to be the reference product in this study. This suggests that networks of CML have information to add to IMERG and can potentially be used for near real-time ground validation of IMERG at time scales from 30 min to 24 h.

The results presented in Table 3.1 and Fig. 3.2 are indicative for CML networks with an average spatial density and time availability comparable to that of the Netherlands (Fig. 3.1b). However, many areas around the world, in particular regions with few surface rainfall observations such as developing countries, will exhibit significantly lower link densities than countries such as the Netherlands. It is to be expected that the performance of CML networks in terms of rainfall estimation would deteriorate for such lower spatial densities.

The density of the considered CML network over the Netherlands is spatially variable, with generally higher densities around urban areas and lower densities in rural areas. In addition, network renewal or replacement with optical fiber cables affects link densities in some areas. This property of the CML network allows a systematic investigation of the effect of spatial network density on LINK performance, by classifying the pixels in Fig. 3.1b in different categories of link density, from low to high, and subsequently computing the

performance indicators CV and r^2 [Eqs. (3.2) and (3.3)] for each class separately. The result of such an analysis is shown in Fig. 3.3, for four spatial density classes of equal width, namely 27 km per IMERG pixel. Approximately 85% of the pixels in Fig. 3.1b fall in the 1st class, 12% in the 2nd class, 2% in the 3rd class, and 1% in the 4th class, over the entire 7-month period considered.

Figure 3.3 shows that the performance of LINK rainfall estimates is in fact hardly affected by spatial network density, neither in terms of the coefficient of variation of the residuals (CV, left panel) nor in terms of the coefficient of determination with regard to the reference product, i.e., the gauge-adjusted weather radar data (r^2 , middle panel). Only for very small network densities, a slight deterioration of the LINK performance in terms of r^2 is noted (right panel). The near independence of LINK performance from network density can be partially explained by the employed interpolation methodology, which takes into account information from the 50 nearest link observations around each individual pixel of the original link interpolation grid (0.92 km²). As a result of this, CML from neighbouring IMERG pixels with a higher link density carry over rainfall information to the current IMERG pixel, even if that has a lower link density. Nevertheless, the results presented in Fig. 3.3 are encouraging from the perspective of the potential of LINK rainfall estimates as means of ground validation of satellite rainfall products in areas with lower link densities, such as encountered in regions with few surface rainfall observations (e.g. developing countries).

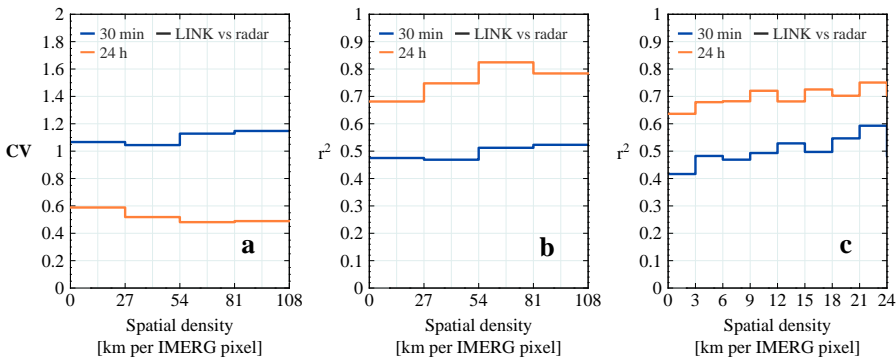


Figure 3.3: Coefficient of variation (CV, left) and coefficient of determination (r^2 , centre and right) for four bins of spatial density of the CML network shown in Fig. 3.1. The statistics are computed for rainfall depths above 0.1 and 1.0 mm (30 min and 24 h durations, respectively) for the period between 1 April 2014 and 1 November 2014. Panel c shows the results obtained for smaller spatial density bins (a discretization of the first bin in panel b). Blue lines are for 30 min. Orange lines are for 24 h.

3.5 Conclusions and Recommendations

We evaluated the performance of three rainfall products derived from satellite (IMERG, CPP, and NIPE), and one from a Dutch CML network (LINK). Gauge-adjusted radar rainfall fields were considered as the ground truth. The information from all platforms was gathered and transformed into rainfall maps with spatiotemporal resolution of $0.1^\circ \times 0.1^\circ$ every 30 min (IMERG resolution). Pixel-by-pixel comparisons were done for the land surface of the Netherlands at half-hourly and daily scales, over a 214-day period ($\sim 10,000$ 30-min rainfall maps). The performance was compiled in three metrics: r^2 , CV and the relative bias. Beyond that, we explored the potential use of link-derived rainfall as ground-validation for satellite rainfall.

LINK is the rainfall product which best reproduces the spatiotemporal distribution of rainfall over the land surface of the Netherlands. For 30 min, its relatively high $r^2 = 0.37$ indicates a linear correlation of ~ 0.6 , twice as high as that of IMERG (~ 0.3). The LINK product underestimates rainfall events by 8.88%. This underestimation is attributed to the limited number of links, whereas for IMERG it is related to the revisit time of GPM constellation (~ 3 h). LINK, IMERG and NIPE yielded low relative biases ($< 10\%$) which becomes suitable from the perspective of hydrological modeling.

CPP is able to broadly match the performance of IMERG, i.e., $r^2 = 0.09$. Such an equivalent performance suggests CPP as a reliable alternative to IMERG for daytime precipitation, given its continuous monitoring over the Netherlands. The least poor performance of NIPE is achieved for nighttime, i.e., $r^2 = 0.02$, which suggests ample room for improvement.

For 24 h, the performance of LINK and IMERG is better than for 30 min. With an $r^2 = 0.36$ and a CV = 1.17, IMERG was found to be better than the NIPE product. With an $r^2 = 0.66$ and a CV = 0.58, LINK strongly improves upon IMERG. These results confirm the potential of IMERG, and especially of LINK, in hydrological applications at relevant spatiotemporal resolutions.

We directly compared LINK vs radar rainfall estimates to assess the potential of CML data for satellite rainfall validation, especially at half-hourly durations. We found that the quality of rainfall estimates from LINK shows no clear dependence on the link density. The average r^2 of LINK vs radar is 0.50 for 30 min, and 0.76 for 24 h, regardless of the spatial link density, even at very small link densities.

The derived LINK maps are based on an interpolation technique which takes the actual availability into account. This interpolation methodology (section 3.2) is expected to have limited influence on the outcome of the rainfall intercomparisons, given that LINK is the result of spatiotemporal aggregation at the relatively coarse IMERG pixel scale (section 3.2). Should evaluations at higher spatiotemporal resolutions be required, the link-derived rainfall products should preferably be based on more sophisticated interpolation techniques, e.g., *D'Amico et al. (2016)*; *Roy et al. (2016)*.

An alternative type of comparison between IMERG and LINK would be to compare not-interpolated link retrievals against IMERG or even IMERG precipitationUncal; thus, the true potential of CML in satellite ground validation could be assessed. Another approach to find if there is indeed a relation between link density and rainfall retrieval would be that of *Rios Gaona et al.* (2015). There, CML rainfall depths were simulated from radar data. In the same way, if CML data is simulated here from radar rainfall depths, one might be able to explore the influence of the spatial density by changing the amount of (simulated) links available.

Pixel-by-pixel comparisons of rainfall products are a drastic evaluation exercise, especially at higher spatiotemporal resolutions. Future work should apply more sophisticated neighborhood verification approaches, such as those proposed by *Ebert* (2010). Such an approach allows comparisons within spatial and/or temporal neighborhoods to evaluate the accuracy of rainfall estimates, given the spatiotemporal requirements of a particular application. The evaluation of the rainfall products at such a high spatiotemporal (IMERG) resolution is important for hydrological applications. It also implies that we ask the most from the observational systems. On the other hand, results are expected to greatly improve at lower spatiotemporal resolutions. For instance, *Roebeling and Holleman* (2009) showed a better performance for CPP at much larger spatial scales. This could also be the case for the experimental product NIPE in spite of its poor performance at higher resolutions. Note that no parallax correction was applied for either CPP or NIPE. If such a correction were to be applied, the validation scores at the pixel scale would likely improve.

Our study is representative of spring, summer, and autumn. Solid precipitation is a known factor that worsens link rainfall estimates *Overeem et al.* (2016a). Results for the LINK product might be transferable to tropical latitudes with few rainfall observations, and similar characteristics to Dutch summer rainfall.

High-quality and -resolution products are beneficial worldwide and very much in need, especially in those areas in which technologies like ground-based weather radar or even standard gauge networks are scarce or too expensive to operate (or maintain). We showed that the performance of satellite rainfall products still shows room for improvement, and that a link-derived rainfall product performs better. Nevertheless, it is remarkable how satellite products like IMERG or CPP offer global estimates of rainfall at high spatiotemporal resolutions. At even higher resolutions, link-derived rainfall estimates are more accurate than those from satellite. This is a clear incentive for such networks to play a more important role in rainfall estimation worldwide.

3.5. Conclusions and Recommendations

Chapter 4

Errors in Dutch Rainfall Maps from CML

Accurate measurements of rainfall are important in many hydrological and meteorological applications, for instance, flash-flood early-warning systems, irrigation, weather forecasting, and climate modelling. Whenever possible, commercial microwave link (CML) networks measure and store the received power of the electromagnetic signal at regular intervals. The decrease in power can be converted to rainfall intensity, and is largely due to the attenuation by raindrops along the link paths. Such an alternative technique fulfils the continuous effort to obtain measurements of rainfall in time and space at higher resolutions, especially in places where traditional rain gauge networks are scarce or poorly maintained.

The uncertainties present in rainfall maps from CML networks are not yet fully comprehended. Here we identify and quantify the sources of uncertainty present in interpolated rainfall maps from link rainfall depths. To disentangle such sources of uncertainty, we classified them into two categories: 1) those associated with the individual link measurements, i.e. the errors involved in link rainfall retrievals, such as wet antenna attenuation, sampling interval of measurements, wet/dry period classification, dry weather baseline attenuation, quantization of the received power, drop size distribution (DSD), and multipath propagation; and 2) those associated with mapping, i.e. the combined effect of the interpolation methodology and the spatial density of link measurements.

We computed $\sim 3,500$ rainfall maps from real and simulated link rainfall depths for 12 days for the land surface of the Netherlands. Simulated link rainfall depths refer to path-averaged rainfall depths obtained from radar data. Real and simulated rainfall maps were compared against quality-controlled gauge-adjusted radar rainfall fields (assumed to be the ground truth). Thus, we were able to not only identify and quantify the sources of uncertainty in such rainfall maps, but also test the actual and optimal performance of one CML network from one of the cellular providers in the Netherlands. Errors in ML measurements were found to be the source that contributes most to the overall uncertainty.

This chapter was originally published as:

Rios Gaona, M. F., Overeem, A., Leijnse, H., and Uijlenhoet, R.: Measurement and interpolation uncertainties in rainfall maps from cellular communication networks, *Hydrol. Earth Syst. Sci.*, 19, 3571–3584, doi:10.5194/hess-19-3571-2015, 2015.

4.1 Introduction

Accurate rainfall estimates are crucial inputs for hydrological models, especially those employed for forecasting flash floods, due to the short timescales in which they develop. Rainfall rates can be retrieved from (commercial) microwave links (CML) because rain droplets attenuate the electromagnetic signal between transmitter and receiver along the link path. The principles behind rainfall estimates from microwave attenuation were investigated by *Atlas and Ulbrich* (1977). They established the nearly linear relationship between the rainfall intensity and the specific attenuation of the signal for frequencies between 10 and 35 GHz.

Messer et al. (2006) and *Leijnse et al.* (2007b) used CML to estimate rainfall rates. Note that networks of such links have not been designed for that purpose. In the last decade several studies have developed methods to improve rainfall estimates from CML measurements (*Leijnse et al.*, 2008, 2010; *Overeem et al.*, 2011; *Schleiss et al.*, 2013; *Chwala et al.*, 2014). In addition, *Goldshtein et al.* (2009) and *Zinevich et al.* (2008, 2009, 2010) proposed methods to estimate rainfall fields via CML networks. *Giuli et al.* (1991) had previously reconstructed rainfall fields from simulated microwave attenuation measurements. *Overeem et al.* (2011) developed an algorithm to estimate rainfall from minimum and maximum received signal levels over 15-min intervals, in which the wet antenna effect is corrected for, and where wet and dry spells are identified from the removal of signal losses not related to rainfall by using nearby links.

Rainfall fields can generally be retrieved from CML networks at a higher resolution than rain gauge networks. This holds not only for the spatial resolution (usually CML outnumber rain gauges) but also for the temporal resolution (link measurements can be obtained for 1 s, 1 min, 15 min, or daily intervals at either instantaneous or minimum and maximum samples of received signal level (RSL) measurements; *Messer et al.*, 2012). The massive deployment of CML provides a complementary network to measure rainfall, especially in countries where rain gauges are scarce or poorly maintained, and where ground-based weather radars are not (yet) deployed (*Doumounia et al.*, 2014).

Overeem et al. (2013) obtained 15-min and daily rainfall depths from one CML network for 12 days for the land surface of the Netherlands ($\sim 35,000 \text{ km}^2$; $\sim 1,750$ links). They interpolated these rainfall depths to obtain rainfall fields to be compared against gauge-adjusted radar rainfall maps. Although the associated biases were small, the corresponding uncertainties were not. The coefficient of determination, i.e. the square of the correlation coefficient, between link-based and gauge-adjusted radar rainfall maps was 0.49 for the 15-min timescale, and 0.73 for the daily timescale. They did not explore the sources of error that impeded these correlations to reach higher values, though. Here, we address this issue with the aim to unravel and understand the sources of error (and their uncertainties) present in the methodology proposed by *Overeem et al.* (2013) to estimate rainfall fields. We split the overall uncertainty in rainfall maps from CML networks into two main sources of error: 1) those associated with the individual link measurements, such as wet antenna attenuation, sampling interval of measurements, wet/dry period

classification, dry weather baseline attenuation, drop size distribution (DSD), and multipath propagation; and 2) those associated with mapping, that is, the combined effect of the interpolation methodology and the spatial density of link measurements. Note that not all the links in the network continuously report data. Only the overall effects of measurement and interpolation errors are addressed here, not all measurement errors separately.

This chapter is organized as follows: Section 4.2 describes the data sets and methodology developed by *Overeem et al.* (2013) to estimate rainfall maps, jointly with the methodologies for this work to derive rainfall maps to identify and quantify error sources. Section 4.3 compares the results obtained here with those presented in *Overeem et al.* (2013). Section 4.4 highlights our major findings. Finally, Sections 4.5 and 4.6 provide a summary, conclusions, and recommendations.

4.2 Materials and Methods

Data

Two categories of data were used: link data and radar data. These two data sets are fully independent given that each one originates from a different source: link measurements, and a combination of radar and rain gauge measurements, respectively. Link and radar data contain rainfall depths from the 12-day validation period studied by *Overeem et al.* (2013), which is spread across the months of June, August, and September 2011. This validation period was selected because of its large number of rainfall events. Figure 4.1 conceptually illustrates the steps we followed to quantify uncertainties in rainfall maps from link networks.

Link data

Link data refer to rainfall depths retrieved from measurements of the attenuation of electromagnetic signals from one CML network in the Netherlands. *Overeem et al.* (2011, 2013) thoroughly explained the methodology to convert measurements of the decrease in the received power to rainfall depths, with reference to a level representative of dry weather. Briefly explained, their methodology is based on four steps: 1) a link is considered to be affected by rainfall if the received power jointly decreases with that of nearby links; 2) a reference signal level representative of dry weather, i.e. the median signal level of all dry periods in the previous 24 h, is determined, and the signal is subtracted from this reference level; the result is the attenuation estimate; 3) links for which accumulated (over 1 day) specific attenuation deviates too much (from that of nearby links) are excluded from the analysis; and 4) 15-min average rainfall intensities are computed from a weighted average of minimum and maximum rainfall intensities obtained by a power-law correlation of specific attenuation (*Atlas and Ulbrich, 1977*). These rainfall intensities are expressed as path-averaged rainfall depths, and are assumed to be representative of the rainfall across the link path. Full details of the algorithm can be found in *Overeem et al.* (2011, 2013).

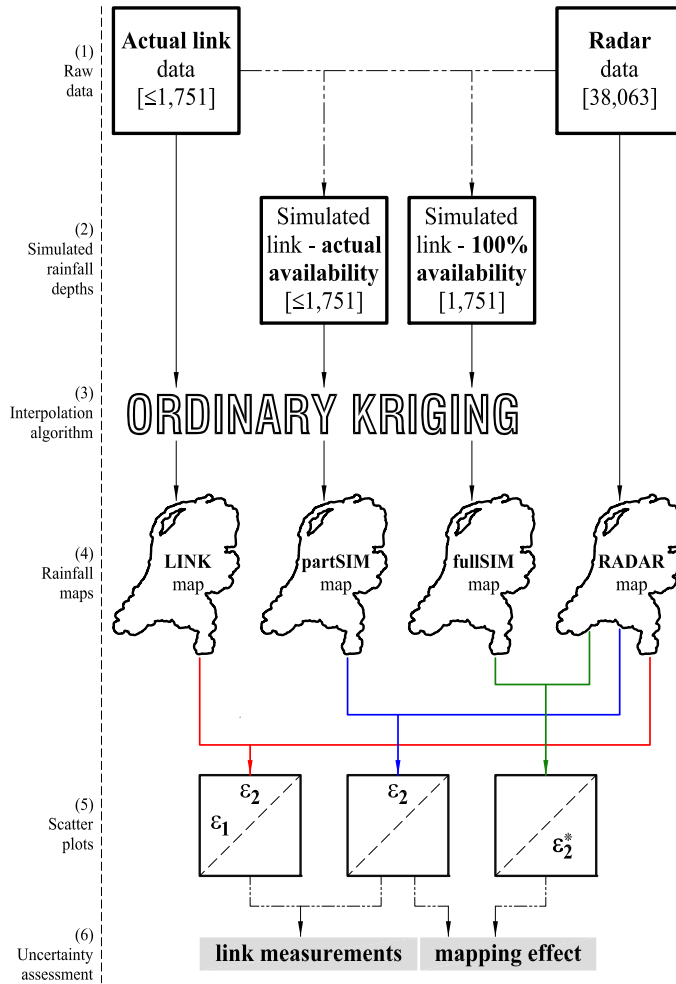


Figure 4.1: Flowchart to visualize the hierarchical process to identify and quantify uncertainties in rainfall maps from link networks. From top to bottom: (1–2) raw data are selected and rainfall depths simulated; (3–4) through the interpolation methodology rainfall maps are obtained; (5) from the comparison between rainfall maps scatter plots are created; and (6) from the comparison between these scatter plots (and their metrics), the error sources are quantified. ϵ_1 and ϵ_2 represent the categories in which the sources of error are classified. Specifically, ϵ_1 indicates the error from link rainfall retrievals, and ϵ_2 indicates the error related to mapping. ϵ_2^* indicates the best case for the mapping-related error (i.e. all links are available all of the time). The number between brackets (1–2) indicates the number of data for every single map or data set.

Data from up to 1, 751 link paths are available, with path lengths from 0.13 to 20.26 km, and frequencies from 12.8 to 39.4 GHz (Fig. 4.2). It is also clear that the network is designed such that the link frequency decreases as path length increases, mainly because low-frequency links suffer less from rain attenuation.

Figure 4.3 presents the spatial distribution of one commercial link network from one of the providers in the Netherlands, as well as the temporal availability for each link path. Due to data storage problems, wet/dry classification, and outlier removal, it is not feasible to have link data for all the possible link paths in the network (1, 751) for every time step. The temporal availability per link varies from 0.9 to 99.9%, with a global average over the entire 12-day data set of 83.5%.

The spatial distribution of the network has two characteristics: 1) there is a strong contrast between urban and rural areas with regard to the spatial distribution of the network; and 2) there are gaps in the network, because of a complete absence of link data or low data availability. Analyses of the link-path orientations show no preferred orientations, i.e. a uniform distribution (such analyses are not presented in this chapter).

Radar data

Radar data are taken from the climatological rainfall data set¹ of two C-band Doppler weather radars operated by the Royal Netherlands Meteorological Institute (KNMI) (*Overeem et al.*, 2009a,b, 2011). The composite image of rainfall depths has a temporal resolution of 5 min, and a spatial resolution (pixel size) of 0.92 km² (rounded to 1 km² in figures, tables, and subsequent analyses), for the entire land surface of the Netherlands (38, 063 pixels). This composite image is adjusted with rainfall depths from one automatic and one manual rain gauge network (32 and 325 gauges, respectively) also operated by KNMI. The spatial and temporal resolution, and its accuracy, make this data set a reliable source of rainfall data. We used the same radar data set as that used in *Overeem et al.* (2013).

Simulated Link Rainfall Depths

Simulated link rainfall depths are averages of radar data based on the topology and time-availability features of the link network. The purpose of simulated link rainfall depths is twofold: 1) to evaluate the performance of the link network assuming that all links provide perfect measurements of path-averaged rainfall at the 15-min interval, and 2) to evaluate the performance of the link network if all links would be available all the time.

Because link data were obtained in intervals of 15 min, sets of three consecutive 5-min radar composite images were summed up on a pixel-by-pixel basis. The simulation allows us to separate mapping errors from other errors. For detailed studies on the effects of link

¹KNMI climatological rainfall data sets are freely available at the IS-ENES climate4impact portal: <http://climate4impact.eu/impactportal/data/catalogbrowser.jsp?catalog=http://opendap.knmi.nl/knmi/thredds/.//radarprecipclim.xml>.

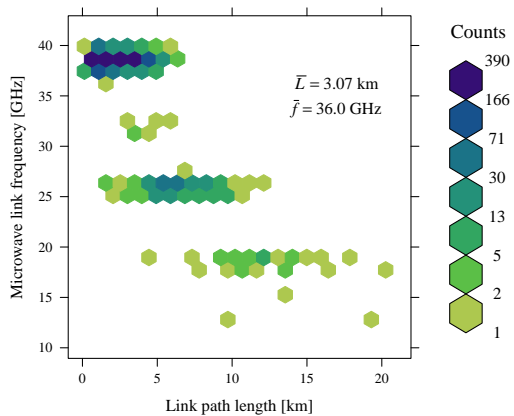


Figure 4.2: Scatter density plot of link frequencies vs. link-path lengths for the 12-day validation period. The colour scale is logarithmic.

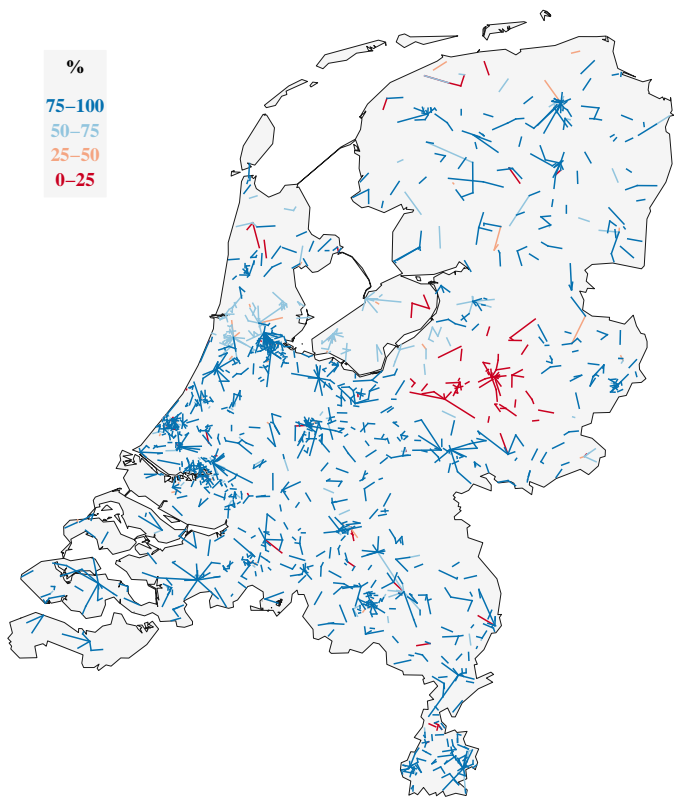


Figure 4.3: Topology of the T-Mobile NL CML network used for this study. The colour scale of the CML network represents the temporal availability of the link data for the 12-day validation period. The average availability is 83.5%.

length and frequency, temporal sampling, power resolution, and wet antenna attenuation in link measurements see *Leijnse et al.* (2008, 2010). After the addition of 5-min radar composite images, the link network topology was overlaid on the 15-min radar composite image, and all pixels under every link path were selected. Then, for every link path and its associated pixels, rainfall depths were averaged. This was a weighted average in which the weight was taken as the fraction of the total link path that overlaps one radar pixel. For instance, if a 1-km link path was located 0.6 km over one pixel and 0.4 km over a contiguous pixel, the average rainfall depth was the sum of 60% of the first pixel's rainfall depth plus 40% of the second pixel's rainfall depth.

Not all link data are available for all the possible link paths in the network (1, 751) at every time step. In addition to the performance of the actual topology of the network, the complete availability of radar data allowed us to simulate the optimal performance of the link network, i.e. the performance that could theoretically be achieved if all links (1, 751) would be available all the time.

Rainfall Maps

The rainfall depths from actual link measurements and both types of simulations (actual and 100% network availability) were spatially interpolated to obtain 15-min rainfall maps with a spatial resolution of 1 km². In all rainfall maps the land surface of the Netherlands was represented by 38,063 pixels. For any given time step, interpolated rainfall maps were compared on a pixel-by-pixel basis against the radar rainfall fields. Hence, 15-min rainfall maps were obtained for the 12-day validation period, i.e. 1,152 rainfall maps in total for each of the four sets of rainfall maps considered (namely, radar, actual links, simulated links with partial availability, and simulated links with 100% availability). In subsequent figures and tables, these four data sets will be identified as RADAR, LINK, partSIM, and fullSIM, respectively (see Fig. 4.1); 15-min rainfall maps were accumulated to daily rainfall maps, i.e. 12 daily rainfall maps per data set.

Ordinary kriging (OK) was employed to generate rainfall maps, because it is the simplest and most straightforward method that accounts for the local variability of the stochastic process, rainfall in this case (*Cressie*, 1990; *Haining et al.*, 2010). Kriging is ideally suited for interpolation of highly irregularly spaced data points. Nevertheless, this method comes with its own limitations, and a number of assumptions should be made for the method to be valid, e.g. isotropy and statistical stationarity. These assumptions are further explained in section 4.6. The path-averaged link rainfall estimates are assigned to the point at the centre of the link, so that these point data can be used in the OK interpolation. This conversion from line-scale to point-scale data is part of our mapping method, and hence errors resulting from this conversion are part of the mapping uncertainty.

Any kriging method heavily relies on the function that describes the spatial covariance, i.e. the semi-variogram. The semi-variogram is a continuous function that describes how the spatial dependence of a random variable changes with distance and direction (*Isaaks and Srivastava*, 1989, ch.7). Like *Overeem et al.* (2013), we chose the semi-variogram appro-

ach of *Van de Beek et al.* (2011) because it is a simple isotropic spherical model developed for the Netherlands on the basis of a 30-year climatological rainfall data set. *Van de Beek et al.* (2011) concluded that the seasonality in range and sill of the semi-variogram can be described by cosine-function models with the day-of-year as the independent variable. Note that they assumed the nugget to be zero. *Van de Beek et al.* (2012) also developed two methodologies that allowed for the spherical semi-variogram to be downscaled from daily to hourly time steps. We chose their second methodology, namely, power-law scaling of cosine-function parameters, because it was shown to perform better. This downscaling methodology was based on hourly rainfall data aggregated to 2, 3, 4, 6, 8, 12, and 24 h. Here we extended this power-law downscaling to smaller timescales, namely, 0.25 h, i.e. 15 min.

For the LINK, partSIM, and fullSIM data sets, 15-min rainfall maps were obtained as follows: first, the spherical semi-variogram parameters were computed and downscaled for the given day of the year. Hence, a single semi-variogram is applied to all 15-min time steps within that given day. The nugget was defined as 10% of the sill. Second, rainfall depths were assigned to the coordinates of the link paths' middle points. Third, rainfall depths were interpolated over the spatial grid of the radar data set. The interpolation algorithm always selects the closest 100 rainfall depths to the pixel for which the interpolation is carried out. This selection was established to speed up the interpolation process; 24-h rainfall maps were obtained from the aggregation of 15-min rainfall maps.

Error and Uncertainty Metrics

To quantify the uncertainty in rainfall maps from CML networks, we used three metrics: 1) the relative bias, 2) the coefficient of variation, and 3) the coefficient of determination.

The relative bias is a relative measure of the average error between the interpolated and radar rainfall fields (considered to be the ground truth):

$$\text{relative bias} = \frac{\bar{R}_{\text{res}}}{\bar{R}_{\text{radar}}} = \frac{\sum_{i=1}^n R_{\text{res},i}}{\sum_{i=1}^n R_{\text{radar},i}}, \quad (4.1)$$

where $R_{\text{res},i} = R_{\text{int},i} - R_{\text{radar},i}$. In Eq. (4.1), n represents all possible pixels and time steps for the 12-day validation period.

The coefficient of variation is a dimensionless measure of dispersion, which is defined as the standard deviation divided by the mean (*Haan, 1977*). In this case we took the standard deviation of the residuals divided by the mean of the reference field (i.e. the mean of the radar rainfall field):

$$CV = \frac{\sqrt{\frac{1}{n-1} \sum_{i=1}^n (R_{res,i} - \bar{R}_{res})^2}}{\bar{R}_{radar}}. \quad (4.2)$$

The coefficient of variation is a measure of uncertainty (similar to the root mean squared error). For instance, a $CV = 0$ would indicate a hypothetical case with no bias and no uncertainty, i.e. a case in which all data points would fall exactly on the 1:1 line.

The coefficient of determination is a measure of the strength of the linear dependence between two random variables, interpolated and radar rainfall depths, in this case. It is simply defined as the square of the correlation coefficient between the interpolated and radar rainfall depths:

$$r^2 = \frac{\left[\sum_{i=1}^n (R_{radar,i} - \bar{R}_{radar}) \cdot (R_{int,i} - \bar{R}_{int}) \right]^2}{\left[\sum_{i=1}^n (R_{radar,i} - \bar{R}_{radar})^2 \right] \cdot \left[\sum_{i=1}^n (R_{int,i} - \bar{R}_{int})^2 \right]}. \quad (4.3)$$

The coefficient of determination represents the fraction of the variance of the reference variable that can be explained by a linear regression. In a case of perfect linear correlation, i.e. $r^2 = 1$, all data points would fall on a straight line without any scatter. Hence, the linear regression would be able to explain 100% of the variance of the reference variable in that case. However, perfect linearity does not imply unbiased estimation because the regression line could not necessarily coincide with the 1:1 line, even if it captures all variability.

4.3 Results

From the actual and simulated link rainfall depths, rainfall maps were obtained for three cases: 1) 15-min rainfall maps from interpolation of 15-min rainfall depths; 2) 24-h rainfall maps from the sum of these 15-min rainfall maps; and 3) 15-min rainfall maps from interpolation of 15-min rainfall depths, in which each pixel (interpolated rainfall depth) was averaged with the surrounding pixels within a 9×9 pixel square. The reason for this posterior average of the rainfall depths was to limit representativeness errors in time (*Overeem et al.*, 2013). Incidentally, this area ($\sim 81 \text{ km}^2$) roughly corresponds to the spatial extent of typical water management units in the Netherlands.

Appendix B.1 presents five examples of 24-h and 15-min rainfall maps. *Overeem et al.* (2013, Supplement) showed daily comparisons between actual link rainfall maps and radar rainfall fields for the 12-day validation period. Here, we present 5 of those 12 cases for reference. These comparisons are extended to both types of simulated link rainfall maps (actual and 100% network availability) (Fig. B.1). Five comparisons of 15-min rainfall maps are also presented (Fig. B.2). These examples provide information on the improvement

in rainfall fields when the sources of error studied here are removed.

For any given time step, interpolated rainfall maps were compared on a pixel-by-pixel basis against radar rainfall fields. This pixel-by-pixel comparison was done via scatter density plots of interpolated against radar rainfall depths (ground truth). Figure 4.4 presents an array of scatter plots, for the three cases of spatiotemporal aggregation, for the actual and both types of simulated link rainfall depths (actual and 100% network availability). Each of the scatter plots in Fig. 4.4 corresponds to all 15-min (or 24-h) rainfall maps within the 12-day validation period. These plots show paired rainfall depths of interpolated and radar rainfall maps, for any pair in which the radar rainfall depth is larger than 0.1 mm.

The scatter density plot of Fig. 4.5 corresponds to the actual and simulated link rainfall depths (actual availability) at the locations of the links, i.e. before any interpolation was applied. Only those pairs for which at least one rainfall depth exceeded 0.1 mm were plotted.

Table 4.1 summarizes the values of the relative bias, the coefficient of variation (of the residuals), and the coefficient of determination (i.e. the squared correlation coefficient) for the three cases of spatiotemporal aggregation, for the actual and both types of simulated link rainfall depths.

4.4 Discussion

From left to right and from top to bottom, the general picture that arises from Fig. 4.4 and Table 4.1 is: 1) a reduced systematic error (relative bias); 2) a smaller random error (CV); and 3) a stronger linear dependence (r^2). This suggests a general improvement of the interpolated link rainfall depths with respect to the radar rainfall depths, as more sources of error are removed from the analysis.

Figure 4.4a, d, and g show the relation between the actual link and radar rainfall depths, for the three cases of spatiotemporal aggregation. The scatter in these plots can be attributed to all possible sources of error in rainfall maps from link measurements, i.e. those associated with the link measurements themselves and those associated with the interpolation of individual measurements (mapping).

The dark blue shading close to the 1:1 line for small rainfall depths in all panels of Fig. 4.4 indicates a good agreement between rainfall estimates from links and radar (note that the colour scale is logarithmic). Conversely, for larger rainfall depths the scatter seems to relatively increase for the actual link measurements (panels a, d, g), while it decreases for the simulated link measurements (all other panels). Such deviations must be the result of errors in individual link measurements as well as the combination of limited spatial coverage of the link network (Fig. 4.3) with the strong variability of rainfall in space. The relative contribution of the measurement errors to the total error hence increases with rainfall amounts.

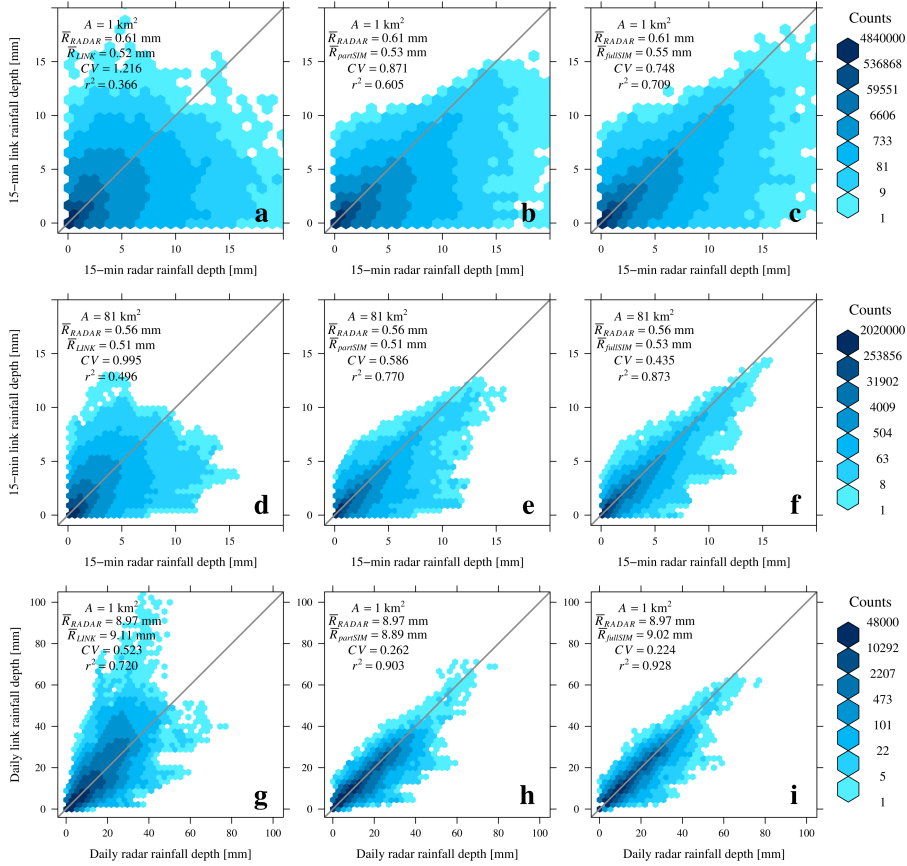


Figure 4.4: Scatter density plots of interpolated link rainfall depths vs. radar rainfall depths for 15 min and 24 h. Top row (a, b, c): 15-min rainfall depths; middle row (d, e, f): 15-min rainfall depths averaged with the surrounding pixels within a 9×9 pixel square; bottom row (g, h, i): daily sum of 15-min rainfall depths. Left column (a, d, g): actual link rainfall maps vs. radar rainfall fields; centre column (b, e, h): simulated link rainfall maps (actual availability) vs. radar rainfall fields; right column (c, f, i): simulated link rainfall maps (100% availability) vs. radar rainfall maps. (d) and (g) are comparable to Overeem et al. (2013). The colour scale is logarithmic.

From Fig. 4.4 and Table 4.1, it is clear as well that the relative bias is most sensitive to the spatial and temporal aggregation level. If all paired rainfall accumulations would have been used (and not only those in which at least the radar rainfall depth exceeds 0.1 mm) one would expect the relative bias to be exactly the same for all aggregation levels, because both aggregation and computation of the bias are linear operators [Eq. (4.1)].

There is a limited improvement in terms of the coefficients of variation and determination, when the scatter plots in the second column of Fig. 4.4 are compared to those in the third column, as well as their respective statistics in Table 4.1. This means that the main reduction of uncertainty is achieved when the actual link measurements are replaced with the simulated link measurements, rather than to increase the actual link network availability to 100% for all links. This implies that a significant fraction of the overall uncertainty must be due to errors and uncertainties in the link measurements themselves, rather than due to errors and uncertainties associated with mapping, at which rainfall maps are reconstructed.

Figure 4.4c, f, and i and the last column of Table 4.1 indicate the best possible performance that can be achieved with the employed link network (if all links would yield perfect measurements of path-averaged rainfall all the time). The remaining scatter can be attributed to the interpolation methodology (including the assignment of path-averaged rainfall intensities to the link's centre point), the spatial variability of rainfall, and the effect of other factors such as the variable and limited density of the link network (more links in urban than in rural areas).

Table 4.1: Relative bias, and coefficients of variation and determination for the three cases of spatiotemporal aggregation (15 min [1 km²], 15 min [81 km²], 24 h [1 km²]), for the three sets of link measurements, i.e. the actual and both types of simulated link rainfall depths (actual and 100% network availability).

	LINK	partSIM	fullSIM
Relative bias (%)			
15 min [1 km ²]	-14.3	-13.0	-9.3
15 min [81 km ²]	-9.1	-9.1	-5.6
24 h [1 km ²]	+1.6	-0.8	+0.7
CV			
15 min [1 km ²]	1.216	0.871	0.748
15 min [81 km ²]	0.995	0.586	0.435
24 h [1 km ²]	0.523	0.262	0.224
<i>r</i> ²			
15 min [1 km ²]	0.366	0.605	0.709
15 min [81 km ²]	0.496	0.770	0.873
24 h [1 km ²]	0.720	0.903	0.928

When 15-min rainfall depths at the 1-km² spatial scale (Fig. 4.4a—c) are summed to daily rainfall depths (Fig. 4.4g—i), the discrepancies in rainfall estimates at 15 min tend to can-

cel each other. This explains the sharp decrease in the coefficient of variation, and the sharp increase in the coefficient of determination between 15-min and 24-h rainfall accumulations, which implies a certain degree of independence among the errors in the 15-min accumulations.

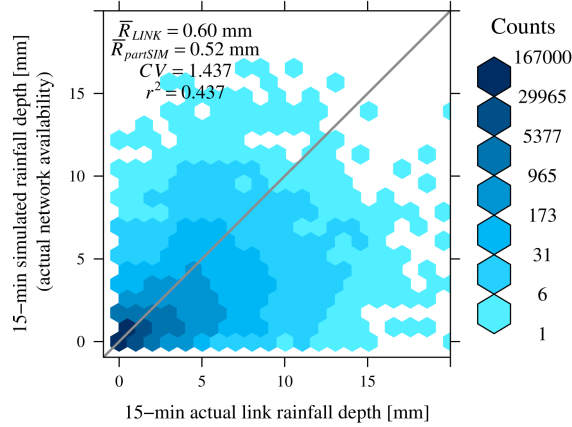


Figure 4.5: Scatter density plot of simulated link rainfall depths (actual availability) vs. actual link rainfall depths for all 15-min time steps in the 12-day validation period. Both simulated and actual link rainfall depths are path-averaged rainfall depths. The colour scale is logarithmic.

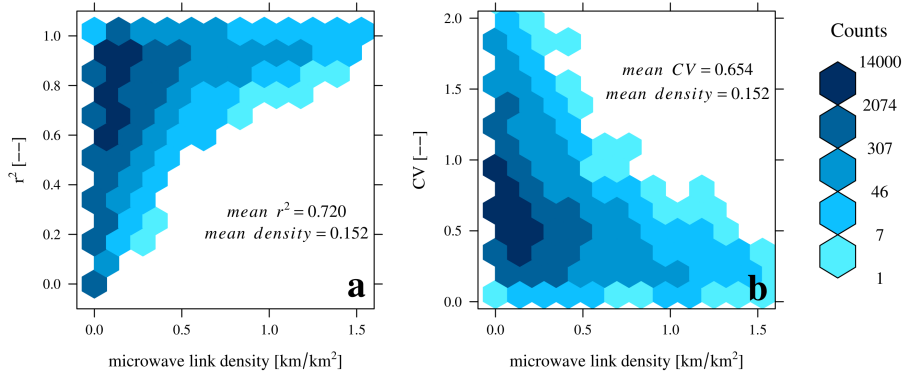


Figure 4.6: Scatter density plots of coefficient of determination (r^2) and coefficient of variation (CV) vs. link density (averaged over 155 km²), for the fullSIM case at 15 min and 1 km² spatial scale. The colour scale is logarithmic.

Figure 4.5 compares simulated against actual link rainfall depths, before any interpolation was applied. This indicates the performance of the 1,751 individual links in terms of rainfall retrieval, regardless of the errors and uncertainties introduced by interpolation

(mapping). Note that the coefficient of variation is larger than that of the 1 km², 15-min rainfall accumulations presented in panel a of Fig. 4.4; and that the coefficient of determination is between those coefficients presented in panels a and d of Fig. 4.4. If we would assume that rainfall retrieval and mapping errors are independent, we would expect the CV in Fig. 4.4 to be greater than that in Fig. 4.5. This means that there is a clear interplay between these two types of errors, and that the assumption of independence does not hold. This may be explained by the fact that we use kriging with a variogram that includes a nugget. In areas with a dense link network, the weight of each individual link is relatively small in the computation of the interpolated rainfall field. This reduces the effect of large errors in a given link. In areas with lower link densities the nugget of the employed variogram has a similar reducing effect on large errors.

From Fig. 4.6 it can be seen that a higher density in the link network guarantees good correlation between the estimated values of rainfall and the ground truth, and a low coefficient of variation of the residuals. From the left panel (Fig. 4.6a), it can be concluded that lower link densities also contribute (and in large proportion) to higher correlation coefficients. This means that without considering errors in link measurements, these latter being the largest source of uncertainty in country-wide rainfall fields, the network density and the mapping methodology considered here are, respectively, high and good enough to retrieve accurate rainfall fields at such country-wide scales (at least in the Netherlands).

4.5 Summary and Conclusions

Our goal was to quantify the errors and uncertainties in rainfall maps CML link networks. In general, these errors can be attributed to different sources like wet antenna attenuation, sampling interval of measurements, wet/dry period classification, dry weather baseline attenuation, drop size distribution (DSD), multi-path propagation, interpolation algorithm and methodology, the availability of link measurements, and the variability of rainfall itself across time and space. For the purpose of this chapter we classified all possible sources of error into two categories: 1) those associated with the link measurements themselves (retrieval algorithm included), and 2) those associated with mapping. Only the overall effects of physical and interpolation errors were addressed here, not all physical errors separately.

To quantify the errors and uncertainties that can be attributed to these two categories, rainfall maps created from three sets of link rainfall depths were compared: actual link measurements, simulated link measurements with the actual network availability, and simulated link measurements with 100% network availability assumed. Simulated link rainfall depths are not affected by errors and uncertainties attributed to actual link measurements; therefore, we could estimate uncertainties attributed to mapping. Based on a pixel-by-pixel comparison, interpolated rainfall maps of the Netherlands were compared against radar rainfall fields (considered to be the ground truth). These comparisons were carried out on the basis of scatter density plots and three metrics: relative bias, coefficient of variation (CV), and coefficient of determination (r^2).

We found that measurement errors themselves are the source of error that contributes most to the overall uncertainty in rainfall maps from CML networks.

In a standard operational framework, data from CML networks may not be continuously available for the entire network. Such data gaps affect the accuracy of the retrieved rainfall intensities. Because we were able to simulate rainfall depths on the basis of radar composites, we could investigate the hypothetical case in which data from a commercial link network would be available for all time steps, and for all possible link paths in the network. This best-case scenario could explain an additional 10% of the variance explained by error-free link measurements with actual network availability for the 15-min accumulation (3% for the 24-h accumulation). Note that these percentages are particular for the region and period considered in this study. Nevertheless, even the best-case scenario showed a remaining and significant amount of uncertainty that could not be removed in rainfall maps. This means that the space-time variability of rainfall is such that it would require an even more dense and robust network of links to generate more accurate rainfall maps at country-wide scales. The uncertainties in link rainfall retrievals found in this chapter are partly explained by the combined effects of rainfall space variability along the link, non-linearity of the retrieval relation, imperfect temporal sampling strategy, quantization of the received power (data stored in integer number of dBs), and wet antenna attenuation (and correction) investigated by *Leijnse et al.* (2008, in particular Fig. 13, upper right panel on p.1487). They reported a CV of ~ 1.0 , which explains a significant part of the CV (1.44) given in Fig. 4.5. Daily rainfall maps from CML showed less uncertainty compared to 15-min rainfall maps, because errors present in 15-min rainfall maps tend to cancel each other when 15-min rainfall maps are aggregated.

4.6 Constraints and Recommendations

The kriging algorithm we used was that of *Pebesma* (2014) and *Pebesma and Wesseling* (1998). The interpolated maps from simulated link rainfall depths represent the outcome of a process in which a linear feature (link path) obtained from the average of volume samples (radar data) is assigned to a point (link-path middle point). Each of these features (area, line, volume, point) represents what in geostatistics is referred to as support, i.e. the spatial resolution at which the random variable is analyzed (*Cressie and Wikle*, 2011, ch.4). The arbitrary change from line to point support introduces a source of error that is implicitly included in the errors related to mapping.

Apart from its simplicity and the 30-year rainfall data set on which it is based, we also chose the isotropic spherical semi-variogram of *Van de Beek et al.* (2011), because a consistent semi-variogram model estimated from link data was not feasible for 15-min rainfall intensities. Isotropic semi-variograms assume equal spatial dependence in all possible directions. Rainfall is generally a phenomenon that exhibits anisotropy in time and space (*Lepioufle et al.*, 2012; *Velasco-Forero et al.*, 2009; *Guillot and Lebel*, 1999; *Amani and Lebel*, 1997). Nevertheless, it is reasonable to assume isotropy for the Netherlands given its relative small area and flat topography. OK assumes the mean to be constant and

unknown within the region of interpolation. When this unknown mean presents substantial changes over short distances, the assumption of statistical stationarity is no longer valid. Universal kriging, kriging with external drift, and regression kriging are more sophisticated interpolation techniques that incorporate trends to account for non-stationarity (e.g. *Schuurmans et al.*, 2007). The performance of these geostatistical techniques to retrieve link rainfall maps was beyond the scope of this research.

If a similar study were to be carried out in a country with different conditions than those present in the Netherlands, three issues should be considered: 1) the spatial and operational configuration of the link network, 2) the climatology of the region where the link network operates, and 3) the spatial scale at which the analysis is carried out.

The first issue, the spatial and operational configuration of the link network, refers to the distribution of link frequencies, lengths, and densities of link networks around the world. For instance, the CML network used in this study has an average link-path length of 3.1 km, a mean frequency of 36.0 GHz, and a global average availability of 83.5% across the Netherlands (Figs. 4.2 and 4.3). Other regions may have more extensive urban and/or rural areas. In particular, for rural areas one expects to find longer link paths, and therefore lower microwave frequencies. Another issue related to the lower frequencies, e.g. 7 GHz, is the low sensitivity to rainfall and the non-linearity of the $R-k$ relationship, mostly in tropical regions (*Doumounia et al.*, 2014). This non-linearity will lead to biases in rainfall intensities in cases of large rainfall variability along the link path (positive biases at lower frequencies where the exponent of the $R-k$ power law is smaller than 1; see *Leijnse et al.*, 2010). Thus, the performance of the rainfall retrieval algorithm for such link networks will differ from the performance found in this study. For instance, in places where link paths are longer (tens of kilometres) the error due to spatial variability of rainfall along the link path becomes more important (*Berne and Uijlenhoet*, 2007; *Leijnse et al.*, 2008, 2010). Moreover, less dense networks with long link paths will provide less detailed information about rainfall.

The second issue, the climatology of the region refers to the local pattern of rainfall that characterizes different regions around the world. The rainfall characteristics of the Netherlands are different from the ones encountered in, e.g., (sub-)tropical regions. For instance, the spherical semi-variogram model applied here was derived from climatological rain gauge data for the Netherlands. Furthermore, rainfall characteristics such as rain-drop size distributions or the distribution of rainfall intensities will affect the optimal values of the parameters of the retrieval algorithm. Therefore, for regions with different rainfall climatologies than the Netherlands, variations should be considered not only in the interpolation methodology but also in the algorithms and their parameters to retrieve rainfall intensities.

The third issue refers to the spatial scale at which rainfall maps are reconstructed. The analyses presented here focussed on 15-min (and 24-h) maps at 1 and 81 km², and the differences in error characteristics are significant. For larger regions, for instance, the uncertainty attributed to mapping could play a major role in the overall error distribution.

Still, the scale at which rainfall can effectively be retrieved depends greatly on the density of the underlying link network. This means that in regions with a much lower link density than in the Netherlands, the effective spatial resolution for which rainfall maps can be derived will be lower.

Chapter 5

CML Rainfall in São Paulo, Brazil

In the last decade there has been a growing interest from the hydrometeorological community regarding rainfall estimation from commercial microwave link (CML) networks. Path-averaged rainfall intensities can be retrieved from the signal attenuation between cell phone towers. Although this technique is still in development, it offers great opportunities for the retrieval of rainfall rates at high spatiotemporal resolutions very close to the Earth's surface. Rainfall measurements at high spatiotemporal resolutions are highly valued in urban hydrology, for instance, given the large impact that flash floods exert on society. Flash floods are triggered by intense rainfall events that develop over short time scales.

Here, we present one of the first evaluations of this measurement technique for a subtropical climate. Rainfall estimation for subtropical climates is highly relevant, since many countries with few surface rainfall observations are located in such areas. The test bed of the current study is the Brazilian city of São Paulo. The open-source algorithm RAINLINK was applied to retrieve rainfall intensities from (power) attenuation measurements. The performance of RAINLINK estimates was evaluated for 5 of the 250 CML in the São Paulo metropolitan area for which we received data, for 81 days between October 2014 and January 2015. The evaluation was done by comparing the retrieved rainfall intensities and accumulations from CML to those from a dense automatic gauge network. Results were found to be promising and encouraging, especially for short links, for which high correlations (> 0.9) and low biases ($\sim 30\%$ and lower) were obtained.

5.1 Introduction

Rainfall is the key input in environmental applications such as hydrological modeling, flash-flood and crop growth forecasting, landslide triggering, quantification of fresh water availability, and waterborne disease propagation. Because it is a natural process with a high spatiotemporal variability (*Hou et al.*, 2008; *Sene*, 2013a), its accurate estimation is a demanding task.

The most common technologies that are currently used to measure rainfall at larger scales are rain gauges, radars and satellites. Each technology presents advantages and drawbacks with regard to the accuracy of rainfall estimates and the spatiotemporal coverage. Rain gauges directly measure the quantity of precipitation that falls on the ground. They offer accurate estimates of rainfall collected at temporal scales from minutes to days. Nevertheless, their rainfall estimates are only representative of their direct vicinity. In addition, in most cases the gauges within a network are unevenly distributed in space. Radar (RADio Detection And Ranging) offers indirect estimates of rainfall, with horizontal resolutions of ~ 1 km (even less depending on the frequency at which the radar operates) every ~ 2 to ~ 5 min. They reach distances of ~ 100 – 300 km, which represents an area of $\sim 125,000$ km², if issues of beam blockage are not present. The accuracy of rainfall estimates from radar depends on how well the measurements of backscattered power from hydrometeors are transformed into rain rates. Satellites offer also indirect estimates of rainfall at several spatiotemporal resolutions. For instance, Geostationary Earth Orbit (GEO) satellites (orbiting the Earth at $\sim 36,000$ km) provide observations at resolutions of ~ 10 – 60 min, and 1 – 4 km (*Sene*, 2013b; *Wang*, 2013), whereas Low Earth Orbit (LEO) satellites (orbiting the Earth at ~ 800 km) can provide observations at resolutions of ~ 1 km or less. Gridded rainfall products from the Global Precipitation Measurement mission (GPM) offer precipitation estimates between 60°N – 60°S at a spatial resolution of $0.1^\circ \times 0.1^\circ$ every 30 min. The main advantage of satellites above radar and gauges is that they provide global and continuous rainfall estimates (oceans included).

Commercial microwave links (CML) are a technology that in the past decade has gained momentum as an alternative means of rainfall estimation. CML rainfall estimates are more representative of rainfall at the ground surface than those offered by satellites or weather radars. Networks of CML are more dense than gauge networks given their worldwide deployment for telecommunication purposes (*Overeem et al.*, 2016a). This worldwide spread of CML has the potential to offer rainfall estimates in places where rain gauges are scarce or poorly maintained, or where ground-based weather radars are not yet deployed or cannot be afforded. The spatiotemporal resolution of rainfall estimates from CML can vary from seconds to minutes, and from hundreds of meters to tens of kilometers. For instance, *Messer et al.* (2012) and *Overeem et al.* (2016a) employ maximum and minimum Received Signal Level (RSL) measurements over 15-min intervals, for CML with (spatial) densities of 0.3 to 3 links per km², and 0.1 to 2.4 km per km² (~ 1 link per 10 km²), respectively. *Messer et al.* (2012) also retrieve rainfall fields from 1-min instantaneous RSL measurements, whereas *Doumounia et al.* (2014) sample RSL at 1 sec for a 29-km link.

The interaction between attenuation and rainfall has long been studied by the electronic community (from the attenuation perspective), and during the last two and a half decades by the hydrological community (from the rainfall perspective). *Hogg* (1968) and *Crane* (1971) review the influence of atmospheric phenomena on mm- and cm-wavelength based satellite communication systems. Later, *Hogg and Chu* (1975) and *Crane* (1977) focus exclusively on the role of rainfall in satellite communication, as rainfall is the major source of propagation issues for frequencies above 4–10 GHz. Recently, *Badron et al.* (2011) and *Chakravarty and Maitra* (2010) have studied rain-induced attenuation in satellite communication at tropical locations, where the attenuation is severe. Even more recently, *Bartès and Mallet* (2013) and *Mercier et al.* (2015) have retrieved high resolution rainfall fields (0.5×0.5 km every 10 sec) from 10.7- and 12.7-GHz Earth-space links used in satellite TV transmission, although at Ku band the estimation of weak rainfall rates is not optimal.

Our main interest here is rainfall estimation from terrestrial links. The idea of rain rate retrieval from attenuation measurements via tomographic techniques was presented by *Giuli et al.* (1991). *Cuccoli et al.* (2013) and *D'Amico et al.* (2016) present reconstructed 2D-rainfall fields from operational ML networks via tomographic techniques. *Rufet et al.* (1996) use a 35-GHz dual-polarization link for rainfall estimation at 0.1–1 km horizontal resolutions. *Holt et al.* (2000), *Rahimi et al.* (2004) and *Upton et al.* (2005) estimate path-averaged rainfall from the differential attenuation of dual-frequency links. *Minda and Nakamura* (2005) use a 50-GHz link of 820 m to estimate rainfall. At such frequencies (or higher) rainfall estimation is sensitive to the raindrop size distribution and raindrop temperature. The synergistic use of MLs, gauges and radars for rainfall estimation is proposed by *Grum et al.* (2005) and *Bianchi et al.* (2013). The first references to estimate rainfall rates from CML are *Messer et al.* (2006) and *Leijnse et al.* (2007b). Sources of uncertainty in rainfall estimates from MLs are studied by *Berne and Uijlenhoet* (2007), *Leijnse et al.* (2010) and *Zinevich et al.* (2010). Methods for country-wide rainfall fields from CML have been developed by *Zinevich et al.* (2008) and *Overeem et al.* (2013).

In the last decade the use of MLs has broadened its spectrum to several other environmental applications beyond rainfall estimation, for instance, melting snow (*Upton et al.*, 2007), water vapour monitoring (*David et al.*, 2009; *Chwala et al.*, 2014), wind velocity estimation (*Messer et al.*, 2012), dense-fog monitoring (*David et al.*, 2013), urban drainage modelling (*Fencl et al.*, 2013), flash flood early warning in Africa (*Hoedjes et al.*, 2014), and air pollution detection (*David and Gao*, 2016).

Here, we evaluate the performance of 5 CML located in the city of São Paulo, Brasil, in terms of their capacity to retrieve rainfall for the period between 20 October 2014 and 9 January 2015 (~ 3 months). Rainfall evaluation against gauge data was coherently possible for 5 links from a network of 117 CML. Previously, *da Silva Mello et al.* (2002) studied the attenuation along MLs due to rainfall for São Paulo. They used 6 links (7–43 km) operating at frequencies between 15 and 18 GHz. Here, instead of considering rainfall to be a nuisance for the propagation of radio signals, we invert the problem by considering the attenuation suffered by such signals to be a valuable source of rainfall information. Since

CML were not intended for rainfall estimation purposes, rainfall retrievals from these devices can be considered a form of opportunistic sensing. They are potentially cost-free as the retrieved rain rates can be regarded as a by-product of power measurements. As subtropical and tropical regions are the ones most deprived of radar (*Heistermann et al.*, 2013) and gauge networks (*Kidd et al.*, 2017; *Lorenz and Kunstmann*, 2012), CML could serve as complementary (or even alternative) networks for rainfall monitoring. Most of the recent studies concerning rainfall retrieval from CML have focused on temperate and Mediterranean climates, e.g., *Overeem et al.* (2016a); *Messer and Sendik* (2015). Thus, our evaluation is one of the first which focuses on a subtropical climate, complementing the study of *Doumounia et al.* (2014), which focused on a semi-arid climate. Focus on accurate rainfall estimation within the subtropics is of high relevance given that in such regions (e.g., São Paulo) intense events develop more often into flash floods and mud slides, which cause damage to property, disruption of business, and occasional casualties (*Pereira Filho*, 2012).

This chapter is organized as follows: Section 5.2 describes the study area, the employed datasets (CML, rain gauges, disdrometers), the retrieval algorithm, and the metrics used to evaluate the rainfall estimates from CML. The results and the related discussion of our major findings are presented alongside in section 5.3. Summary, conclusions and recommendations are provided in Section 5.4.

5.2 Study Area, Data and Methods

Description of Study Area

The city of São Paulo is located ~60 km from the Atlantic Ocean at ~770 masl, where see breeze fronts commonly push from the SE against prevailing continental NW winds (cold fronts). In general, the incoming see breeze interacts with the warmer and drier (urban) heat island of São Paulo, producing very deep convection with heavy rainfall, wind gusts, lightning and hail (*Vemado and Pereira Filho*, 2016; *Machado et al.*, 2014; *Pereira Filho*, 2012). *de Oliveira et al.* (2002) characterize the local climate as typical of subtropical regions of Brazil, with a dry winter (June-August) and a wet summer (December-March). With regard to the climatology of São Paulo¹, February is the warmest month with 22.4° C, and July the coldest with 15.8° C. Climatological averages for temperature and humidity, for November and December (the full two months of the studied period), are 20.2 and 21.1° C, and 78% and 80%, respectively. August is the driest month with 39.6 mm of precipitation, and January the wettest with 237.4 mm. The (climatological) yearly accumulated rainfall is 1441 mm. *Overeem et al.* (2016a) reported winter time issues in rainfall estimates from CML. Thus, for the subtropical climate of São Paulo, such winter issues are not expected to play a role, which is advantageous for accurate rainfall estimation.

¹The climatological data presented here covers the period from 1961 to 1990 and corresponds to the station “Mir. de Santana” located in the heart of São Paulo city (−46.6 lon, −23.5 lat, 792 masl). These data are freely available at the INMET (METeorological National Institute) web portal: <http://www.inmet.gov.br/portal/index.php?r=home2/index>.

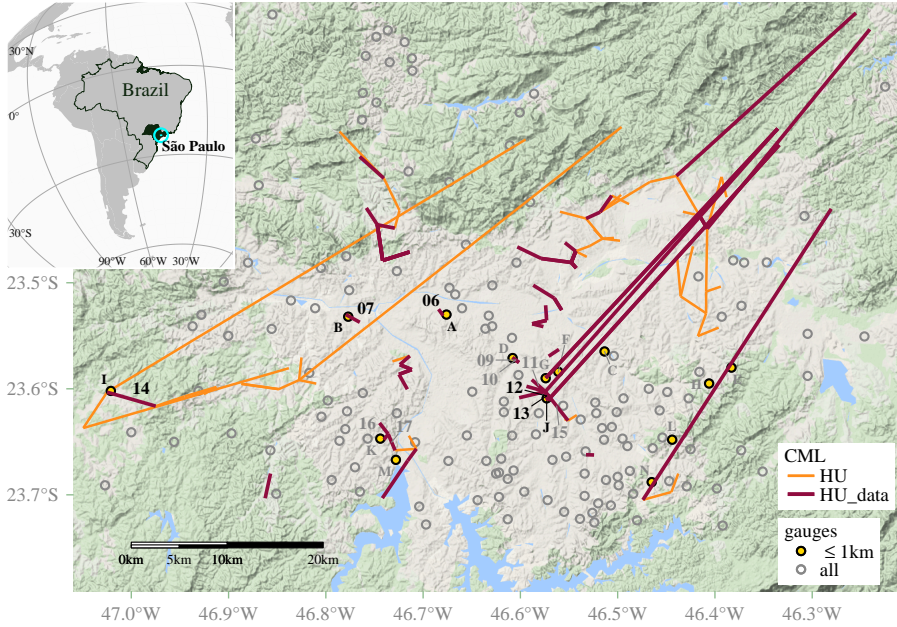


Figure 5.1: Topology of one CML network in the city of São Paulo, Brazil. 117 Huawei (HU) CML are shown (101 link paths). CML in red are the ones where unequivocal power level assignment was feasible (HU_data). CML which have both lengths above 20 km and frequencies above 15 GHz were not analyzed. Thus, only 11 CML were retained given the proximity of rain gauges to their link paths, i.e., ≤ 1 km (yellow circles). All circles represent gauges with 10-min resolution available for the studied period (20 October 2014 to 9 January 2015). The black numbers refer to the CML that showed clear rainfall signals as compared to nearby gauges, i.e. for which $r^2 \geq 0.75$ (see also Tab. 5.1). The letters refer to the corresponding gauges. CML data was provided by the Planetary Skin Institute / Italia Mobile². Gauge data was retrieved from the CEMADEN database. The geographical location of São Paulo is given in the upper left corner. The DEM was obtained from Google maps.

Data

We received power measurements from two brands of CML: Ericsson (ER) and Huawei (HU). Power levels were registered every 15 min from 0100 UTC 20 October 2014 to 0045 UTC 8 January 2015, i.e., 81 days exactly. Their quantization level was 0.1 dB. Minimum and maximum levels of received and transmitted power were available for HU CML (101 link paths, see Fig. 5.1), whereas only minimum received powers were available for ER CML (149). Because our CML-based rainfall retrieval algorithm RAINLINK (Sec. 5.2) is only able to retrieve rain rates from minimum and maximum power levels, we discarded the ER CML. Due to issues in the log-file of the attenuation measurements, it was only possible

²We received CML data from a third party. It was not possible to verify the topology of the network, shown in Fig. 5.1 on-site, which we suspect not always to be accurate given the orientation of the long links.

to correctly and unequivocally assign power levels to 66 HU CML (16 full-duplex and 34 simplex). From the 66 HU CML, we selected 17 CML given their proximity to rain gauges (≤ 1 km or less). Our experience tells us that CML with both lengths above 20 km and frequencies above 15 GHz are not common in CML networks (they are highly unlikely from a link network design perspective: long links experience more attenuation in rain, and should hence operate at low frequencies to limit this attenuation). Hence, we discarded the data specifications for 6 CML as dubious and did not consider them in our analyses, which reduced the number of CML considered to 11. Finally, from the 11 remaining CML, we only kept the 5 CML which showed clear rainfall signals as compared to nearby rain gauges, i.e. for which $r^2 \geq 0.75$. The other 6 CML showed a nearly complete absence of correlation with nearby gauges ($r^2 \sim 0.3$ for one CML-gauge pair and $r^2 < 0.1$ for the other five CML-gauge pairs). This was due to issues with the CML attenuation data and/or with malfunctioning gauges. Figure 5.2 shows the scatter plot of frequency against link length for all HU CML. For RAINLINK to work, it is necessary that the power level of the transmitted signal is essentially constant. For the remaining 5 CML evaluated here, the mean difference between 15-minute transmitted power levels is ~ 0.0 dB, with a maximum of 0.5 dB (for the 81 days considered).

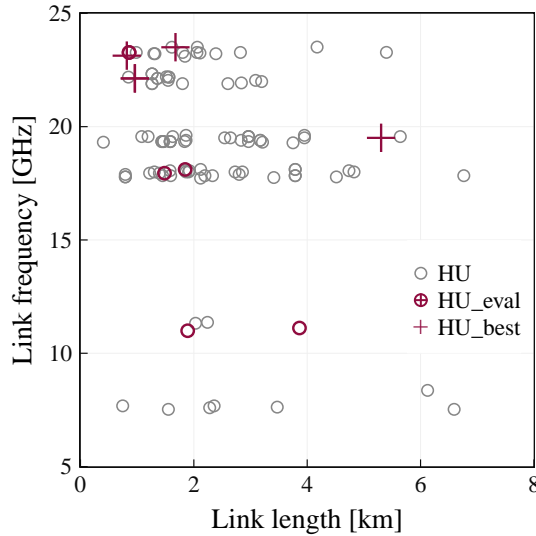


Figure 5.2: Scatter plot of link frequency against link length for all HU CML (gray circles) shown in Fig. 5.1. Red markers indicate those 11 CML for which the evaluation was possible (Tab. 5.1). The crosses represent the 5 HU CML which showed clear rainfall signals as compared to nearby gauges, i.e. for which $r^2 \geq 0.75$ (Sec. 5.3).

Rainfall depths from 152 stations were retrieved from the National Early Warning and Monitoring Centre of Natural Disasters (CEMADEN), Brasil³. These 152 stations offer 10-

³Gauge data from Brazil is freely available at <http://www.cemaden.gov.br/mapainterativo/>.

min rainfall depths for the period and region under study (Fig. 5.1). Stations located within 1-km distance from the evaluated link paths were selected. Hence, only 11 stations were used to evaluate rainfall estimates in São Paulo from CML.

Thanks to the CHUVA project (Machado *et al.*, 2014), we retrieved one-minute drop size distributions (DSD) from three Parsivel disdrometers located in the region “Vale do Paraíba”, ~93 km east of the study area⁴. DSD data were collected from 1 November 2011 to 14 March 2012.

Rainfall Retrieval Algorithm

Rainfall estimation from CML is based on power measurements from the electromagnetic signal along a link path, i.e., between transmitter and receiver. Rainfall rates can be retrieved from the decrease in power, which is largely due to the attenuation of the electromagnetic signal by raindrops along the link path. The power-law relation between attenuation and rainfall (along a link path) was established by Olsen *et al.* (1978) and Atlas and Ulbrich (1977) as:

$$A = aR^b \quad (5.1)$$

where A is the specific attenuation [$\text{dB} \cdot \text{km}^{-1}$] along the link path attributed to rainfall and R is the rainfall rate [$\text{mm} \cdot \text{h}^{-1}$]. The coefficient a and exponent b depend on the frequency and polarization of the electromagnetic signal, the DSD, and (to a much lesser extent) on the raindrop temperature. At the frequencies CML commonly operate, the exponent b in Eq. (5.1) is ~ 1.0 . Atlas and Ulbrich (1977) state that the near-linearity between rain rates and specific attenuation (in the 20–40 GHz band) “makes it possible to use the total path loss as a direct measure of \bar{R} [average rain rate] independent of the form of the distribution of R [rain rate] along the path”.

Both the degree to which Eq. (5.1) holds and the values of a and b are determined by the DSD. In order to study how strongly this relation deviates from other relations found in the literature, we determine values of a and b based on measured DSDs from the São Paulo region. For each 1-min DSD, we compute the corresponding rainfall intensity and specific attenuation at the three most common frequency bands in São Paulo (11, 18, and 23 GHz). Specific attenuation is computed for vertically polarized signals (most CML operate using this polarization) using T-Matrix scattering computations (e.g. Mishchenko, 2000), assuming raindrop oblateness as a function of its volume-equivalent diameter given by Andsager *et al.* (1999), and a raindrop temperature of 287.15 K. The values of a and b are subsequently determined by nonlinear fitting of Eq. (5.1) to the computed values of R and A .

Figure 5.3 shows the resulting power-law relations for the three different frequency bands. Also shown in this figure are the power-law relations derived for rainfall in the Netherlands as used by Overeem *et al.* (2016b) and those recommended by the International Te-

⁴ DSD data from Parsivel and other disdrometers for the region of São Paulo (and other regions across Brazil) are freely available at <http://chuvaproject.cptec.inpe.br/soschuva/>

telecommunication Union (ITU). It is clear from this figure that there are certainly differences, and that these differences at high rainfall intensities are largest for the 11-GHz band. For the higher frequencies, these differences are more limited, especially for high rainfall intensities. This is in line with what has been found earlier (e.g. *Berne and Uijlenhoet, 2007; Leijnse et al., 2008*).

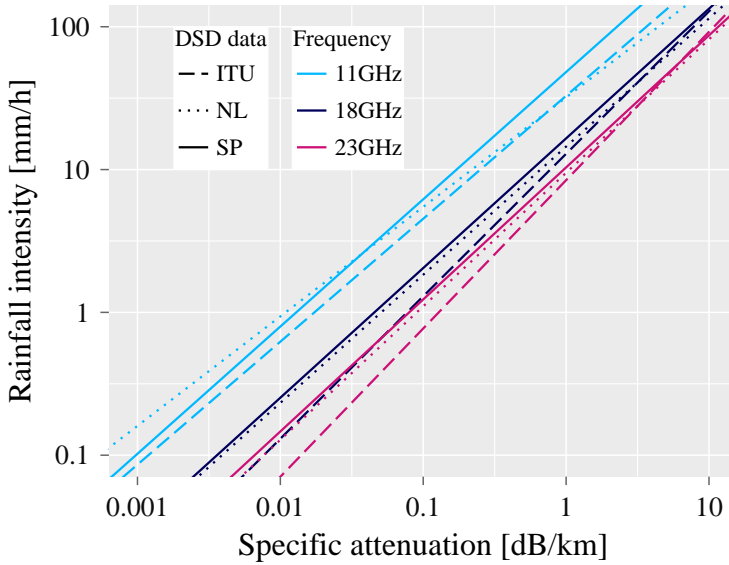


Figure 5.3: Rainfall intensity against specific attenuation for the a and b parameters of three DSD models, i.e. local (SP - continuous line), suggested by ITU-R Recommendation P.838-3 (ITU - dashed line), and RAINLINK's default (NL - dotted line). The $A-R$ relations are presented for three frequencies: 11, 18, and 23 GHz.

RAINLINK (*Overeem et al., 2016b*) is an R package (*R Core Team, 2016*) in which rain rates and area-wide rainfall maps can be derived from CML attenuation measurements. A very brief description of the algorithm is as follows: 1) wet-dry classification — a link is considered for non-zero rainfall retrievals if the received power jointly decreases with that of nearby links; 2) attenuation estimates are obtained from the difference between RSL and the reference signal level representative of dry weather (the median signal level of all dry periods in the previous 24 h); 3) outlier removal — exclusion of links for which the specific attenuation (accumulated over 24 h) deviates too much from that of nearby links; 4) 15-min average rainfall intensities are computed from a weighted average of minimum and maximum rainfall intensities obtained by the (inverse) power-law of Eq. (5.1); and 5) through Ordinary Kriging the rainfall intensities are interpolated into rainfall maps for the land surface of the Netherlands. This latter step was not implemented in this study. *Overeem et al. (2016b)* give a more detailed and in-depth review and/or description about all the technicalities within the RAINLINK package.

Error and Uncertainty Metrics

We evaluated the rainfall estimates from RAINLINK through 1) the relative bias, 2) the coefficient of variation (CV), and 3) the coefficient of determination (r^2).

For a given CML, the relative bias is a relative measure of the average error between the RAINLINK estimates $R_{\text{RAINLINK},i}$ and the gauge rainfall measurements $R_{\text{gauge},i}$ (the latter considered as the ground truth):

$$\text{relative bias} = \frac{\bar{R}_{\text{res}}}{\bar{R}_{\text{gauge}}} = \frac{\sum_{i=1}^n R_{\text{res},i}}{\sum_{i=1}^n R_{\text{gauge},i}}, \quad (5.2)$$

where $R_{\text{res},i} = R_{\text{RAINLINK},i} - R_{\text{gauge},i}$ and n represents all possible time steps for the (rainfall) event under consideration. $R_{\text{res},i}$ are the residuals, i.e., the difference between $R_{\text{RAINLINK},i}$ and $R_{\text{gauge},i}$. \bar{R}_{res} and \bar{R}_{gauge} are the average of the residuals and gauge rainfall measurements (in mm), respectively. The relative bias ranges from -1 to $+\infty$, where 0 represents unbiased rainfall estimates.

The coefficient of variation is a dimensionless measure of dispersion (Haan, 1977), defined in this case as the standard deviation of the residuals $\sqrt{\widehat{\text{Var}}(R_{\text{res}})}$ divided by the mean of the gauge rainfall measurements, for the evaluated CML:

$$\text{CV} = \frac{\sqrt{\widehat{\text{Var}}(R_{\text{res}})}}{\bar{R}_{\text{gauge}}}. \quad (5.3)$$

The CV is a measure of uncertainty. It ranges from 0 (a hypothetical case with no uncertainty) to ∞ .

The coefficient of determination is a measure of the strength of the linear dependence between two random variables, RAINLINK estimates and gauge rainfall measurements in this case. It is defined as the square of the correlation coefficient between $R_{\text{RAINLINK},i}$ and $R_{\text{gauge},i}$:

$$r^2 = \frac{\widehat{\text{Cov}}^2(R_{\text{gauge}}, R_{\text{RAINLINK}})}{\widehat{\text{Var}}(R_{\text{gauge}}) \cdot \widehat{\text{Var}}(R_{\text{RAINLINK}})}, \quad (5.4)$$

where $\widehat{\text{Var}}(R_{\text{gauge}})$ and $\widehat{\text{Var}}(R_{\text{RAINLINK}})$ are the variance of gauge rainfall measurements and RAINLINK estimates, respectively; and $\widehat{\text{Cov}}^2(R_{\text{gauge}}, R_{\text{RAINLINK}})$ the squared covariance between these two variables. r^2 ranges from 0 to 1, this latter the case of perfect linear correlation, i.e., all data points would fall on a straight line without any scatter. Perfect linearity does not imply unbiased estimates because the regression line does not have to coincide with the 1:1 line, even if it captures all variability.

The metrics were computed on 30-min paired rainfall depths, both above 0 mm to only account for (significant) rainfall events. 30-min aggregation was necessary given the temporal resolutions of the datasets, i.e., 10 min for gauge and 15 min for link-retrieved data.

5.3 Results and Discussion

Evaluation of 30-min Rainfall Rates

Figure 5.4 shows minimum and maximum received powers and the derived CML rainfall rates, as well as the rain rates from the nearest gauge. It can be seen that the minimum and maximum received powers are strongly negatively correlated with the gauge rainfall rates. Two clear rainfall events are found for CML 14. One can see that the stronger the rainfall event is, the larger is the attenuation registered by this CML. The largest decrease in received power, ~ 50 dB, is found for the rainfall event on 12 December 2014, where gauge I measured 20 mm in 10 min.

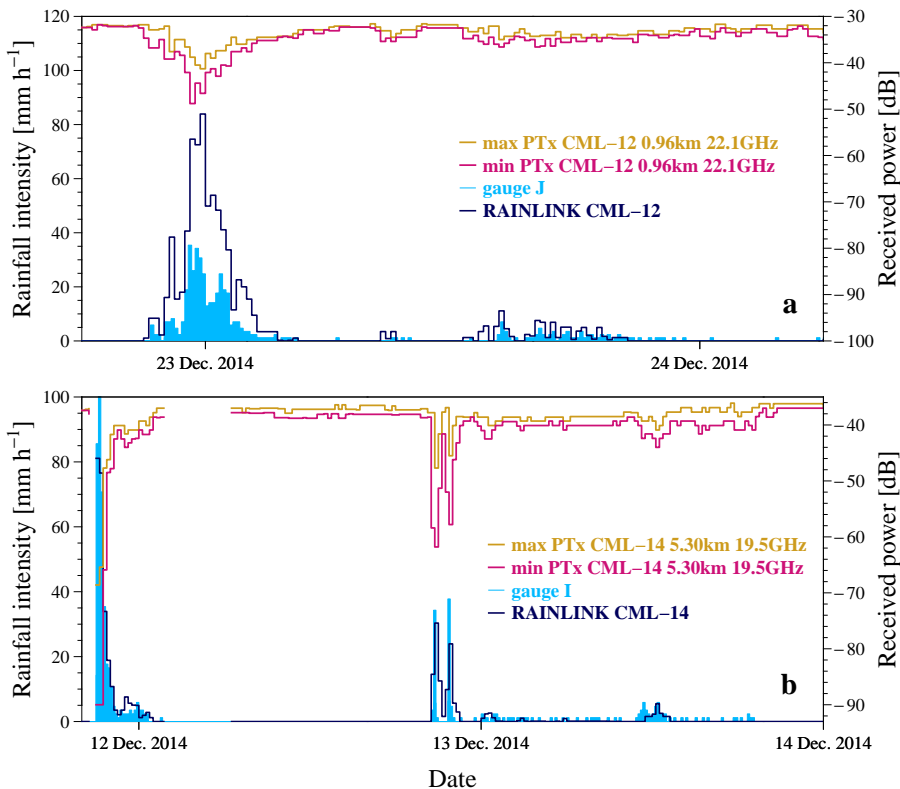


Figure 5.4: Time series of gauge measurements (light blue), RAINLINK estimates (dark blue), and minimum and maximum received powers (pink and gold, respectively) for a couple of rainfall events for CML 12 (a), and for CML 14 (b).

The quality of rainfall estimates differs between CML 12 and CML 14. For CML 14 the rainfall rates correspond well with those from gauge I. In contrast, for CML 12 only the dynamics, i.e. the variation with time corresponds, whereas the CML rainfall rates are much larger than those from gauge I for the event around 23 December 2014.

Uncertainties in gauge and attenuation measurements themselves are the two sources of error that mainly constraint our evaluation. Our work compares CML rainfall estimates against rain gauge measurements, which are considered here as the “ground truth”. Nonetheless, a gauge is only representative of its surrounding area and does not account for the spatial variability of rainfall along the link path. Representativeness errors will increase for longer link paths and for more intense rainfall events. For tropical regions where intense rainfall is associated to small convective raincells/systems, *da Silva Mello et al.* (2014) showed that due to smaller raincells only a part of the link-path contributes to the attenuation causing thus an effective link-rain rate smaller than the one(s) measured by gauges.

In Figure 5.4 the best results are obtained for the longest link (5.3 km), whereas representativeness errors could already play a larger role. The worst result is found for the shortest link (0.96 km). This may be related to the fact that rain-induced attenuation along the link path may be relatively small compared to the attenuation caused by wet antennas, i.e., the wet antennas may explain the large overestimation found for CML 12.

Table 5.1 provides a more extensive verification employing five CML shown in Fig. 5.1. The results presented in Table 5.1 come from the manual selection of significant rainfall events for each particular CML. A rainy event is identified if both rainfall depths (CML and gauges) are above 0.0 mm for more than two consecutive 30-min steps, i.e., if it lasted more than 1 h. Hence, if the evaluation of CML estimates yields a $r^2 \geq 0.75$ we can be sure that CML and gauge estimates show similarities, which is the case for the selected five CML in Table 5.1. Given the fact that the CML and gauge measurements are totally independent, it is likely that the high values of r^2 indicate that both types of observations contain a true rain signal.

Table 5.1: Relative bias, and coefficients of variation (CV) and determination (r^2) for $A-R$ relations: local (SP), suggested by ITU-R Recommendation P.838-3 (ITU), and RAINLINK's default (NL). The metrics presented correspond to CML estimates for which $r^2 \geq 0.75$ (i.e., 5 out of 11 CML evaluated). n indicates the number of rainfall pairs (comparisons) the metrics are computed on. The mean rain gauge depth (\bar{R}_{gauge}) for the n pairs is also presented.

CML	Length [km]	Freq. [GHz]	gage	r^2			CV			\bar{R}_{gauge} SP	relative bias			n
				NL	ITU	SP	NL	ITU	SP		SP	ITU	NL	
14	5.30	19.5	I	0.85	0.85	0.85	0.70	0.73	0.70	2.69	+9.3	-2.7	-9.1	93
06	0.82	23.1	A	0.87	0.85	0.85	0.98	0.83	0.92	3.69	+32.9	+24.4	+31.6	22
07	1.68	23.5	B	0.75	0.76	0.76	0.96	0.88	0.90	3.86	+33.5	+26.2	+34.5	92
13	0.96	22.1	J	0.87	0.85	0.84	1.67	1.44	1.64	2.64	147.3	127.8	135.0	96
12	0.96	22.1	J	0.86	0.84	0.84	1.89	1.66	1.88	2.50	153.3	133.5	143.0	102

A high value of r^2 , although promising, does not automatically imply that CML rainfall estimates are accurate. Hence, it is important to also compute other metrics, such as CV and the relative bias. CML 6, 7 and 14 provide relatively low values of CV, i.e. below 1. The relative bias for CML 6 and 7 is relatively high ($\sim 30\%$), whereas the relative bias for CML 14 is within 10%. CML 12 and 13 do likely perceive a rain signal given the high values of r^2 , but their values of CV are much larger than 1, and their relative bias is roughly 130%, implying a large rainfall overestimation by CML. This might be caused by wet antenna attenuation being more dominant for those short links, although this is not found for the short CML 6.

The results for different $A-R$ relations are quite similar, indicating that differences in climatologies play a smaller role. For CML 12 and 13 the relative bias becomes more severe for the $A-R$ relation derived from São Paulo data.

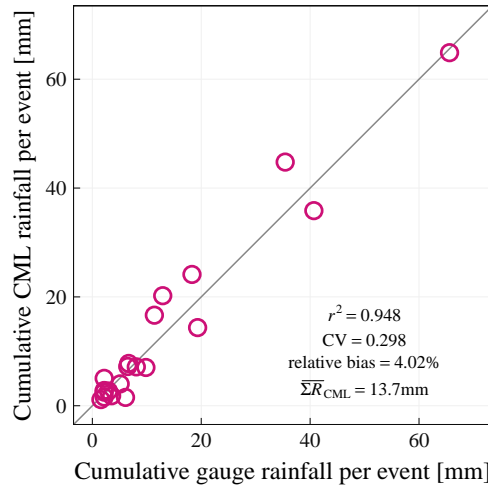


Figure 5.5: Scatter plot of aggregated CML rainfall against aggregated gauge rainfall for all selected rainy events (20) in the evaluation of CML 14. A rainfall event is selected if both rainfall depths are above 0.0 mm, and for a duration of 1 h or more.

Evaluation of Event Rainfall Accumulations

The clear potential of CML technology for rainfall estimation (for subtropical climatologies) is presented through the outstanding performance of CML 14 (Fig. 5.4b, and Table 5.1). We further explore the performance of this CML by studying all registered rainfall events for the period under consideration, i.e. 20 rainy events (excluding one event for which the CML attenuations were clearly erroneous). Figure 5.5 presents a scatter plot of aggregated CML rainfall against aggregated gauge rainfall for these 20 selected rainfall

events. In the figure one can see how CML 14 accurately measures very intense, as well as light rainfall events. The r^2 for the aggregated rainfall of these 20 events is 0.95, with a very low CV of 0.30, and a relative bias of 4%. Hence, the rainfall estimates from CML 14 agree well with those from a gauge based on a large dataset. This gives an indication that the RAINLINK package is suitable to retrieve rainfall employing CML data from a subtropical climate, even though many of its parameters have not been optimized for such a climate. Since biases propagate in the hydrological model forecasts, the low relative bias found for CML 14 is of great importance if its rainfall estimates would be used as input for a hydrological model.

The results presented in Fig. 5.5 correspond to RAINLINK retrievals where no wet-dry classification is applied, in order to focus on the performance of individual CML without utilizing information from surrounding CML. Moreover, this shows the usefulness of RAINLINK in case few nearby CML are available. If the wet-dry classification from RAINLINK, i.e. the nearby link approach, is applied, slightly improved metrics are obtained.

5.4 Summary, Conclusions and Recommendations

CML networks are an opportunistic technique for rainfall estimation, with the potential to be used worldwide given the spread of CML-based telecommunication systems/platforms during the last two decades. Here we presented one of the first evaluations of CML rainfall retrievals for a subtropical climate. Subtropical regions could benefit from this technique given that rainfall events are often more extreme and usually fewer surface rainfall measurements are collected. We evaluated rainfall retrievals from power attenuation measurements for five CML from a network located in the city of São Paulo. We employed the package RAINLINK (Overeem *et al.*, 2016b) to retrieve rainfall from these CML.

CML rainfall estimates were evaluated against those from the nearest rain gauge at 30-min intervals for the period from 20 October 2014 to 9 January 2015. We focused our analyses on the five CML for which $r^2 \geq 0.75$. Three out of five CML gave good results in terms of CV. One CML also had a low relative bias. Subsequently, the quality of rainfall estimates from this best performing CML was evaluated employing 20 events from the entire three-month period. The good results indicate that RAINLINK can be successfully applied to CML data from a subtropical climate, even though most parameters have been optimized for the temperate climate of the Netherlands.

In order for RAINLINK to capture the rainfall characteristics from the region of São Paulo, we derived a - b coefficients of power-law $A-R$ relations [Eq. (5.1)] from local DSD data⁵. The a and b coefficients are a function of the polarization and frequency of the link, DSD and raindrop temperature. The ITU/NL sets proved to be very useful and accurate enough when local a - b coefficients cannot be derived. The NL set is characteristic for the hydro-climatology of the Netherlands, and is the default set in RAINLINK.

⁵We enormously thank Timothy Hugh Raupach from EPFL (Switzerland) for his contribution to the DSD data analysis.

The 5.3-km CML was the one with the best performance for the NL $A-R$ relation, i.e., $r^2 = 0.851$, $CV = 0.70$, and relative bias of -9.11% (-2.67% for the ITU set). Such a low relative bias indicates the suitability of CML rainfall retrievals in hydrological modeling, for instance.

A more thorough evaluation should be done to systematically study and explain differences between CML and gauge rainfall estimates. For instance, the influence of rainfall variability along link paths could be studied. This can be achieved if local radar measurements are compared against CML estimates, which would allow to better track the rain events and their incidence over link paths, being especially relevant for longer link paths. We also encourage future work on sensitivity analysis focused on the optimization of RAINLINK parameters to improve the accuracy of rainfall estimates in subtropical regions. Missing maximum signal level data, and unexpected combinations of link lengths and microwave frequencies, decided us to remove many CML from the original dataset. This shows that accurate metadata, such as link coordinates, are essential.

CML are still far from replacing currently standard technologies such as radars, rain gauges (and even satellites), but their opportunistic use is rather valuable as a complementary network for high-resolution rainfall estimation. To conclude, we were able to obtain good results for one link, which confirms the great potential of this technique if the data and metadata are properly stored.

5.4. Summary, Conclusions and Recommendations

Chapter 6

Synthesis

6.1 Summary

In Chapter 2 the first year of the GPM research product (IMERG) was evaluated for the land surface of the Netherlands. IMERG is a gridded product with a spatiotemporal resolution of $0.1^\circ \times 0.1^\circ$ every 30 min. IMERG data sets were evaluated against the spatiotemporal aggregation (at IMERG resolution) of radar rainfall fields which have a native resolution of $\sim 1 \text{ km}^2$ every 5 min. The evaluation was done for half-hourly, daily, monthly, and yearly durations through pixel-by-pixel comparisons, and cumulative daily rainfall for the entire land surface of the Netherlands. It was found that IMERG tends to systematically underestimate rainfall by 2%, for the *precipitationCal* data set.

In Chapter 3 not only IMERG was evaluated again for the land surface of the Netherlands but also two more satellite rainfall products, and one from CML. The two extra GEO-satellite products, i.e., CPP and NIPE have been designed for the hydrometeorological conditions of the Netherlands. This is also the case for CML-derived rainfall maps. Here, the evaluation was only based on pixel-by-pixel comparisons. IMERG was the satellite product which outperformed its other two counterparts, CPP and NIPE. Rainfall maps from CML were the product with the best performance with a correlation of ~ 0.6 , which is twice as good as the one obtained for IMERG. It was explored if the spatial density of CML would be a crucial factor in satellite validation at IMERG resolution (it isn't).

Chapter 4 quantified the uncertainties in rainfall maps derived from CML data associated with the spatiotemporal availability of the CML data itself, and the methodology of interpolation. The evaluation was carried out for spatiotemporal resolutions of $\sim 1 \text{ km}^2$ every 15 min and 24 h. CML rainfall was simulated from radar data. This derived data set represented perfect rainfall measurements that potentially come from CML networks where all links retrieve power measurements at all times, i.e., no availability issues. It was found that measurement errors were the source that contributes most to the overall uncertainty in rainfall maps from CML networks.

In Chapter 5 rainfall was retrieved from a Brazilian CML network through the freeware R-

package RAINLINK. This package was developed for the climatological conditions of the Netherlands, and for the topology of the local CML networks. Because of the tropical climatology of Brazil, this was a perfect opportunity to test the applicability of RAINLINK to other conditions than those for which it was originally designed. The evaluation was done at half-hourly durations against aggregated data from a local automatic gauge network of which the native resolution is 10 min. Only for one CML the bias was below 10%, which is an indication that RAINLINK is suitable for rainfall estimation in (sub)tropical climates.

6.2 If Something Has to Be Concluded, It Should Be This

The following general conclusions are based on the evaluation of the rainfall products carried out in this thesis:

- CML offer the most accurate rainfall estimates at higher spatiotemporal resolutions, i.e., $\sim 1 \text{ km}^2$ and sub-hourly. CML rainfall products were the ones which consistently captured the inherent variability of rainfall at small spatiotemporal scales. We saw how in Chapter 3 it is the product with the lowest coefficient of variation (CV), and the highest coefficient of determination (r^2), which represents a correlation of 0.61, with regard to the product of reference, i.e., radar rainfall fields. This correlation is practically the same to the one obtained in Chapter 4 (also 0.61, with CV=1.2). The similarity of these results boosts the validity of this technology, as these numbers were computed for different topologies, evaluation periods, and accumulated durations. For instance, in Chapter 3 the evaluation was for 7 months, at 30 min, for $\sim 1,400$ links, whereas in Chapter 4 the evaluation was for 12 days, at 15 min, for $\sim 1,700$ links. Overeem *et al.* (2016a) obtained a correlation of 0.6 at hourly accumulations, for two-and-a-half years of data from almost 3,400 CML for the land surface of the Netherlands at $\sim 1 \text{ km}^2$.
- RAINLINK is a good first approach for CML rainfall retrievals in subtropical latitudes. The evaluation of CML rainfall from the city of São Paulo (Brazil) yielded promising results. Results are not really conclusive at this point because the evaluation carried out was only possible for 11 CML from a 200-link network for an evaluation period of three months. Nevertheless, there was one case in which the performance of RAINLINK was remarkable. Such a performance corresponded to a 5.3-km CML which yielded a correlation of 0.92, a CV of 0.7, and a relative bias below 10% (2% for an alternative scenario). This performance was achieved without modifying the default parameters RAINLINK comes with. Hence, it is expected that after a more detailed fine-tuning of the embedded parameters within the package, jointly with a more extensive data set, more promising results will come. This was an exciting exercise because (as far as we know) it was the first time that RAINLINK was applied to latitudes close to the Equator where rainfall properties, and network topology, vastly differ from those RAINLINK was designed for.
- Satellite rainfall estimates from the brand new GPM mission gave good results for the hydrometeorological conditions of the Netherlands. With the transition from TRMM to GPM it was possible to evaluate the first full year of rainfall measurements from

space for the land surface of the Netherlands. The performance of IMERG was not as good as the one obtained from CML. At half-hourly durations and $0.1^\circ \times 0.1^\circ$ resolution the correlation was 0.33 with $CV=1.9$ (Chapters 2 and 3). This implies a large discrepancy between the ground truth and the rainfall estimated by GPM. Nevertheless, when it comes to the relative bias, IMERG underestimates rainfall by just $\sim 2\%$, whereas CML rainfall retrievals underestimate rainfall by $\sim 14\%$. The low relative bias of IMERG suggests the suitability of such a high-resolution gridded product for hydrological modelling, for instance.

6.3 Discussion

The current and leading technology in high-resolution rainfall estimation is radar. Although it is true that CML could potentially offer rainfall estimates at sub-kilometer and sub-minute resolutions, and that satellites provide global rainfall estimates, radar is the technology which actually offers accurate rainfall estimates at spatiotemporal resolutions of $\sim 1 \text{ km}^2$ (or higher) every 5 min on average (or less), on an operational basis. The robustness of radar technology is the product of ~ 80 years of evolution. Therefore, it would be hard for any other technology to take that privilege away. What CML and satellite technologies now offer is the possibility to reach places radar can't, and counterbalance the limitations radar is prone to. It should be underlined one last time that the aim of this thesis is not to promote satellite and/or CML technologies as future replacements of radar, but to carry out the evaluation of state-of-the-art technologies in rainfall monitoring over the land surface of the Netherlands (and beyond).

CML rainfall retrievals proved to be accurate and valuable at higher resolutions, that is, $\sim 1 \text{ km}^2$ in space and at sub-hourly durations. Even for the Brazilian case, in which the performance was outstanding for rainfall occurring along a 5.3-km link-path sampled at 15-min resolution. For the Dutch case, it seems that the top correlation achieved for CML-based rainfall maps is around 0.6. In Chapter 4 it was demonstrated how this correlation could be improved by 10% if we would manage to perfectly operate a CML network. Chapters 3 and 4 also showed how the accuracy of CML rainfall retrievals is not directly linked to the number of CML available in a given area, i.e., the density of the network. The largest source of uncertainty in CML rainfall maps comes from (sources of) errors in the measurements themselves. Unfortunately, in this thesis none of the possible errors induced by the measurement process like sampling, quantization, wet-antenna attenuation, drop size distribution, and many others were further explored. Nevertheless, with regard to the contribution of CML measurements towards the enhancement of hydrological sciences, especially rainfall estimation, what I can advocate for is a joint effort between scientists and (cellular) communication providers. Especially bigger efforts from the latter are required to release the power measurements, if recorded at all.

We like to think of CML as rain gauges due to their conceptual similarities. CML are closer to the ground than what radar rainfall estimates can offer. CML are deployed in networks, which tend to be more dense in urban than in rural areas. The advantage with

regard to gauge networks is mainly the proportion of CML to gauges (10:1 to 50:1) due to the boom in cellular communications. The proximity of these links to the ground and the linearity of the retrieval relation yield accurate rainfall estimates, and thus, potentially high-resolution products. It was argued that the accuracy of rainfall estimates does not improve as the link density is higher, but large data sets of CML measurements would certainly provide the opportunity to explore new approaches and gain a deeper understanding of the science and statistics of rainfall. These very same are the advantages that CML offer to radar, and which radar could benefit from. While the time for phased-array radars comes into operational fruition, current radars scan all directions within 5 min, whereas CML could offer rainfall estimates at the sub-minute scale. In the same way, and despite the coverage that radar offers, CML could be a better representation of the ground truth.

If IMERG has to be held accountable for what the numbers reflect on its performance, it would most likely be disregarded, especially when better rainfall products such as those from radar and CML are within our reach. This would be indeed a very harsh assessment because despite the low correlation (0.33), IMERG succeeds in aspects radar and CML don't, regardless of the high-resolution estimates they provide. We saw in Chapters 2 and 3 how this low correlation could be attributed to the few direct measurements the GPM constellation is able to retrieve over the Dutch land surface. Not only does this lower sampling in the direct detection of rainfall (from the dual-frequency precipitation radar) contribute to a poor performance but also the large proportion of passive measurements from top cloud properties (many kilometers up in the sky). Hence, it is definitely expected that actual surface measurements of rainfall outperform satellite-derived ones. Nevertheless, the strength of IMERG lies in the joint effort between multinational satellite platforms, reached in the 17 years in which TRMM orbited the Earth measuring rainfall over the tropics. It is worth to briefly mention once more that the main advantage of satellite retrievals of rainfall is their global coverage. Thus, places where radar technology is not affordable or where poor gauge networks are in place or where CML-derived rainfall is still to be tested can hugely benefit from this source of precipitation measurements, if at least an internet connection does exist in such places. Satellite measurements not only are key for places deprived of more conventional networks to measure rainfall but also provide rainfall measurements over the vast oceans which also regulate Earth's water and energy budget. More than to promote IMERG as an alternative source of rainfall measurements for an already well-gauged country, this thesis evaluated the expected capabilities and accuracy of IMERG in places with a similar rainfall climatology as experienced in the Netherlands. In such places, at least, we can be confident that IMERG offers high-resolution estimates of rainfall accurate enough to be used in hydrological modelling or for water management purposes.

6.4 Outlook

I want to go back to my ontological disclaimer: It is realistically not possible to seize the (rainfall) ground truth. Thus, whatever we measure is hopeless to compare against a truth that does not exist. Nevertheless, what is possible is that what we measure could be a clo-

ser representation of that truth we strive to achieve. We saw one example of this predicament in Chapter 5 where CML rainfall retrievals were evaluated against a (dense) gauge network. The data from this gauge network represented the “ground truth”; yet still its validity could not be assessed, neither confirmed nor rejected. The evaluation results were sourly split, luckily they tended to be on the promising side, i.e., with correlations above 0.8. It is therefore reasonable to assume that if gauge and CML rainfall retrievals are both inaccurate, there would naturally be little or no correlation whatsoever. Nonetheless, it is virtually impossible (very unlikely) that two totally independent measurements would consistently yield similar and inaccurate rainfall retrievals in the same proportion. This is why CML 14 in Chapter 5 is a promising (and outstanding) result for rainfall estimation in the subtropics, and helps to prove my ontological point. Acknowledging that we actually do not know the ground truth, the case of CML 14 tells us that two independent sources practically measure(d) the same characteristics (to a certain extent) of the phenomenon being observed. Hence, and for strictly technical purposes, neither of them (CML or gauges) represent the ground truth but at the same time both of them could hold the ground truth. So why prefer one above the other? We cannot deny that, unlike rain gauges, CML still have to put up a lengthy fight before becoming operational networks in rainfall monitoring at global scale. But we should never prefer one technology above the other. Hence, the synergistic use of all of them is what I think will put us one step closer to that ground truth we strive to achieve, and one step further away from such an ontological dichotomy.

In this thesis we evaluated and quantified the performance of two state-of-the-art products in monitoring rainfall at high spatiotemporal resolutions. Doing so is very important because we need to know how large the error in rainfall measurements is (if any), and what are the sources that cause it. I believe that future work should focus less on pinpointing sources of uncertainty in such technologies, and more on the synergistic use of current and available technologies and/or platforms for rainfall estimation like satellites, radars, CML, gauges, and even tweets! (*de Vasconcelos et al.*, 2016). This combinatorial approach would certainly offer the tools to truthfully estimate rainfall. On the other hand, the work by *Kirstetter et al.* (2015) is one of the first steps in acknowledging the impossibility to measure the truth, the whole truth, and nothing but the truth... so help us [.]

Appendices

- A. Comparisons between IMERG and RADAR rainfall maps — Chapter 2**
- B. Comparisons between CML and RADAR rainfall maps — Chapter 4**

A.1 The 30-min and 24-h scales

Figure A.1 shows 12 30-min comparisons between radar and IMERG rainfall fields. A wide range of cases was selected, for instance, good cases such as 2000 UTC 26 May, 0930 UTC 8 July, and 1430 UTC 22 August 2014, where rainfall partially and entirely fell over the Netherlands, and some cases in which IMERG either missed precipitation or/and did not accurately measure it, such as 0900 UTC 21 March 2014 and 1700 UTC 9 January 2015. Of special interest in this figure is the good performance of IMERG for one of the most intense events in 2014, that is, Fig. A.1 (second and third rows) that correspond to 6 30-min time steps on 28 July 2014 (each separated by 1 h). In Fig. A.1 (second and third rows) it is shown how, despite some difficulties to capture high rainfall intensities, IMERG is able to accurately track the storm at such medium-catchment scale.

Figure A.2 shows 12 24-h comparisons between radar and IMERG rainfall fields. Good and bad cases of the performance of IMERG were selected. One pattern seen in this figure is how IMERG on the 24-h scale tends to overestimate high intense rainfall events (pattern also observed in Fig. 2.2, top right). Such are the cases for 0800 UTC 27 May, 0800 UTC 29 July, and 0800 UTC 12 December 2014.

A.2 The monthly scale

Figure A.3 shows 12 monthly comparisons between radar and IMERG rainfall fields. In most cases IMERG is able to reproduce the spatial variability of rainfall, especially in those cases where monthly rainfall is below 120 mm, for instance, from September to November 2014. When extreme events (above 160 mm) were developed either locally or sparsely through the Netherlands, IMERG fails to accurately capture such intense events, for instance, May and August 2014. In these IMERG rainfall fields, it is possible to identify the signature of the spatial scale on which the GPCC gauge analyses are based.

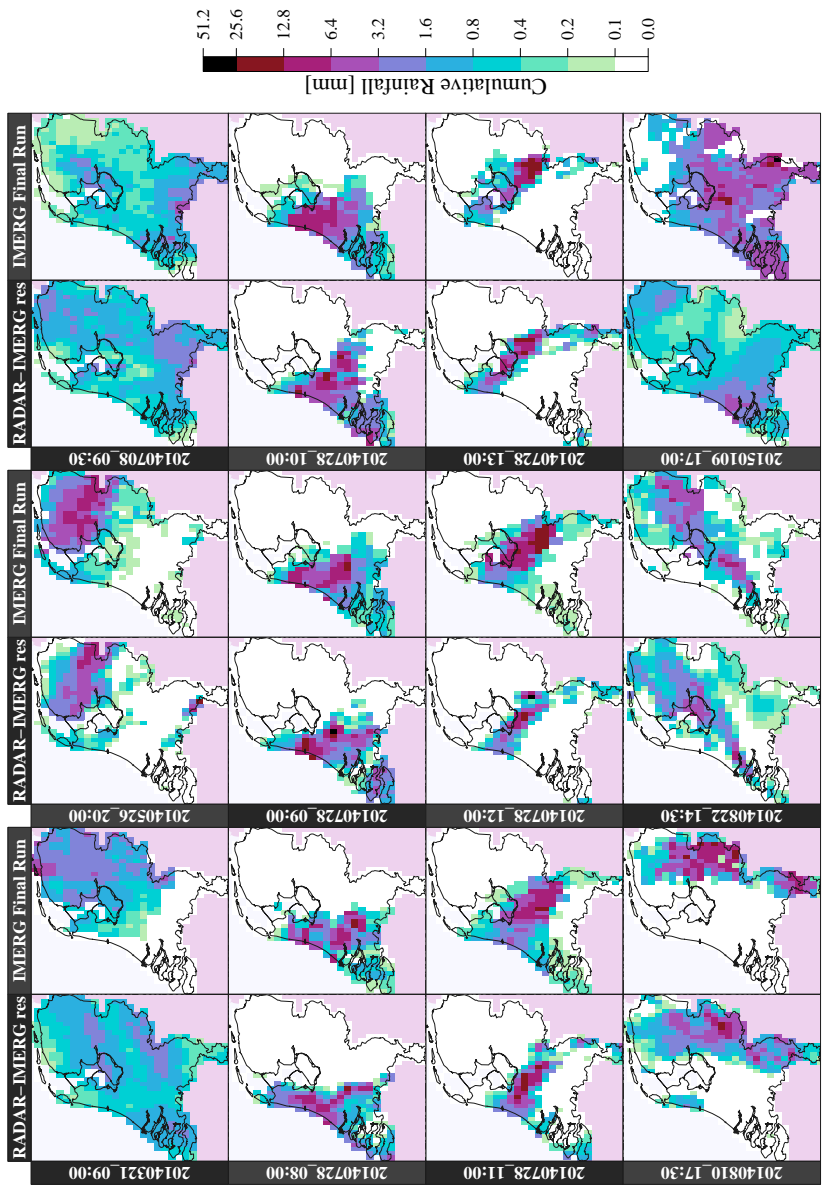


Figure A.1: Comparison of 30-min rainfall maps between IMERG Final Run and radar at IMERG resolution. All the cases in the second and third rows follow the most intense rainfall event in the Netherlands for 2014. The column labels indicate the end time (UTC) and date for which the 30-min maps were obtained.

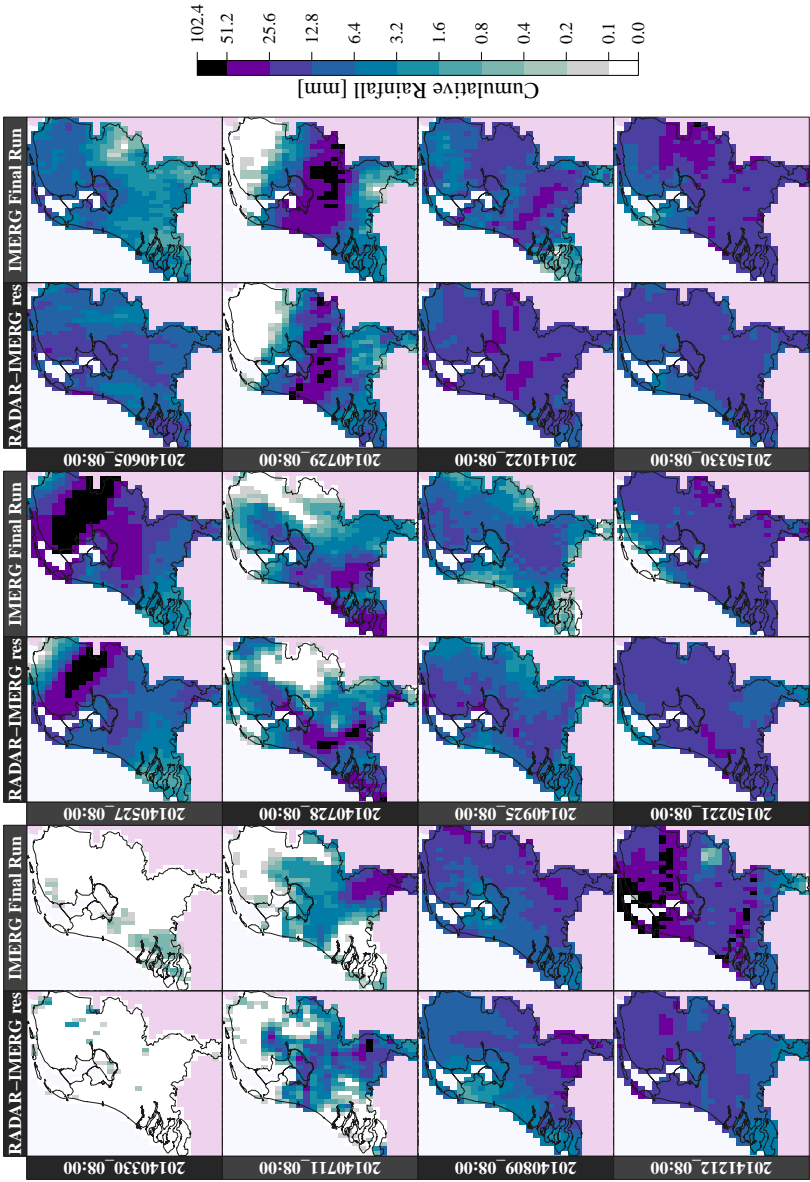


Figure A.2: Comparison of 24-h rainfall maps between IMERG Final Run and radar at IMERG resolution. The column labels indicate the end time (UTC) and date for which the 24-h maps were obtained.

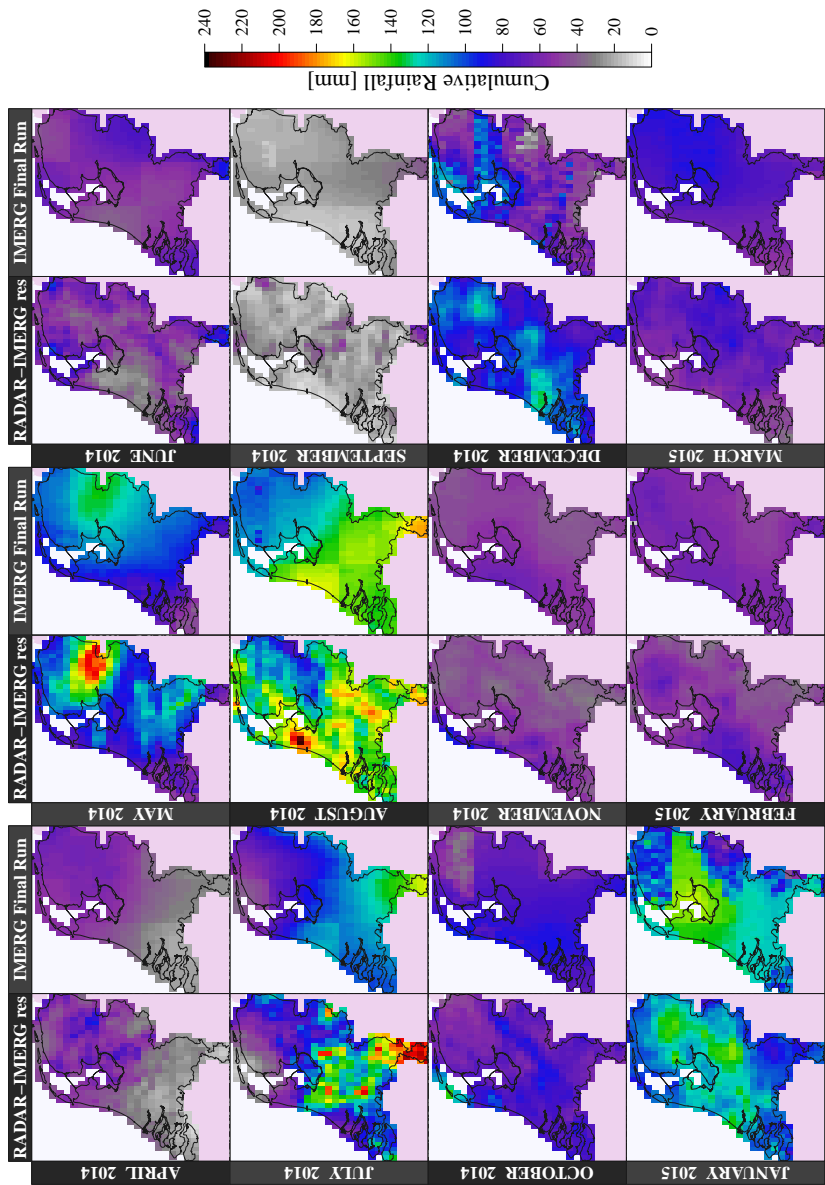


Figure A.3: Comparison of monthly rainfall maps between IMERG Final Run and radar at IMERG resolution. The column labels indicate the end time (UTC) and date for which the 30-min maps were obtained.

B.1 The 24-h and 15-min scales

In Fig. B.1, the LINK column (rows 20110907_08:00 and 20110819_08:00, top and bottom, respectively) shows how daily rainfall depths are greatly overestimated by link data, especially in places where there is intense rainfall, and the density of the network is higher. Simulated rainfall depths (actual availability) show improvement of rainfall fields with regard to link-based rainfall fields. Conversely, to actual link rainfall maps, simulated rainfall fields based on the actual availability of the network present a slight underestimation of rainfall depths. Simulated link rainfall fields (actual and 100% network availability) are similar because the effect of actual or 100% availability among 15-min intervals is smoothed out by the sum of 15-min rainfall fields.

Figure B.2 shows how accurate rainfall events are captured across the Netherlands at 15-min intervals. Note how the accuracy is improved for the best-case scenario of 100% network availability (fullSIM column).

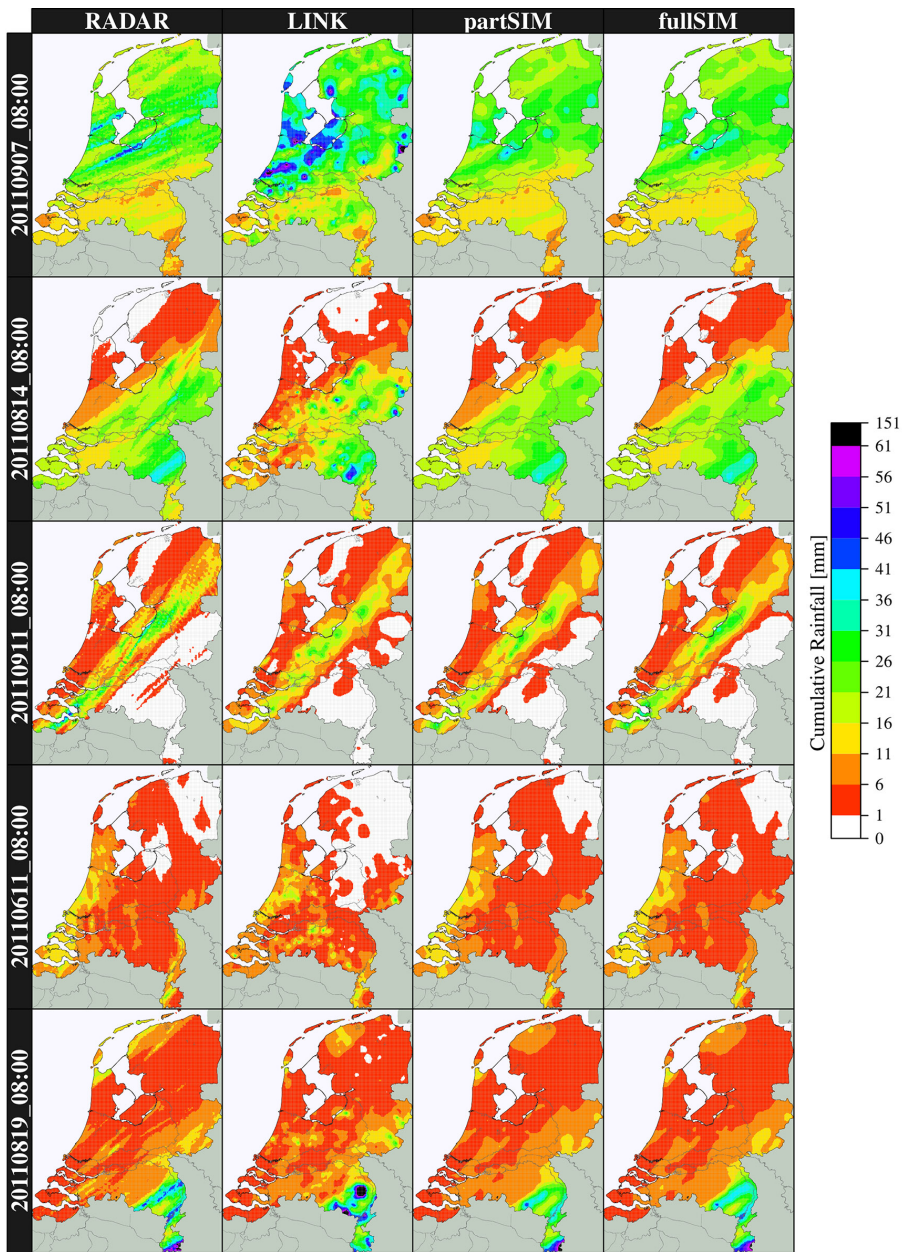


Figure B.1: Comparison of daily interpolated rainfall maps with regard to radar rainfall fields (ground truth; left column). The rows show five of the 12 days of the validation period. Daily rainfall maps were aggregated from 15-min rainfall maps. The row labels indicate the end UTC for which the maps were obtained.

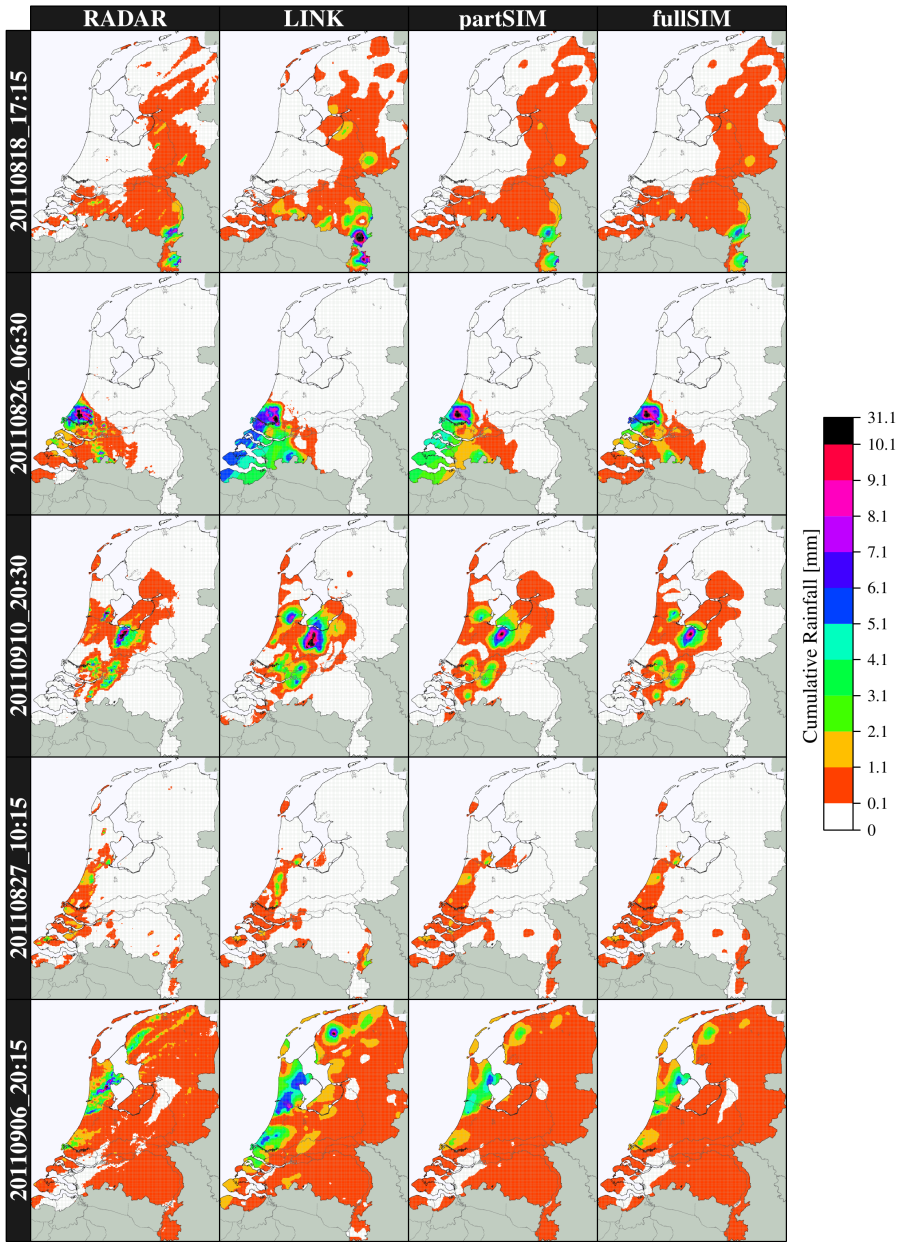


Figure B.2: Comparison of 15-min interpolated rainfall maps with regard to radar rainfall fields (ground truth, left column). The rows show five of the 1,152 time steps (cases) present in the 12-day validation period. The row labels indicate the start UTC for which the maps were obtained.

Bibliography

- Amani, A., and T. Lebel (1997), Lagrangian kriging for the estimation of Sahelian rainfall at small time steps, *J Hydrol*, 192(1–4), 125–157, doi: 10.1016/S0022-1694(96)03104-6.
- Amos, J. (2014), Smart umbrellas ‘could collect rain data’, BBC News [online], May 2014, <http://www.bbc.com/news/science-environment-27222282>, (accessed Feb 15, 2017).
- Andsager, K., K. V. Beard, and N. F. Laird (1999), Laboratory measurements of axis ratios for large raindrops, *J Atmos Sci*, 56(15), 2673–2683, doi: 10.1175/1520-0469(1999)056<2673:LMOARF>2.0.CO;2.
- Atlas, D., and L. J. Batan (1990), *Radar in meteorology: Battan memorial and 40th anniversary radar meteorology conference*, American Meteorological Society, Boston, conference proceedings.
- Atlas, D., and C. W. Ulbrich (1977), Path- and area-integrated rainfall measurement by microwave attenuation in the 1–3 cm band, *J Appl Meteorol*, 16(12), 1322–1331, doi: 10.1175/1520-0450(1977)016<1322:PAAIRM>2.0.CO;2.
- Badron, K., A. F. Ismail, J. Din, and A. Tharek (2011), Rain induced attenuation studies for v-band satellite communication in tropical region, *J Atmos Sol-terr Phy*, 73(5–6), 601–610, doi: 10.1016/j.jastp.2010.12.006.
- Barthès, L., and C. Mallet (2013), Rainfall measurement from the opportunistic use of an earth–space link in the ku band, *Atmos Meas Tech*, 6(8), 2181–2193, doi: 10.5194/amt-6-2181-2013.
- Becker, A., P. Finger, A. Meyer-Christoffer, B. Rudolf, K. Schamm, U. Schneider, and M. Ziese (2013), A description of the global land-surface precipitation data products of the Global Precipitation Climatology Centre with sample applications including centennial (trend) analysis from 1901–present, *Earth Syst Sci Data*, 5(1), 71–99, doi: 10.5194/essd-5-71-2013.
- Berne, A., and R. Uijlenhoet (2007), Path-averaged rainfall estimation using microwave links: Uncertainty due to spatial rainfall variability, *Geophys Res Lett*, 34(7), doi: 10.1029/2007GL029409.
- Berne, A., G. Delrieu, J.-D. Creutin, and C. Obled (2004), Temporal and spatial resolution of rainfall measurements required for urban hydrology, *J Hydrol*, 299(3–4), 166–179, doi: 10.1016/j.jhydrol.2004.08.002.
- Bianchi, B., P. Jan van Leeuwen, R. J. Hogan, and A. Berne (2013), A variational approach to retrieve rain rate by combining information from rain gauges, radars, and microwave links, *J Hydrometeorol*, 14(6), 1897–1909, doi: 10.1175/JHM-D-12-094.1.
- Biswas, A. K. (1970), *History of Hydrology*, 348 pp., North-Holland Publishing Company, Amsterdam, the Netherlands, ISBN 7204-8018-3.
- Bitew, M. M., and M. Gebremichael (2011), Evaluation of satellite rainfall products through hydrologic simulation in a fully distributed hydrologic model, *Water Resour Res*, 47(6), W06526, doi: 10.1029/2010WR009917.
- Bitew, M. M., M. Gebremichael, L. T. Ghebremichael, and Y. A. Bayissa (2012), Evaluation of high-resolution satellite rainfall products through streamflow simulation in a hydrological modeling of a small mountainous watershed in Ethiopia, *J Hydrometeorol*, 13(1), 338–350, doi: 10.1175/2011JHM1292.1.
- Black, A. W., G. Villarini, and T. L. Mote (2017), Effects of rainfall on vehicle crashes in six U.S. states, *Wea Climate Soc*, 9(1), 53–70, doi: 10.1175/WCAS-D-16-0035.1.

Bibliography

- Brasjen, N., and J. Meirink (2015), Precipitation estimation from MSG-SEVIRI infrared satellite imager, in *Proceedings for the 2015 EUMETSAT Meteorological Satellite Conference*, 21–25 September, Toulouse, France.
- Brutsaert, W. (2005), *Hydrology: An Introduction*, 618 pp., Cambridge University Press, Cambridge, UK, ISBN 978-0-521-82479-8.
- Buderi, R. (1997), *The Invention That Changed the World: How a Small Group of Radar Pioneers Won the Second World War and Launched a Technological Revolution*, 1st ed., 576 pp., Touchstone, New York, USA, ISBN 0-684-83529-0.
- Burt, C., and M. Stroud (2007), *Extreme Weather: A Guide & Record Book*, climate change ed., 303 pp., W.W. Norton, New York, USA, ISBN 978-0-393-33015-1.
- Carlton, J. (2017), California storms bring destruction and drought relief: Back-to-back storms have stoked optimism that there will finally be enough water for everything from agriculture to golf courses, *The Wall Street Journal* [online], Jan 2017, <https://search.proquest.com/docview/1857946768?accountid=27871>, (accessed Feb 9, 2017).
- Cervený, R. S., J. Lawrimore, R. Edwards, and C. Landsea (2007), Extreme weather records: Compilation, adjudication, and publication, *Bull Amer Meteor Soc*, 88(6), 853–860, doi: 10.1175/BAMS-88-6-853.
- Chakravarty, K., and A. Maitra (2010), Rain attenuation studies over an earth–space path at a tropical location, *J Atmos Sol-terr Phys*, 72(1), 135–138, doi: 10.1016/j.jastp.2009.10.018.
- Chwala, C., H. Kunstmann, S. Hipp, and U. Siart (2014), A monostatic microwave transmission experiment for line integrated precipitation and humidity remote sensing, *Atmos Res*, 144, 57–72, doi: 10.1016/j.atmosres.2013.05.014.
- Crane, R. K. (1971), Propagation phenomena affecting satellite communication systems operating in the centimeter and millimeter wavelength bands, *IEEE*, 59(2), 173–188, doi: 10.1109/PROC.1971.8123.
- Crane, R. K. (1977), Prediction of the effects of rain on satellite communication systems, *IEEE*, 65(3), 456–474, doi: 10.1109/PROC.1977.10498.
- Cressie, N. (1990), The origins of kriging, *Math Geol*, 22(3), 239–252, doi: 10.1007/BF00889887.
- Cressie, N., and C. K. Wile (2011), *Statistics for spatio-temporal data*, Wiley series in probability and statistics, 1st ed., 624 pp., Wiley, Oxford, UK, ISBN 978-0-471-69274-4.
- Crutzen, P. J., and E. F. Stoermer (2000), The “Anthropocene”, *IGBP Global Change Newsletter*, (41), 17–18.
- Cuccoli, F., L. Baldini, L. Facheris, S. Gori, and E. Gorgucci (2013), Tomography applied to radiobase network for real time estimation of the rainfall rate fields, *Atmos Res*, 119, 62–69, doi: 10.1016/j.atmosres.2011.06.024.
- da Silva Mello, L., M. S. Pontes, I. Fagundes, M. P. C. Almeida, and F. J. A. Andrade (2014), Modified rain attenuation prediction method considering the effect of wind direction, *J Microw Optoelectron Electromagn Appl*, 13, 254–267, doi: 10.1590/S2179-10742014000200012.
- da Silva Mello, L. A. R., E. Costa, and R. S. L. de Souza (2002), Rain attenuation measurements at 15 and 18 GHz, *Electron Lett*, 38(4), 197–198, doi: 10.1049/el:20020105.
- Dacre, H. F., P. A. Clark, O. Martinez-Alvarado, M. A. Stringer, and D. A. Lavers (2015), How do atmospheric rivers form?, *Bull Amer Meteor Soc*, 96(8), 1243–1255, doi: 10.1175/BAMS-D-14-00031.1.
- D’Amico, M., A. Manzoni, and G. L. Solazzi (2016), Use of operational microwave link measurements for the tomographic reconstruction of 2-D maps of accumulated rainfall, *IEEE Geosci Remote Sens Lett*, 13(12), 1827–1831, doi: 10.1109/LGRS.2016.2614326.
- Dauphas, N. (2003), The dual origin of the terrestrial atmosphere, *Icarus*, 165(2), 326–339, doi: 10.1016/S0019-1035(03)00198-2.
- David, N., and H. O. Gao (2016), Using cellular communication networks to detect air pollution, *Environ Sci Technol*, 50(17), 9442–9451, doi: 10.1021/acs.est.6b00681.
- David, N., P. Alpert, and H. Messer (2009), Technical note: Novel method for water vapour monitoring using wireless communication networks measurements, *Atmos Chem Phys*, 9(7), 2413–2418, doi: 10.5194/acp-

- 9-2413-2009.
- David, N., P. Alpert, and H. Messer (2013), The potential of commercial microwave networks to monitor dense fog—feasibility study, *J Geophys Res*, 118(20), 11,750–11,761, doi: 10.1002/2013JD020346.
- de Oliveira, A. P., A. J. Machado, J. F. Escobedo, and J. Soares (2002), Diurnal evolution of solar radiation at the surface in the city of são paulo: seasonal variation and modeling, *Theor Appl Climatol*, 71(3), 231–249, doi: 10.1007/s007040200007.
- de Vasconcelos, L. E. C., E. C. M. dos Santos, M. L. F. Neto, N. J. Ferreira, and L. G. de Vasconcelos (2016), *Using Tweets for Rainfall Monitoring, Information Technology: New Generations. Advances in Intelligent Systems and Computing*, vol. 448, pp. 1157–1167, Springer International Publishing, Cham, Switzerland, doi: 10.1007/978-3-319-32467-8_100, ISBN 978-3-319-32467-8.
- de Vos, L., H. Leijnse, A. Overeem, and R. Uijlenhoet (2017), The potential of urban rainfall monitoring with crowdsourced automatic weather stations in Amsterdam, *Hydrol Earth Syst Sci*, 21(2), 765–777, doi: 10.5194/hess-21-765-2017.
- Dinku, T., F. Ruiz, S. J. Connor, and P. Ceccato (2010), Validation and intercomparison of satellite rainfall estimates over Colombia, *J Appl Meteor Climatol*, 49(5), 1004–1014, doi: 10.1175/2009JAMC2260.1.
- Dolman, A. H. (2008), The role of the hydrological cycle in the climate system, in *Climate and the Hydrological Cycle*, edited by M. F. P. Bierkens, A. H. Dolman, and P. A. Troch, IAHS Special Publication 8, chap. 1, pp. 1–21, IAHS Press, Wallingford, UK, ISBN 978-1-901502-54-1.
- Doumounia, A., M. Gosset, F. Cazenave, M. Kacou, and F. Zougmore (2014), Rainfall monitoring based on microwave links from cellular telecommunication networks: First results from a West African test bed, *Geophys Res Lett*, 41(16), 6016–6022, doi: 10.1002/2014GL060724.
- Ebert, E. E. (2008), Fuzzy verification of high-resolution gridded forecasts: a review and proposed framework, *Meteor Appl*, 15(1), 51–64, doi: 10.1002/met.25.
- Ebert, E. E. (2010), Neighborhood verification of high resolution precipitation products, in *Satellite Rainfall Applications for Surface Hydrology*, edited by M. Gebremichael and F. Hossain, pp. 127–143, Springer Netherlands, doi: 10.1007/978-90-481-2915-7_8.
- Ebert, E. E., J. E. Janowiak, and C. Kidd (2007), Comparison of near-real-time precipitation estimates from satellite observations and numerical models, *Bull Amer Meteor Soc*, 88(1), 47–64, doi: 10.1175/BAMS-88-1-47.
- Ehlers, R., and B. Brown (2016), The 2016-17 budget: The state's drought response, Legislative Analyst's Office (LAO) [online], Feb 2016, 32 pp., <http://www.lao.ca.gov/reports/2016/3343/drought-response-020516.pdf>, (accessed Feb 9, 2017).
- Fencl, M., J. Rieckermann, M. Schleiss, D. Stránský, and V. Bareš (2013), Assessing the potential of using telecommunication microwave links in urban drainage modelling, *Water Sci Technol*, 68(8), 1810–1818, doi: 10.2166/wst.2013.429.
- Fleming, J. R. (2004), Sverre Petterssen and the contentious (and momentous) weather forecasts for D-Day, *Endeavour*, 28(2), 59–63, doi: 10.1016/j.endeavour.2004.04.007.
- Gale, E. L., and M. A. Saunders (2013), The 2011 thailand flood: climate causes and return periods, *Weather*, 68(9), 233–237, doi: 10.1002/wea.2133.
- Gebregiorgis, A., and F. Hossain (2014), Estimation of satellite rainfall error variance using readily available geophysical features, *IEEE Trans Geosci Remote Sens*, 52(1), 288–304, doi: 10.1109/TGRS.2013.2238636.
- Gebregiorgis, A. S., and F. Hossain (2015), How well can we estimate error variance of satellite precipitation data around the world?, *Atmos Res*, 154, 39–59, doi: 10.1016/j.atmosres.2014.11.005.
- Gimeno, L., R. Nieto, M. Vázquez, and D. Lavers (2014), Atmospheric rivers: A mini-review, *Front Earth Sci*, 2, 2, doi: 10.3389/feart.2014.00002.
- Giuli, D., A. Toccafondi, G. B. Gentili, and A. Freni (1991), Tomographic reconstruction of rainfall fields through microwave attenuation measurements, *J Appl Meteorol*, 30(9), 1323–1340, doi: 10.1175/1520-0450(1991)030<1323:TRORFT>2.0.CO;2.

Bibliography

- Goldshtein, O., H. Messer, and A. Zinevich (2009), Rain rate estimation using measurements from commercial telecommunications links, *IEEE T Signal Proces*, 57(4), 1616–1625, doi: 10.1109/TSP.2009.2012554.
- Gran, R. (2014), NASA rainfall satellite out of fuel, but continues to provide data, NASA [online], Aug 2014, <https://www.nasa.gov/content/goddard/nasa-rainfall-satellite-out-of-fuel-but-continues-to-provide-data>, (accessed Mar 3, 2017).
- Gray, E., and H. Hanson (2013), Global Precipitation Measurement core observatory, NASA [online], Nov 2013, 20 pp., https://pmm.nasa.gov/sites/default/files/document_files/GPM%20Mission%20Brochure.pdf, (accessed Mar 3, 2017).
- Grum, M., S. Kraemer, H.-R. Verworn, and A. Redder (2005), Combined use of point rain gauges, radar, microwave link and level measurements in urban hydrological modelling, *Atmos Res*, 77(1–4), 313–321, doi: 10.1016/j.atmosres.2004.10.013.
- GSMA (2016), Unlocking rural coverage: Enablers for commercially sustainable mobile network expansion, GSM Association [online], Jul 2016, 32 pp., http://www.gsma.com/publicpolicy/wp-content/uploads/2016/09/GSMA2016_Report_UnlockingRuralCoverage-EnablersForCommerciallySustainableMobileNetworkExpansionReport.pdf, (accessed Feb 15, 2017).
- Guillot, G., and T. Lebel (1999), Approximation of Sahelian rainfall fields with meta-Gaussian random functions, *Stoch Env Res Risk A*, 13(1–2), 113–130, doi: 10.1007/s004770050035.
- Haan, C. T. (1977), *Statistical Methods in Hydrology*, 1st ed., 378 pp., Iowa State University Press, Ames, USA, ISBN 8-8138-1510-X.
- Haining, R. P., R. Kerry, and M. A. Oliver (2010), Geography, spatial data analysis, and geostatistics: An overview, *Geogr Anal*, 42(1), 7–31, doi: 10.1111/j.1538-4632.2009.00780.x.
- Hallis, L. J., G. R. Huss, K. Nagashima, G. J. Taylor, S. A. Halldórsson, D. R. Hilton, M. J. Mottl, and K. J. Meech (2015), Evidence for primordial water in Earth's deep mantle, *Science*, 350(6262), 795–797, doi: 10.1126/science.aac4834.
- Heistermann, M., S. Jacobi, and T. Pfaff (2013), Technical note: An open source library for processing weather radar data (wradlib), *Hydrol Earth Syst Sci*, 17(2), 863–871, doi: 10.5194/hess-17-863-2013.
- Henson, B. (2017), More than 180,000 under evacuation orders as Oroville dam spillways compromised, WunderBlog® News & Blogs, Category 6™ [online], Feb 2017, <https://www.wunderground.com/blog/JeffMasters/more-than-180000-under-evacuation-orders-as-oroville-dam-spillways-co>, published on February 13, 2017, (accessed Feb 13, 2017).
- Henson, R. (2014), *The thinking person's guide to climate change*, 515 pp., AMS Books, Boston, USA, ISBN 978-1-935704-73-7.
- Hirschmann, M. M. (2006), Water, melting, and the deep earth H₂O cycle, *Annu Rev Earth Pl Sc*, 34(1), 629–653, doi: 10.1146/annurev.earth.34.031405.125211.
- Hoedjes, J. C. B., A. Kooiman, B. H. P. Maathuis, M. Y. Said, R. Becht, A. Limo, M. Mumo, J. Nduhiu-Mathenge, A. Shaka, and B. Su (2014), A conceptual flash flood early warning system for africa, based on terrestrial microwave links and flash flood guidance, *ISPRS Int J Geo-Inf*, 3(2), 584–598, doi: 10.3390/ijgi3020584.
- Hogg, D. C. (1968), Millimeter-wave communication through the atmosphere, *Science*, 159(3810), pp. 39–46.
- Hogg, D. C., and T.-S. Chu (1975), The role of rain in satellite communications, *P IEEE*, 63(9), 1308–1331, doi: 10.1109/PROC.1975.9940.
- Holt, A. R., J. W. F. Goddard, G. J. G. Upton, M. J. Willis, A. R. Rahimi, P. D. Baxter, and C. G. Collier (2000), Measurement of rainfall by dual-wavelength microwave attenuation, *Electron Lett*, 36(25), 2099–2101, doi: 10.1049/el:20001468.
- Hong, Y., and J. J. Gourley (2014), *Radar Hydrology*, chap. Advanced Radar Technologies for Quantitative Precipitation Estimation, pp. 87–108, CRC Press, Boca Raton, USA, doi: 10.1201/b17921-6, ISBN 978-1-4665-1461-4.

- Hong, Y., R. F. Adler, and G. Huffman (2007a), An experimental global prediction system for rainfall-triggered landslides using satellite remote sensing and geospatial datasets, *IEEE Trans Geosci Remote Sens*, 45(6), 1671–1680, doi: 10.1109/TGRS.2006.888436.
- Hong, Y., R. F. Adler, F. Hossain, S. Curtis, and G. J. Huffman (2007b), A first approach to global runoff simulation using satellite rainfall estimation, *Water Resour Res*, 43(8), WR005739, doi: 10.1029/2006WR005739.
- Horowitz, A. (2016), New Orleans's new flood maps: An outline for disaster, The New York Times [online], Jun 2016, <https://www.nytimes.com/2016/06/01/opinion/new-orleans-new-flood-maps-an-outline-for-disaster.html?rref=collection%2Ftimestopic%2FHurricane%20Katrina&r=0>, (accessed Feb 17, 2017).
- Hou, A. Y., G. Skofronick-Jackson, C. D. Kummerow, and J. M. Shepherd (2008), *Precipitation: Advances in Measurement, Estimation and Prediction*, chap. Global precipitation measurement, pp. 131–169, Springer Berlin Heidelberg, Berlin, Heidelberg, doi: 10.1007/978-3-540-77655-0_6.
- Hou, A. Y., R. K. Kakar, S. Neeck, A. A. Azarbarzin, C. D. Kummerow, M. Kojima, R. Oki, K. Nakamura, and T. Iguchi (2014), The Global Precipitation Measurement mission, *Bull Amer Meteor Soc*, 95(5), 701–722, doi: 10.1175/BAMS-D-13-00164.1.
- Huffman, G., D. Bolvin, D. Braithwaite, K. Hsu, R. Joyce, and P. Xie (2014), Integrated Multi-satellite Retrievals for GPM (IMERG), V03D, NASA's Precipitation Processing Center [online], <ftp://arthurhou.pps.eosdis.nasa.gov/gpmdata/>, (accessed Jan 6, 2017).
- Huffman, G. J., R. F. Adler, M. M. Morrissey, D. T. Bolvin, S. Curtis, R. Joyce, B. McGavock, and J. Susskind (2001), Global precipitation at one-degree daily resolution from multisatellite observations, *J Hydrometeor*, 2(1), 36–50, doi: 10.1175/1525-7541(2001)002<0036:GPAODD>2.0.CO;2.
- Huffman, G. J., D. T. Bolvin, E. J. Nelkin, D. B. Wolff, R. F. Adler, G. Gu, Y. Hong, K. P. Bowman, and E. F. Stocker (2007), The TRMM Multisatellite Precipitation Analysis (TMPA): Quasi-global, multiyear, combined-sensor precipitation estimates at fine scales, *J Hydrometeor*, 8(1), 38–55, doi: 10.1175/JHM560.1.
- Huffman, G. J., D. T. Bolvin, D. Braithwaite, K. Hsu, R. Joyce, and P. Xie (2015a), NASA Global Precipitation Measurement Integrated Multi-satellite Retrievals for GPM (IMERG). Algorithm Theoretical Basis Document, version 4.5, NASA [online], Nov 2015, 30 pp., http://pmm.nasa.gov/sites/default/files/document_files/IMERG_ATBD_V4.5.pdf, (accessed Feb 21, 2017).
- Huffman, G. J., D. T. Bolvin, and E. J. Nelkin (2015b), Integrated Multi-satellite Retrievals for GPM (IMERG) Technical Documentation. NASA/GSFC Code 612 Tech. Doc., NASA [online], Jun 2015, 48 pp., https://pmm.nasa.gov/sites/default/files/document_files/IMERG_doc.pdf, (accessed Feb 21, 2017).
- Huffman, G. J., D. T. Bolvin, and E. J. Nelkin (2015c), Day 1 IMERG Final Run release notes. NASA Tech. Doc., NASA [online], Jan 2015, 9 pp., https://pmm.nasa.gov/sites/default/files/document_files/IMERG_FinalRun_Day1_release_notes.pdf, (accessed Feb 21, 2017).
- Impact Forecasting (2012), Annual global climate and catastrophe report, Aon Benfield [online], Jan 2012, no. 8042–12/2011, 80 pp., http://thoughtleadership.aonbenfield.com/documents/20120110_if_annual_global_climate_cat_report.pdf, (accessed Feb 9, 2017).
- Impact Forecasting (2017), 2016 Annual global climate and catastrophe report, Aon Benfield [online], Jan 2017, 75 pp., <http://thoughtleadership.aonbenfield.com/Documents/20170117-ab-if-annual-climate-catastrophe-report.pdf>, (accessed Feb 9, 2017).
- IPCC (2013), *Climate Change 2013: The Physical Science Basis. Contribution of Working Group I to the Fifth Assessment Report of the Intergovernmental Panel on Climate Change*, 1535 pp., Cambridge University Press, Cambridge, UK and New York, USA, doi: 10.1017/CBO9781107415324.
- Isaaks, E. H., and R. Srivastava (1989), *Applied Geostatistics*, 561 pp., Oxford University Press, New York, USA, iISBN 0-19-505013-4.
- ITU (2016), Measuring the information society report 2016, International Telecommunication Union [online], iISBN 978-92-61-21431-9, 274 pp., <http://www.itu.int/en/ITU-D/Statistics/Documents/publications/misr2016/MISR2016-w4.pdf>, (accessed Feb 15, 2017).

Bibliography

- Joyce, R. J., J. E. Janowiak, P. A. Arkin, and P. Xie (2004), CMORPH: A method that produces global precipitation estimates from passive microwave and infrared data at high spatial and temporal resolution, *J Hydrometeorol*, 5(3), 487–503, doi: 10.1175/1525-7541(2004)005<0487:CAMTPG>2.0.CO;2.
- Khan, S., Y. Hong, J. Wang, K. Yilmaz, J. Gourley, R. Adler, G. Brakenridge, F. Policell, S. Habib, and D. Irwin (2011), Satellite remote sensing and hydrologic modeling for flood inundation mapping in Lake Victoria basin: Implications for hydrologic prediction in ungauged basins, *IEEE Trans Geosci Remote Sens*, 49(1), 85–95, doi: 10.1109/TGRS.2010.2057513.
- Kidd, C., and G. Huffman (2011), Global precipitation measurement, *Meteor Appl*, 18(3), 334–353, doi: 10.1002/met.284.
- Kidd, C., and V. Levizzani (2011), Status of satellite precipitation retrievals, *Hydrol Earth Syst Sci*, 15(4), 1109–1116, doi: 10.5194/hess-15-1109-2011.
- Kidd, C., V. Levizzani, J. Turk, and R. Ferraro (2009), Satellite precipitation measurements for water resource monitoring, *J Amer Water Resour Assoc*, 45(3), 567–579, doi: 10.1111/j.1752-1688.2009.00326.x.
- Kidd, C., V. Levizzani, and S. Laviola (2010), *Rainfall: State of the Science*, chap. Quantitative Precipitation Estimation from Earth Observation Satellites, pp. 127–158, American Geophysical Union, Washington, D. C., doi: 10.1029/2009GM000920.
- Kidd, C., P. Bauer, J. Turk, G. J. Huffman, R. J. Joyce, K.-L. Hsu, and D. Braithwaite (2012), Intercomparison of high-resolution precipitation products over northwest Europe, *J Hydrometeorol*, 13(1), 67–83, doi: 10.1175/JHM-D-11-042.1.
- Kidd, C., A. Becker, G. J. Huffman, C. L. Muller, P. Joe, G. Skofronick-Jackson, and D. B. Kirschbaum (2017), So, how much of the Earth's surface is covered by rain gauges?, *Bull Amer Meteor Soc*, 98(1), 69–78, doi: 10.1175/BAMS-D-14-00283.1.
- Kirschbaum, D., and K. G. Patel (2016), Precipitation data key to food security and public health, *EOS Earth & Space Science News* [online], Apr 2016, vol. 97, no. 7, pp. 10, <https://doi.org/10.1029/2016E0045583>, published on 09 February 2016, (accessed Feb 13, 2017).
- Kirschbaum, D., R. F. Adler, D. Adler, C. Peters-Lidard, and G. Huffman (2012), Global distribution of extreme precipitation and high-impact landslides in 2010 relative to previous years, *J Hydrometeorol*, 13(5), 1536–1551, doi: 10.1175/JHM-D-12-02.1.
- Kirstetter, P.-E., Y. Hong, J. J. Gourley, S. Chen, Z. Flamig, J. Zhang, M. Schwaller, W. Petersen, and E. Amitai (2012), Toward a framework for systematic error modeling of spaceborne precipitation radar with NOAA/NSSL ground radar-based national mosaic QPE, *J Hydrometeorol*, 13(4), 1285–1300, doi: 10.1175/JHM-D-11-0139.1.
- Kirstetter, P.-E., Y. Hong, J. J. Gourley, Q. Cao, M. Schwaller, and W. Petersen (2014), *Research Framework to Bridge from the Global Precipitation Measurement Mission Core Satellite to the Constellation Sensors Using Ground-Radar-Based National Mosaic QPE*, chap. 4, pp. 61–79, John Wiley & Sons, Inc, doi: 10.1002/9781118872086.ch4.
- Kirstetter, P.-E., J. J. Gourley, Y. Hong, J. Zhang, S. Moazamigoodarzi, C. Langston, and A. Arthur (2015), Probabilistic precipitation rate estimates with ground-based radar networks, *Water Resour Res*, 51(3), 1422–1442, doi: 10.1002/2014WR015672.
- KNMI (2015), KNMI'14 climate scenarios for the Netherlands; a guide for professionals in climate adaptation, KNMI [online], Jan 2015, 34 pp., http://www.klimaatsscenarios.nl/brochures/images/Brochure_KNMI14_EN_2015.pdf, (accessed Feb 17, 2017).
- Kousky, C., and E. Michel-Kerjan (2015), Examining flood insurance claims in the united states: Six key findings, *J Risk Insur*, pp. n/a–n/a, doi: 10.1111/jori.12106.
- Kucera, P. A., E. E. Ebert, F. J. Turk, V. Levizzani, D. Kirschbaum, F. J. Tapiador, A. Loew, and M. Borsche (2013), Precipitation from space: Advancing earth system science, *Bull Amer Meteor Soc*, 94(3), 365–375, doi: 10.1175/BAMS-D-11-00171.1.
- Kummerow, C. D., S. Ringerud, J. Crook, D. Randel, and W. Berg (2011), An observationally generated a priori database for microwave rainfall retrievals, *J Atmos Oceanic Technol*, 28(2), 113–130, doi: 10.1175/

- 2010JTECHA1468.1.
- Leijnse, H., R. Uijlenhoet, and J. N. M. Stricker (2007a), Rainfall measurement using radio links from cellular communication networks, *Water Resour Res*, 43(W03201), WR005631, doi: 10.1029/2006WR005631.
- Leijnse, H., R. Uijlenhoet, and J. N. M. Stricker (2007b), Hydrometeorological application of a microwave link: 2. precipitation, *Water Resour Res*, 43(4), WR004989, doi: 10.1029/2006WR004989.
- Leijnse, H., R. Uijlenhoet, and J. Stricker (2008), Microwave link rainfall estimation: Effects of link length and frequency, temporal sampling, power resolution, and wet antenna attenuation, *Adv Water Resour*, 31(11), 1481–1493, doi: 10.1016/j.advwatres.2008.03.004.
- Leijnse, H., R. Uijlenhoet, and A. Berne (2010), Errors and uncertainties in microwave link rainfall estimation explored using drop size measurements and high-resolution radar data, *J Hydrometeor*, 11(6), 1330–1344, doi: 10.1175/2010JHM1243.1.
- Lepioufle, J.-M., E. Leblois, and J.-D. Creutin (2012), Variography of rainfall accumulation in presence of advection, *J Hydrol*, 464–465(0), 494–504, doi: 10.1016/j.jhydrol.2012.07.041.
- Lorenz, C., and H. Kunstmann (2012), The hydrological cycle in three state-of-the-art reanalyses: Intercomparison and performance analysis, *J Hydrometeor*, 13(5), 1397–1420, doi: 10.1175/JHM-D-11-088.1.
- Machado, L. A. T., M. A. F. Silva Dias, C. Morales, G. Fisch, D. Vila, R. Albrecht, S. J. Goodman, A. J. P. Calheiros, T. Biscaro, C. Kummerow, J. Cohen, D. Fitzjarrald, E. L. Nascimento, M. S. Sakamoto, C. Cunningham, J.-P. Chaboureau, W. A. Petersen, D. K. Adams, L. Baldini, C. F. Angelis, L. F. Sapucci, P. Salio, H. M. J. Barbosa, E. Landulfo, R. A. F. Souza, R. J. Blakeslee, J. Bailey, S. Freitas, W. F. A. Lima, and A. Tokay (2014), The chuva project: How does convection vary across brazil?, *Bull Amer Meteor Soc*, 95(9), 1365–1380, doi: 10.1175/BAMS-D-13-00084.1.
- Marshall, J., W. Hitschfeld, and K. Gunn (1955), Advances in radar weather, pp. 1–56, Elsevier, doi: 10.1016/S0065-2687(08)60310-6.
- Masters, J. (2007), A new rainfall world record, WunderBlog® News & Blogs, Category 6™ [online], Mar 2007, <https://www.wunderground.com/blog/JeffMasters/a-new-rainfall-world-record>, published on March 13, 2007, (accessed Feb 12, 2017).
- Mei, Y., E. I. Nikolopoulos, E. N. Anagnostou, and M. Borga (2016), Evaluating satellite precipitation error propagation in runoff simulations of mountainous basins, *J Hydrometeor*, 17(5), 1407–1423, doi: 10.1175/JHM-D-15-0081.1.
- Melsen, L. (2017), Putting hydrological modelling practice to the test, Ph.D. thesis, Wageningen, the Netherlands, doi: 10.18174/408585, Wageningen University thesis nr. 6626, ISBN 978-94-6343-122-4.
- Mercier, F., L. Barthès, and C. Mallet (2015), Estimation of finescale rainfall fields using broadcast TV satellite links and a 4DVAR assimilation method, *J Atmos Oceanic Technol*, 32(10), 1709–1728, doi: 10.1175/JTECH-D-14-00125.1.
- Messer, H., and O. Sendik (2015), A new approach to precipitation monitoring: A critical survey of existing technologies and challenges, *IEEE Signal Proc Mag*, 32(3), 110–122, doi: 10.1109/MSP.2014.2309705.
- Messer, H., A. Zinevich, and P. Alpert (2006), Environmental monitoring by wireless communication networks, *Science*, 312(5774), 713, doi: 10.1126/science.1120034.
- Messer, H., A. Zinevich, and P. Alpert (2012), Environmental sensor networks using existing wireless communication systems for rainfall and wind velocity measurements, *IEEE Instru Meas Mag*, 15(2), 32–38, doi: 10.1109/MIM.2012.6174577.
- Minda, H., and K. Nakamura (2005), High temporal resolution path-average rain gauge with 50-ghz band microwave, *J Atmos Oceanic Technol*, 22(2), 165–179, doi: 10.1175/JTECH-1683.1.
- Mishchenko, M. I. (2000), Calculation of the amplitude matrix for a nonspherical particle in a fixed orientation, *Appl Opt*, 39(6), 1026–1031, doi: 10.1364/AO.39.001026.
- Nerini, D., Z. Zulkafli, L.-P. Wang, C. Onof, W. Buytaert, W. Lavado-Casimiro, and J.-L. Guyot (2015), A comparative analysis of TRMM-rain gauge data merging techniques at the daily time scale for distributed rainfall-runoff

Bibliography

- modeling applications, *J Hydrometeor*, 16(5), 2153–2168, doi: 10.1175/JHM-D-14-0197.1.
- Nijssen, B., and D. P. Lettenmaier (2004), Effect of precipitation sampling error on simulated hydrological fluxes and states: Anticipating the global precipitation measurement satellites, *J Geophys Res*, 109(D2), JD003497, doi: 10.1029/2003JD003497.
- Nikolopoulos, E. I., E. N. Anagnostou, F. Hossain, M. Gebremichael, and M. Borga (2010), Understanding the scale relationships of uncertainty propagation of satellite rainfall through a distributed hydrologic model, *J Hydrometeor*, 11(2), 520–532, doi: 10.1175/2009JHM1169.1.
- NOAA-NWS (2014), World record point precipitation measurements, NOAA-NWS Hydrometeorological Design Studies Center [online], May 2014, http://www.nws.noaa.gov/oh/hdsc/record_precip/record_precip_world.html, (accessed Feb 12, 2017).
- NRC (2008), *Earth observations from space: The first 50 years of scientific achievements*, 142 pp., National Academies Press, Washington D.C., USA, doi: 10.17226/11991, ISBN 978-0-309-11095-2.
- Oki, T., and S. Kanae (2006), Global hydrological cycles and world water resources, *Science*, 313(5790), 1068–1072, doi: 10.1126/science.1128845.
- Olsen, R., D. Rogers, and D. Hodge (1978), The αR^b relation in the calculation of rain attenuation, *IEEE T Antenn Propag*, 26(2), 318–329, doi: 10.1109/TAP.1978.1141845.
- Overeem, A., T. A. Buishand, and I. Holleman (2009a), Extreme rainfall analysis and estimation of depth-duration-frequency curves using weather radar, *Water Resour Res*, 45(10), WR007869, doi: 10.1029/2009WR007869.
- Overeem, A., I. Holleman, and A. Buishand (2009b), Derivation of a 10-year radar-based climatology of rainfall, *J Appl Meteor Climatol*, 48(7), 1448–1463, doi: 10.1175/2009JAMC1954.1.
- Overeem, A., H. Leijnse, and R. Uijlenhoet (2011), Measuring urban rainfall using microwave links from commercial cellular communication networks, *Water Resour Res*, 47(12), WR010350, doi: 10.1029/2010WR010350.
- Overeem, A., H. Leijnse, and R. Uijlenhoet (2013), Country-wide rainfall maps from cellular communication networks, *P Natl Acad Sci Usa*, 110(8), 2741–2745, doi: 10.1073/pnas.1217961110.
- Overeem, A., H. Leijnse, and R. Uijlenhoet (2016a), Two and a half years of country-wide rainfall maps using radio links from commercial cellular telecommunication networks, *Water Resour Res*, 52, n/a–n/a, doi: 10.1002/2016WR019412.
- Overeem, A., H. Leijnse, and R. Uijlenhoet (2016b), Retrieval algorithm for rainfall mapping from microwave links in a cellular communication network, *Atmos Meas Tech*, 9(5), 2425–2444, doi: 10.5194/amt-9-2425-2016.
- Palot, M., S. Jacobsen, J. Townsend, F. Nestola, K. Marquardt, N. Miyajima, J. Harris, T. Stachel, C. McCammon, and D. Pearson (2016), Evidence for H₂O-bearing fluids in the lower mantle from diamond inclusion, *Lithos*, 265, 237–243, doi: 10.1016/j.lithos.2016.06.023.
- Pebesma, E. J. (2014), Gstat user's manual, Gstat [online], Apr 2014, 108 pp, <http://www.gstat.org/gstat.pdf>, (accessed Mar 4, 2017).
- Pebesma, E. J., and C. G. Wesseling (1998), Gstat: a program for geostatistical modelling, prediction and simulation, *Computers & Geosciences*, 24(1), 17–31, doi: 10.1016/S0098-3004(97)00082-4.
- Peel, M. C., B. L. Finlayson, and T. A. McMahon (2007), Updated world map of the Köppen-Geiger climate classification, *Hydrol Earth Syst Sci*, 11(5), 1633–1644, doi: 10.5194/hess-11-1633-2007.
- Pereira Filho, A. J. (2012), A mobile x-pol weather radar for hydrometeorological applications in the metropolitan area of são paulo, brazil, *Geosci Instrum Method Data Syst*, 1(2), 169–183, doi: 10.5194/gi-1-169-2012.
- Posner, A. J., and K. P. Georgakakos (2016), An early warning system for landslide danger, *EOS Earth & Space Science News* [online], Dec 2016, vol. 97, no. 24, pp. 16–21, <https://doi.org/10.1029/2016E0062323>, published on 03 November 2016, (accessed Feb 13, 2017).
- Postel, S. (1997), Dividing the waters, *MIT Technology Review* [online], Apr-May 1997, vol. 100, no. 3, pp. 54–

- 62, <https://search.proquest.com/docview/195345814?accountid=27871>, (accessed Feb 9, 2017).
- Quetelard, H., P. Bessemoulin, R. S. Cervený, T. C. Peterson, A. Burton, and Y. Boodhoo (2009), Extreme weather: World-record rainfalls during tropical cyclone Gamede, *Bull Amer Meteor Soc*, 90(5), 603–608, doi: 10.1175/2008BAMS2660.1.
- R Core Team (2016), *R: A Language and Environment for Statistical Computing*, R Foundation for Statistical Computing, Vienna, Austria.
- Rabiei, E., U. Haberlandt, M. Sester, D. Fitzner, and M. Wallner (2016), Areal rainfall estimation using moving cars – computer experiments including hydrological modeling, *Hydrol Earth Syst Sci*, 20(9), 3907–3922, doi: 10.5194/hess-20-3907-2016.
- Rahimi, A., G. Upton, and A. Holt (2004), Dual-frequency links—a complement to gauges and radar for the measurement of rain, *J Hydrol*, 288(1–2), 3–12, doi: 10.1016/j.jhydrol.2003.11.008.
- Reges, H. W., N. Doesken, J. Turner, N. Newman, A. Bergantino, and Z. Schwalbe (2016), CoCoRaHS: The evolution and accomplishments of a volunteer rain gauge network, *Bull Amer Meteor Soc*, 97(10), 1831–1846, doi: 10.1175/BAMS-D-14-00213.1.
- Rios Gaona, M. F., A. Overeem, H. Leijnse, and R. Uijlenhoet (2015), Measurement and interpolation uncertainties in rainfall maps from cellular communication networks, *Hydrol Earth Syst Sci*, 19(8), 3571–3584, doi: 10.5194/hess-19-3571-2015.
- Rios Gaona, M. F., A. Overeem, H. Leijnse, and R. Uijlenhoet (2016), First-year evaluation of GPM rainfall over the Netherlands: IMERG Day1 Final Run (V03D), *J Hydrometeorol*, 17(11), 2799–2814, doi: 10.1175/JHM-D-16-0087.1.
- Roebeling, R. A., and I. Holleman (2009), SEVIRI rainfall retrieval and validation using weather radar observations, *Journal of Geophysical Research: Atmospheres*, 114(D21), n/a–n/a, doi: 10.1029/2009JD012102, d21202.
- Roebeling, R. A., E. L. A. Wolters, J. F. Meirink, and H. Leijnse (2012), Triple collocation of summer precipitation retrievals from SEVIRI over Europe with gridded rain gauge and weather radar data, *J Hydrometeorol*, 13(5), 1552–1566, doi: 10.1175/JHM-D-11-089.1.
- Rogers, R. R., and P. L. Smith (1996), *A Short History of Radar Meteorology*, pp. 57–98, American Meteorological Society, Boston, USA, doi: 10.1007/978-1-940033-84-6_4.
- Rose, C. R., and V. Chandrasekar (2006), A GPM dual-frequency retrieval algorithm: DSD profile-optimization method, *J Atmos Oceanic Technol*, 23(10), 1372–1383, doi: 10.1175/JTECH1921.1.
- Roy, V., S. Gishkori, and G. Leus (2016), Dynamic rainfall monitoring using microwave links, *EURASIP J Adv Signal Process*, 2016(1), 77, doi: 10.1186/s13634-016-0367-6.
- Ruf, C. S., K. Aydin, S. Mathur, and J. P. Bobak (1996), 35–ghz dual-polarization propagation link for rain-rate estimation, *J Atmos Oceanic Technol*, 13(2), 419–425, doi: 10.1175/1520-0426(1996)013<0419:GDPPLF>2.0.CO;2.
- Sarachi, S., K.-I. Hsu, and S. Sorooshian (2015), A statistical model for the uncertainty analysis of satellite precipitation products, *J Hydrometeorol*, 16(5), 2101–2117, doi: 10.1175/JHM-D-15-0028.1.
- Savenije, H. H. G., A. Y. Hoekstra, and P. van der Zaag (2014), Evolving water science in the anthropocene, *Hydrol Earth Syst Sci*, 18(1), 319–332, doi: 10.5194/hess-18-319-2014.
- Scheel, M. L. M., M. Rohrer, C. Huggel, D. Santos Villar, E. Silvestre, and G. J. Huffman (2011), Evaluation of TRMM Multi-satellite Precipitation Analysis (TMPA) performance in the Central Andes region and its dependency on spatial and temporal resolution, *Hydrol Earth Syst Sci*, 15(8), 2649–2663, doi: 10.5194/hess-15-2649-2011.
- Schilling, W. (1991), Rainfall data for urban hydrology: What do we need?, *Atmos Res*, 27(1–3), 5–21, doi: 10.1016/0169-8095(91)90003-F.
- Schleiss, M., J. Rieckermann, and A. Berne (2013), Quantification and modeling of wet-antenna attenuation for commercial microwave links, *IEEE Geosci Remote Sens Lett*, 10(5), 1195–1199, doi: 10.1109/LGRS.2012.

Bibliography

- 2236074.
- Schneider, U., A. Becker, P. Finger, A. Meyer-Christoffer, B. Rudolf, and M. Ziese (2015a), GPCC Full Data Reanalysis Version 7.0 at 0.5°: Monthly land-surface precipitation from rain-gauges built on GTS-based and historic data, doi: 10.5676/DWD_GPCC/FD_M_V7_050.
- Schneider, U., A. Becker, P. Finger, A. Meyer-Christoffer, and M. Ziese (2015b), GPCC Monitoring Product: Near real-time monthly land-surface precipitation from rain-gauges based on SYNOP and CLIMAT data, doi: 10.5676/DWD_GPCC/MP_M_V5_100.
- Schuermans, J. M., M. F. P. Bierkens, E. J. Pebesma, and R. Uijlenhoet (2007), Automatic prediction of high-resolution daily rainfall fields for multiple extents: The potential of operational radar, *J Hydrometeor*, 8(6), 1204–1224, doi: 10.1175/2007JHM792.1.
- Sene, K. (2013a), *Flash Floods: Forecasting and Warning*, chap. Rainfall Forecasting, pp. 101–132, Springer Netherlands, Dordrecht, doi: 10.1007/978-94-007-5164-4_4.
- Sene, K. (2013b), *Flash Floods: Forecasting and Warning*, chap. Precipitation Measurement, pp. 33–70, Springer Netherlands, Dordrecht, doi: 10.1007/978-94-007-5164-4_2.
- Shiklomanov, I., and A. Sokolov (1983), Methodological basis of world water balance investigation and computation, in *New approaches in water balance computations. Proc. of the Hamburg workshop*, edited by A. V. der Beken and A. Herrman, no. 148 in IAHS, pp. 77–92, IAHS, Wallingford, Oxfordshire.
- Skofronick-Jackson, G., W. A. Petersen, A. Y. Hou, E. F. Stocher, J. Kaye, and R. Kakar (2013), Global Precipitation Measurement (GPM) science implementation plan. NASA Tech. Rep., NASA [online], Apr 2013, 162 pp., https://pmm.nasa.gov/sites/default/files/document_files/GPM%20Science%20Implementation%20Plan%20-%20April%202013.pdf, (accessed Feb 21, 2017).
- Smyth, J. R. (1987), β -Mg₂SiO₄: A potential host for water in the mantle?, *Am Mineral*, 72(11–12), 1051–1055.
- Solomon, S. (2011), *Water: The Epic Struggle for Wealth, Power, and Civilization*, 1st ed., 608 pp., HarperCollins, New York, USA, ISBN 978-0-06-054831-5.
- Somanathan, T. V., and V. A. Nageswaran (2015), Derivatives and emerging markets – part II, in *The Economics of Derivatives*, pp. 165–178, Cambridge University Press, Cambridge, UK, doi: 10.1017/CBO9781316134566.014.
- Strangeways, I. (2006), Early attempts to measure rainfall, in *Precipitation*, chap. 7, pp. 139–150, Cambridge University Press, Cambridge, UK, doi: 10.1017/CBO9780511535772.011, ISBN 978-0-521-85117-6.
- Su, F., Y. Hong, and D. P. Lettenmaier (2008), Evaluation of TRMM Multisatellite Precipitation Analysis (TMPA) and its utility in hydrologic prediction in the La Plata basin, *J Hydrometeor*, 9(4), 622–640, doi: 10.1175/2007JHM944.1.
- Talbot, D. (2015a), Desalination out of desperation, MIT Technology Review [online], Jan-Feb 2015, vol. 118, no. 1, pp. 44–48, <https://search.proquest.com/docview/1677666919?accountid=27871>, (accessed Feb 7, 2017).
- Talbot, D. (2015b), Megascale desalination, MIT Technology Review [online], Mar-Apr 2015, vol. 118, no. 2, pp. 49, <https://search.proquest.com/docview/1677666764?accountid=27871>, (accessed Feb 7, 2017).
- Tang, G., Z. Zeng, D. Long, X. Guo, B. Yong, W. Zhang, and Y. Hong (2015), Statistical and hydrological comparisons between TRMM and GPM Level-3 products over a mid-latitude basin: Is Day-1 IMERG a good successor for TMPA 3B42V7?, *J Hydrometeor*, doi: 10.1175/JHM-D-15-0059.1.
- Tapiador, F. J., F. Turk, W. Petersen, A. Y. Hou, E. Garcia-Ortega, L. A. Machado, C. F. Angelis, P. Salio, C. Kidd, G. J. Huffman, and M. de Castro (2012), Global precipitation measurement: Methods, datasets and applications, *Atmos Res*, 104–105, 70–97, doi: 10.1016/j.atmosres.2011.10.021.
- Tian, Y., and C. D. Peters-Lidard (2010), A global map of uncertainties in satellite-based precipitation measurements, *Geophys Res Lett*, 37(24), GLO46008, doi: 10.1029/2010GL046008.
- Tian, Y., C. D. Peters-Lidard, J. B. Eyllander, R. J. Joyce, G. J. Huffman, R. F. Adler, K.-I. Hsu, F. J. Turk, M. Garcia,

- and J. Zeng (2009), Component analysis of errors in satellite-based precipitation estimates, *J Geophys Res*, 114(D24), JD011949, doi: 10.1029/2009JD011949.
- Tobin, K. J., and M. E. Bennett (2010), Adjusting satellite precipitation data to facilitate hydrologic modeling, *J Hydrometeor*, 11(4), 966–978, doi: 10.1175/2010JHM1206.1.
- Upton, G., A. Holt, R. Cummings, A. Rahimi, and J. Goddard (2005), Microwave links: The future for urban rainfall measurement?, *Atmos Res*, 77(1–4), 300–312, doi: 10.1016/j.atmosres.2004.10.009.
- Upton, G. J. G., R. J. Cummings, and A. R. Holt (2007), Identification of melting snow using data from dual-frequency microwave links, *IET MICROW ANTENNA P*, 1(2), 282–288, doi: 10.1049/iet-map:20050285.
- Van de Beek, C. Z., H. Leijnse, P. J. J. F. Torfs, and R. Uijlenhoet (2011), Climatology of daily rainfall semi-variance in the Netherlands, *Hydrol Earth Syst Sci*, 15(1), 171–183, doi: 10.5194/hess-15-171-2011.
- Van de Beek, C. Z., H. Leijnse, P. Torfs, and R. Uijlenhoet (2012), Seasonal semi-variance of Dutch rainfall at hourly to daily scales, *Adv Water Resour*, 45(0), 76–85, doi: 10.1016/j.advwatres.2012.03.023.
- Velasco-Forero, C. A., D. Sempere-Torres, E. F. Cassiraga, and J. J. Gómez-Hernández (2009), A non-parametric automatic blending methodology to estimate rainfall fields from rain gauge and radar data, *Adv Water Resour*, 32(7), 986–1002, doi: 10.1016/j.advwatres.2008.10.004.
- Vemado, F., and A. J. Pereira Filho (2016), Severe weather caused by heat island and sea breeze effects in the metropolitan area of são paulo, brazil, *Advances in Meteorology*, 2016, 13 pages, doi: 10.1155/2016/8364134, Article ID 8364134.
- Vergara, H., Y. Hong, J. J. Gourley, E. N. Anagnostou, V. Maggioni, D. Stampoulis, and P.-E. Kirstetter (2014), Effects of resolution of satellite-based rainfall estimates on hydrologic modeling skill at different scales, *J Hydrometeor*, 15(2), 593–613, doi: 10.1175/JHM-D-12-0113.1.
- Villarini, G., and W. F. Krajewski (2007), Evaluation of the research version TMPA three-hourly $0.25^\circ \times 0.25^\circ$ rainfall estimates over Oklahoma, *Geophys Res Lett*, 34(5), GL029147, doi: 10.1029/2006GL029147.
- Villarini, G., and W. F. Krajewski (2010), Review of the different sources of uncertainty in single polarization radar-based estimates of rainfall, *Surv Geophys*, 31(1), 107–129, doi: 10.1007/s10712-009-9079-x.
- Wada, Y., L. P. H. van Beek, F. C. Sperna Weiland, B. F. Chao, Y.-H. Wu, and M. F. P. Bierkens (2012), Past and future contribution of global groundwater depletion to sea-level rise, *Geophys Res Lett*, 39(9), n/a–n/a, doi: 10.1029/2012GL051230, l09402.
- Wang, P. K. (2013), *Physics and Dynamics of Clouds and Precipitation*, Cambridge University Press, doi: 10.1017/CBO9780511794285, Cambridge Books Online.
- Wentz, F. J. (2015), A 17-yr climate record of environmental parameters derived from the Tropical Rainfall Measuring Mission (TRMM) microwave imager, *J Climate*, 28(17), 6882–6902, doi: 10.1175/JCLI-D-15-0155.1.
- Wilks, D. (2011), Forecast verification, in *Statistical Methods in the Atmospheric Sciences, International Geophysics*, vol. 100, edited by D. S. Wilks, chap. 8, pp. 301–394, Academic Press, doi: 10.1016/B978-0-12-385022-5.00008-7.
- World Bank (2012), *2012 Information and Communications for Development: Maximizing Mobile*, 244 pp., World Bank, Washington D.C., USA, doi: 10.1596/978-0-8213-8991-1, ISBN 978-0-8213-8991-1.
- Wu, H., R. F. Adler, Y. Hong, Y. Tian, and F. Policelli (2012), Evaluation of global flood detection using satellite-based rainfall and a hydrologic model, *J Hydrometeor*, 13(4), 1268–1284, doi: 10.1175/JHM-D-11-087.1.
- Xue, X., Y. Hong, A. S. Limaye, J. J. Gourley, G. J. Huffman, S. I. Khan, C. Dorji, and S. Chen (2013), Statistical and hydrological evaluation of TRMM-based Multi-satellite Precipitation Analysis over the Wangchu basin of Bhutan: Are the latest satellite precipitation products 3B42V7 ready for use in ungauged basins?, *J Hydrol*, 499, 91–99, doi: 10.1016/j.jhydrol.2013.06.042.
- Yang, S., and S. W. Nesbitt (2014), Statistical properties of precipitation as observed by the TRMM precipitation radar, *Geophys Res Lett*, 41(15), 5636–5643, doi: 10.1002/2014GL060683, 2014GL060683.
- Yong, B., D. Liu, J. J. Gourley, Y. Tian, G. J. Huffman, L. Ren, and Y. Hong (2015), Global view of real-time TRMM Multisatellite Precipitation Analysis: Implications for its successor Global Precipitation Measurement mis-

Bibliography

- sion, *Bull Amer Meteor Soc*, 96(2), 283–296, doi: 10.1175/BAMS-D-14-00017.1.
- Zinevich, A., P. Alpert, and H. Messer (2008), Estimation of rainfall fields using commercial microwave communication networks of variable density, *Adv Water Resour*, 31(11), 1470–1480, doi: 10.1016/j.advwatres.2008.03.003.
- Zinevich, A., H. Messer, and P. Alpert (2009), Frontal rainfall observation by a commercial microwave communication network, *J Appl Meteor Climatol*, 48(7), 1317–1334, doi: 10.1175/2008JAMC2014.1.
- Zinevich, A., H. Messer, and P. Alpert (2010), Prediction of rainfall intensity measurement errors using commercial microwave communication links, *Atmos Meas Tech*, 3(5), 1385–1402, doi: 10.5194/amt-3-1385-2010.

Statement of Authorship Contribution

Chapters 1 (introduction) and 6 (synthesis) come exclusively from the mind of Manuel Felipe Ríos Gaona. For all other chapters, the contribution from co-authors is provided below.

NB	=	Noud Brasjen (Weerplaza)	AO	=	Aart Overeem (KNMI/WUR)
HL	=	Hidde Leijnse (KNMI)	MFRG	=	Manuel Felipe Ríos Gaona (WUR)
JFM	=	Jan-Fokke Meirink (KNMI)	RU	=	Remko Uijlenhoet (WUR)

Chapter 2

Conception or design of the work:	RU, MFRG, AO
Data collection:	MFRG
Data analysis and interpretation:	MFRG, AO, RU
Drafting the article:	MFRG
Critical revision of the article:	AO, HL, RU, MFRG
Approval of the published version:	MFRG, AO, HL, RU

Chapter 3

Conception or design of the work:	AO
Data collection:	NB, AO, MFRG
Data analysis and interpretation:	MFRG, AO, JFM, HL, RU
Drafting the article:	MFRG
Critical revision of the article:	AO, JFM, HL, RU, MFRG
Approval of the version to be published:	MFRG, AO, JFM, HL, RU

Chapter 4

Conception or design of the work:	AO, HL, RU
Data collection:	AO, MFRG
Data analysis and interpretation:	MFRG, AO, HL, RU
Drafting the article:	MFRG
Critical revision of the article:	AO, HL, RU, MFRG
Approval of the published version:	MFRG, AO, HL, RU

Chapter 5

Conception or design of the work:	AO, RU
Data collection:	AO, MFRG
Data analysis and interpretation:	MFRG, HL, RU, AO
Drafting the article:	MFRG, RU, HL, AO
Critical revision of the chapter:	HL, RU, AO, MFRG
Approval of the version to be submitted:	MFRG, AO, HL, RU

Summary

This thesis is about the evaluation of several rainfall products retrieved from satellites and microwave link networks for the land surface of the Netherlands and São Paulo.

In **Chapter 2** the first year of the GPM research product (IMERG) was evaluated for the land surface of the Netherlands. IMERG is a gridded product with a spatiotemporal resolution of $0.1^\circ \times 0.1^\circ$ ($\sim 77 \text{ km}^2$ at the latitude of the Netherlands) every 30 min. The evaluation was done for both data sets of IMERG, i.e., *precipitationUncal* and *precipitationCal*. The latter is calibrated through a global network of rain gauges, the former is not. IMERG data sets were evaluated against the spatiotemporal aggregation (at IMERG resolution) of radar rainfall fields which have a native resolution of $\sim 1 \text{ km}^2$ every 5 min. The evaluation was done for half-hourly, daily, monthly, and yearly durations through pixel-by-pixel comparisons, and cumulative daily rainfall for the entire land surface of the Netherlands. It was found that IMERG tends to systematically underestimate rainfall by 2%, for the *precipitationCal* data set. For the *precipitationUncal* this yearly underestimation rises to 11%, which shows the effective improvement in satellite rainfall retrievals from gauge calibration.

In **Chapter 3** not only IMERG was evaluated again for the land surface of the Netherlands but also two more satellite rainfall products, and one from CML. The evaluation is done for a seven-month period. The two extra GEO-satellite products, i.e., CPP and NIPE have been designed for the hydrometeorological conditions of the Netherlands. This is also the case for CML-derived rainfall maps. From all the products evaluated in this chapter, IMERG is the product with the lowest resolution; therefore, and for inter-comparison purposes, the spatiotemporal resolution of all the other products were upscaled to match that of IMERG. Here, the evaluation was only based on pixel-by-pixel comparisons. IMERG was the satellite product which outperformed its other two counterparts, CPP and NIPE. This latter is still an experimental product and the one with the poorest performance. Rainfall maps from CML were the product with the best performance with a correlation of ~ 0.6 , which is twice as good as the one obtained for IMERG. This better performance suggested the added value that CML might have in the eventual validation of satellite rainfall retrievals. Hence, it was explored if the spatial density of CML would be a crucial factor in satellite validation at IMERG resolution. There was no clear evidence for this to be the case.

Chapter 4 quantified the uncertainties in rainfall maps derived from CML data associated with the spatiotemporal availability of the CML data itself, and the methodology of

interpolation. The evaluation was carried out for $\sim 1,100$ rainfall maps with spatiotemporal resolutions of $\sim 1 \text{ km}^2$ every 15 min. As with Chapters 2 and 3, the evaluation was done via pixel-by-pixel comparisons against aggregated radar rainfall maps at 15-min and daily durations. CML rainfall was simulated from radar data to quantify these types of uncertainty. This derived data set represented perfect rainfall measurements that potentially come from CML networks where all links retrieve power measurements at all times, i.e., no availability issues. It was found that only 10% of the uncertainty can be attributed to availability issues in the CML data set, from a CML network of $\sim 1,700$ links with an average availability of 83%. Measurement errors were the source that contributes most to the overall uncertainty in rainfall maps from CML networks.

In **Chapter 5** rainfall was retrieved from a Brazilian CML network through the freeware R-package RAINLINK. RAINLINK is an R package that computes rainfall intensities from minimum and maximum received power measurements (attenuation). This package was developed for the climatological conditions of the Netherlands, and for the topology of the local CML networks. Because of the subtropical climatology of Brazil, this was a perfect opportunity to test the applicability of RAINLINK to other conditions than those for which it was originally designed. The city of São Paulo was the testbed for which rainfall retrievals from 16 CML were evaluated for a three-month period. The evaluation was done at half-hourly durations against aggregated data from a local automatic gauge network of which the native resolution is 10 min. Without totally adapting the algorithm to the local conditions (something that would require a more extensive and intensive evaluation), in 9 out of 16 cases CML rainfall retrievals from RAINLINK gave a correlation of 0.84 with a lower variability but high biases. Only for one CML the relative bias was below 10%, which is an indication that RAINLINK is suitable for rainfall estimation in subtropical climates.

The main results are summarized as follows: CML offer the most accurate rainfall estimates at higher spatiotemporal resolutions, i.e., $\sim 1 \text{ km}^2$ sub-hourly. RAINLINK is a good first approach for CML rainfall retrievals in tropical latitudes. The evaluation of CML data from the city of São Paulo (Brazil) yielded promising results with regard to rainfall retrievals from the RAINLINK package. Satellite rainfall estimates from the brand-new GPM mission perform well for the hydrometeorological conditions of the Netherlands.

Agradecimientos

First things first. To my late mom. She did not have the opportunity to ever set foot in a classroom, but if I managed to finish this PhD, and wander the academic path that led me to this point (and why not, any other future adventure), it was because of the infinite wisdom and love she nurtured me with. To my biologic mother. We have shared very little but she brought me to this world... so what else can one ask for? Muchas gracias mama(s), todo lo bueno que tengo para ofrecer lo aprendí de sumercé. A toda mi demás familia cercana, todos ustedes en algún punto de sus vidas contribuyeron de una otra forma en mi formación y educación. En especial mi hermana Claudia, quién suplió el rol paterno; a mi hermano Alberto, el cuál siempre que pudo me apoyo económicamente; y a mi tía Carmen que me quiere como si fuera hijo propio. A Tomásín “pingüin”, José, Tito, Nelson, Luz, Omar, Henry, Ángel, Janeth, mi tío Matías, Frank, mi madrina Ofelia, mi padrino Jorge H., Laura, Jorge Iván, Janeth R., señoras Rebeca y Ana Lucía, don Vicente y don Joaquín, Joaco, y a aquellos que ya no están con nosotros (mis tías Emma y Ursulita, Ricardo y Enrique): a todos ustedes siempre los tengo presente, palabras más palabras menos, gracias mil.

Second of all, and not less important, to Sara Porras Gutiérrez. Not a single vowel (or consonant or number) that was written in this thesis, could have existed without the encouragement, support, help, an love of my only one and beautiful wife Sara. If I have to write all that she did (or maybe sacrificed) for me, for following me to the Netherlands and to any part of the world, I would have to print an equally large thesis-book like this (but we all agree that one is enough, isn't it?). For now, all I can say is that she's everything to me, and as long as she stays by my side there is no paper, thesis and/or research I can't get done. She is the power and most of the motivation that propels me to face the daily routine.

Before and during my days as PhD candidate in the Netherlands, I had the fortune to meet quite remarkable people, but I could not have survived without the help and support from Koen Siteur, Sija Francisca Stofberg, and Lieke Anna Melsen. Coincidentally, all of them are Dutch and Doctors (double D's - happy-face emoji goes here). Koen and Sija, whom I became friends with during my MSc studies, helped me to (literally) survive the Netherlands. In many occasions they provided me with a place to crash [in/at], nutritive and delicious Dutch food (to the extend of whatever that means can be true and wholesome), Dutch circle parties, and tons of advice of what to do, how to behave, and how to correctly pronounce the Dutch-godforsaken *U*. I failed them in all of the last four aspects; and for that I'm very sorry but I'm pretty sure they still have some room for forgiveness in their hearts. Koen, for lack of a better word, you're a brother (*broer*, *frère*, *fratello*, *hermano*) to me. My devotion to Lieke was born right at the beginning of my PhD. She walked me through

Acknowledgements

every step of this road, from A to Z. She guided me inside and outside my job, and hadn't she taken responsibility for dutifully filling out our taxes, the *belastingdienst* would've already kicked us out of Holland long time ago (don't you worry, I perfectly know the difference between Holland and the Netherlands). More than the nerdiness she embraces, what I learnt from her is to always reply with a smile no matter what crap situation you're in. I never ever met her angry. Special mention goes to my roomie Tjitske Janelle Geertsema (also a future double D - wink-face emoji goes here). She was very kind to me, only had positive comments, and the only one who always understood my silly humor, I think. I will surely miss forever the fist-bump greeting we learnt to cherish. Within her precious blue eyes, inspiration never was difficult to find; but if you ask her, she'll tell you that I'm just being *slijmbal*.

Special acknowledgements to my teammates from one of the oldest football clubs in the Netherlands, the Go-Ahead Victoria Combination (GVC). They brought me into their "dinosaur" category, and allowed me to spend some energy on the training days and on the match-weekends. They even allowed me to captain them on the battlefield, I mean, the football pitch. To all of you guys *hartelijk bedankt* for giving me a space to show my football talent (almost none), score some magnificent goals, and step aside from academia to breath some inspirational air. Special mentions go to Reurt Boelema who is a very good and noble friend, despite his temperament; Rick Breg, Jeroen Veraart, and Joost de Jong (maybe to his amazement). Acknowledgements should also go to my Colombian friends Miguel Angel Hernandez Fuerte, Sergio Porras Gutierrez, Dayron Fernando Valencia Guerrero, Martín Paez Mora, y Canyica. Despite all the distance between us, our long-standing friendship, comradeship, and chatting was the best medicine in those recurrent times of procrastination. Wherever you're, you're the best comedians and coolest friends a guy like me can have. Martín, amiguito, cumplir el sueño de ir a "La Grande Boucle" (2015) fue la mejor experiencia y divertimento que tuve durante los casi cuatro años de Doctorado!

Finally, I want express my infinite gratitude to my supervisors Aart Overeem, Hidde Leijne, and Remko Uijlenhoet, whom I like to refer to as *Les Trois Mousquetaires* (me far from being the equivalent of d'Artagnan, of course). More than to the knowledge I gained from them, my gratitude is meant for the insurmountable patience they had to put up with every single time I was against their guidance. To Aart, I thank him because every Friday he was there to sacredly comply with his supervisor tasks and to ask for results I never had. I'm pretty sure that any coming PhD student he'll supervise from now on will give him less than half the trouble I did. To Hidde, the most intelligent supervisor I had. I still can't find any argument I had with him in which I wasn't wrong. To Remko, he did what he could to make me feel at home, and propitiated a very amicable work environment. I think the only issue I really struggled with while doing the PhD was to consider him as my boss and not as my friend; and if I really learnt something from him, it was to be a Calvinist. My wife and I will always be grateful for the gamble he took in hiring me to commit to this endeavour. Thank you so very much... and see you next time.

Curriculum Vitae

Manuel Felipe Ríos Gaona
27 August 1981, Bogotá D.C.

2013-2017	PhD in Hydrometeorology, Wageningen University Chair Group <i>Hydrology and Quantitative Water Management</i>
2010-2011	MSc Earth Sciences, Utrecht University Specialization <i>Hydrology</i> Internship at Deltares, Utrecht, the Netherlands Thesis at KNMI, De Bilt, the Netherlands
2002-2007	BEng Civil Engineering, Universidad Nacional de Colombia Minor <i>Water & Environment</i>
2000-2005	Land Surveyor, SENA–CCIM, Bogotá D.C., Colombia



*Netherlands Research School for the
Socio-Economic and Natural Sciences of the Environment*

D I P L O M A

For specialised PhD training

The Netherlands Research School for the
Socio-Economic and Natural Sciences of the Environment
(SENSE) declares that

Manuel Felipe Ríos Gaona

born on 27 August 1981 in Bogotá D.C., Colombia

has successfully fulfilled all requirements of the
Educational Programme of SENSE.

Wageningen, 20 June 2017

the Chairman of the SENSE board

Prof. dr. Huub Rijnaarts

the SENSE Director of Education

Dr. Ad van Dommelen

The SENSE Research School has been accredited by the Royal Netherlands Academy of Arts and Sciences (KNAW)



K O N I N K L I J K E N E D E R L A N D S E
A K A D E M I E V A N W E T E N S C H A P P E N



The SENSE Research School declares that **Mr Manuel Ríos Gaona** has successfully fulfilled all requirements of the Educational PhD Programme of SENSE with a work load of 30 EC, including the following activities:

SENSE PhD Courses

- o Environmental research in context (2014)
- o Research in context activity: 'Government review of the IPCC AR5 SYR report' (2014)

Other PhD and Advanced MSc Courses

- o PhD career coaching, Wageningen University (2016)
- o Brain Training, Wageningen University (2015)
- o Reviewing a scientific paper, Wageningen University (2015)
- o Scientific writing, Wageningen University (2014)
- o Bayesian statistics, Wageningen University (2014)
- o Spatial and spatio-temporal modelling of meteorological and climatic variables Using Open Source software (R + OSGeo), University of Belgrade - Faculty of Civil Engineering (2014)
- o Summer school on Remote Sensing of Clouds and Precipitation, Meteorological Institute, University Bonn (2013)

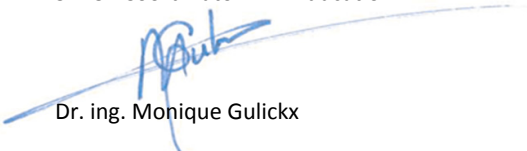
Management and Didactic Skills Training

- o Supervising BSc student with thesis entitled 'Evaluation of near real-time rainfall estimates from satellite' (2016)

Oral Presentations

- o *Intercomparison of rainfall products from radars, satellites and commercial link networks.* 9th ERAD 2016 - European Conference on Radar in Meteorology and Hydrology, 10-14 October 2016, Antalya, Turkey
- o *First-year evaluation of IMERG - Final Run in the Netherlands.* European Geosciences Union EGU - General Assembly, 17-22 April 2016, Vienna, Austria
- o *Assessing spatial and temporal uncertainties, in Rainfall maps from cellular communication networks.* DailyMeteo.org/2014 Conference, 23-27 June 2014, Belgrade, Serbia
- o *Rainfall field estimation using simulated microwave link information.* IPC11 – 11th International Precipitation Conference, 30 June - 3 July 2013, Ede-Wageningen, The Netherlands

SENSE Coordinator PhD Education



Dr. ing. Monique Gulickx

The research described in this thesis was financially supported by The Netherlands Organisation for Scientific Research NWO (project ALW-GO-AO/11-15).

Cover design by Manuel Felipe Ríos Gaona.

The size of the circles indicates the relative altitude with regard to the lowest point within the Netherlands. The color scale represents the rainfall field for the almost four years I lived in the Netherlands while doing this thesis, i.e., from May 4, 2013 to March 21, 2017. Blue, for the lowest rainfall, to yellow, for the highest. The rainfall field is the aggregation of 5-min rainfall accumulations obtained from the gauge-corrected radar data set developed at KNMI. The red circles indicate DEM spots for which no rainfall is estimated. The only two filled circles correspond to the geographical location of WUR and home. Finally, the cover was entirely produced in R, software exclusively used in the analysis of the huge amount of rainfall fields this thesis deals with.

Printed by GVO printers & designers B.V.

